Visibility Laboratory
University of California
Scripps Institution of Oceanography
San Diego 52, California

ATMOSPHERIC OPTICAL MEASUREMENTS DURING HIGH ALTITUDE BALLOON FLIGHT, PART I

Almerian R. Boileau

December 1959
Index Number NS 714-100

Bureau of Ships
Contract NObs-72092

SIC REFERENCE 59-32-(1)

Approved:

Seibert Q. Duntley

Seibert Q. Duntley, Director
Visibility Laboratory

Approved for Distribution:

Roger Revelle

Roger Revelle, Director
Scripps Institution of Oceanography

TABLE OF CONTENTS

	Page
INTRODUCTION AND SUMMARY- -	1
PROCEDURE -	2
Balloon Track Chart -	4
Color Photograph of Sky - - - - - - - - - - - - - - - - -	7
Temperature Profile -	25
Sun's Zenith and Azimuth Angles - - - - - - - - - - - - -	27
PRESENTATION OF DATA -	28
Catalogue of Graphs -	29
Data vs. Altitude -	31
Data vs. Azimuthal Angle - - - - - - - - - - - - - - - - -	66
DISCUSSION -	90
Preface -	90
Notation and Instrumentation - - - - - - - - - - - - - - -	90
Recorded Optical Quantities - - - - - - - - - - - - - - -	93
Computed Optical Property - - - - - - - - - - - - - - - -	95
Operational Procedure - - - - - - - - - - - - - - - - - -	96
Cycling of Filters -	98
APPENDIX -	102
REFERENCES	
ACKNOWLEDGEMENTS	

SIO Ref. 59-32-(1)

Atmospheric Optical Measurements during High Altitude Balloon Flight, Part I*

by

Almerian R. Boileau

INTRODUCTION AND SUMMARY

Certain optical measurements of the atmosphere were made by the Visibility Laboratory, University of California, La Jolla Campus, 21 June 1958, over central Minnesota. These were recorded from daybreak to mid-morning during the time four optically instrumented balloons launched by Air Force Cambridge Research Center recorded related data at a higher altitude.

The data recorded by the Visibility Laboratory are presented herein as a catalogue of the recorded optical measurements as they varied with altitude, time of day, azimuthal angle with respect to the sun, and meteorological conditions.

* This report is a result of research which has been supported by the Geophysics Research Directorate, Air Force Cambridge Research Center, Bedford, Massachusetts, and the Bureau of Ships, U. S. Navy.

PROCEDURE

U. S. Air Force XB-29, No. 4224725, took off for Flight 120 from the Air Force Base at Wold-Chamberlain Airport, Minneapolis-St. Paul at 0415, 21 June 1958 and proceeded to Crosby, Minnesota. This airplane carried optical and meteorological instruments from the Visibility Laboratory, University of California, La Jolla Campus. At the time of this flight there were in operation eight optical instruments and one meteorological instrument, viz., a vortex thermometer. The purpose of this flight was to record atmospheric optical data at the same time that related data were recorded at a higher altitude by means of balloon-borne equipment. When the airplane arrived above Crosby, before sun rise, it was at 20000 feet.

The balloon launching had been scheduled to take place from an open mine pit near Crosby starting at 0500 of the 21st. The balloons, four in number, were launched by Winzen Research, Inc., under the direction of Dr. V. J. Stakutis from the Thermal Radiation Laboratory, Geophysics Research Directorate of the Air Force Cambridge Research Center, Air Research and Development Command. Each balloon carried an instrumented package which contained photometers and recording devices. The launching proceeded on schedule, the balloons being launched, as observed from the B-29, at 0500, 0521, 0536, and 0551.

The plan for the B-29 was to record data from 20000 feet down to 2000 feet (approximately 1000 feet above the terrain) in the general vicinity of the balloons. The optical equipments have light level thresholds below which they will not operate. These thresholds vary for the different instruments. Because a complete set of data was wanted the starting of the exercise was delayed until the least sensitive instrument would record. In the meantime the airplane orbited in the vicinity of 20000 feet following the balloons in their drift.

The balloons first drifted southeast until they were over the south shore of Mille Lacs Lake, then westward. The balloon tracks are shown in Figure 1. The B-29 was flown on different flight paths during data recording, but by always returning to the vicinity of the balloons the B-29 followed the same general track as the balloons.

The approximate positions of the airplane at the times indicated is shown by the underlined times.

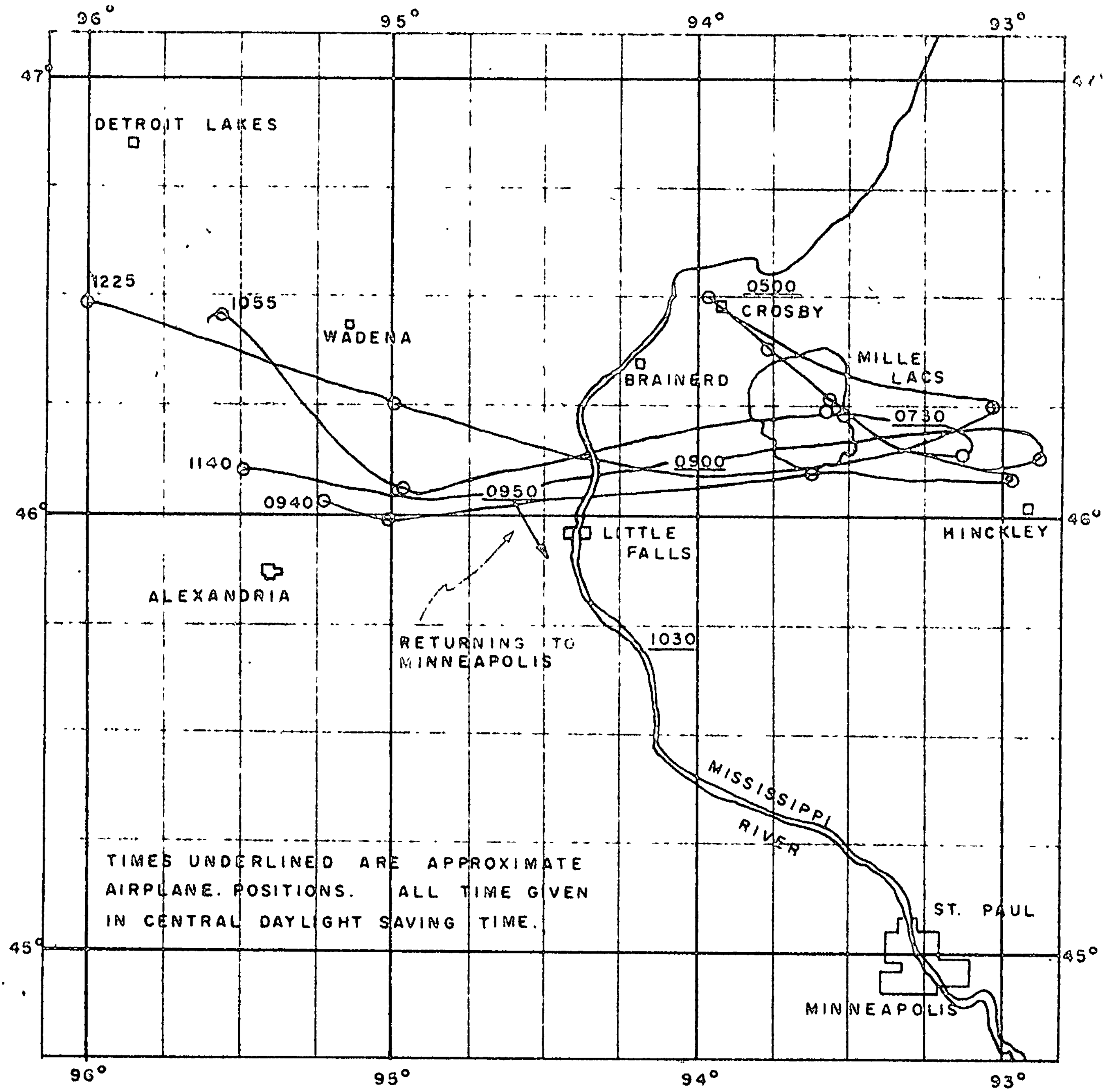

Balloon tracks are shown in solid lines. The time of release of each instrumented package from the balloon which carried it is indicated by the time at the end of each track. The underlined times are approximate airplane positions.

FIGURE 1
FLIGHT 120
JUNE 21, 1958
CENTRAL MINNESOTA

The recording of data commenced at 0635 and continued until 1038, at which time the equipment was secured and the airplane returned to Minneapolis. During this time data were recorded as follows:

Central Daylight Saving Time	
0635 - 0704	At 21000 feet
0713 - 0730	20000 feet to 11300 feet
0738 - 0753	At 11000 feet
0758 - 0811	11200 feet to 2000 feet
0813 - 0820	At 2000 feet
0830 - 0835	6500 feet to 2000 feet
0907 - 0920	At 22000 feet
0925 - 0935	20000 feet to 16400 feet
0942 - 0949	At 17200 feet
1019 - 1030	10200 feet to 2000 feet
1033 - 1037	At 2000 feet

What was the weather like? Photographs, (Kodachrome transparencies) taken at 0700, at 21000 feet, show scattered clouds at a lower level. Photographs taken at 0753, at 11000 feet, show clouds at this altitude and above. By 0945, at 17200 feet, there was a dense cloud layer below the airplane. When a hole was found and the airplane descended to below the cloud layer the layer was seen to be some 6000 feet thick. Color prints from the transparencies taken at the various station altitudes are enclosed as Figure 2 through 18 immediately following this page. The photographs were taken by the project engineer sitting in the bombardier's position while the pilot executed right hand, 30° bank, turns. One result of photographing through the airplane's nose windows was the photographing of reflections of objects inside the airplane. These reflections are very apparent in some of the photographs.

The photographs also show the terrain over which the data were recorded, this being fields, trees, and lakes. In Figure 2, top photograph, Mille Lacs Lake can be seen. In each of two photographs, the bottom photograph of Figure 2 and the top photograph of Figure 3, a river can be seen. It is not the Mississippi in either case; but is believed to be a tributary (or perhaps tributaries) to the St. Croix River.

In Figure 6 the two top photographs show Mille Lacs Lake, and in the bottom photograph one of the tributaries to the St. Croix River can be discerned. The two small lakes shown in the top photograph of Figure 7 probably are those near the town of Mora.

Figure 8, 9, and 10 show the typical terrain. There are so many lakes of various size in this area that those shown could not be identified.

Pages 7 through 23 of the original report carried color photographs showing the visible atmospheric conditions. These photographs are not included in this second printing of the report. The conditions as shown in the color photographs are described to some extent, however, by the descriptive notes in Fig. 19, page 25.

Temperature was recorded during descending runs as registered by an ML-471/AMQ-8 indicating resistance thermometer. A plot of temperature as a function of altitude and time is shown in Figure 19 immediately following this page. In the figure are observations of cloud conditions at the times indicated. In addition, lines representing pseudo-adiabats are plotted near the temperature profiles.

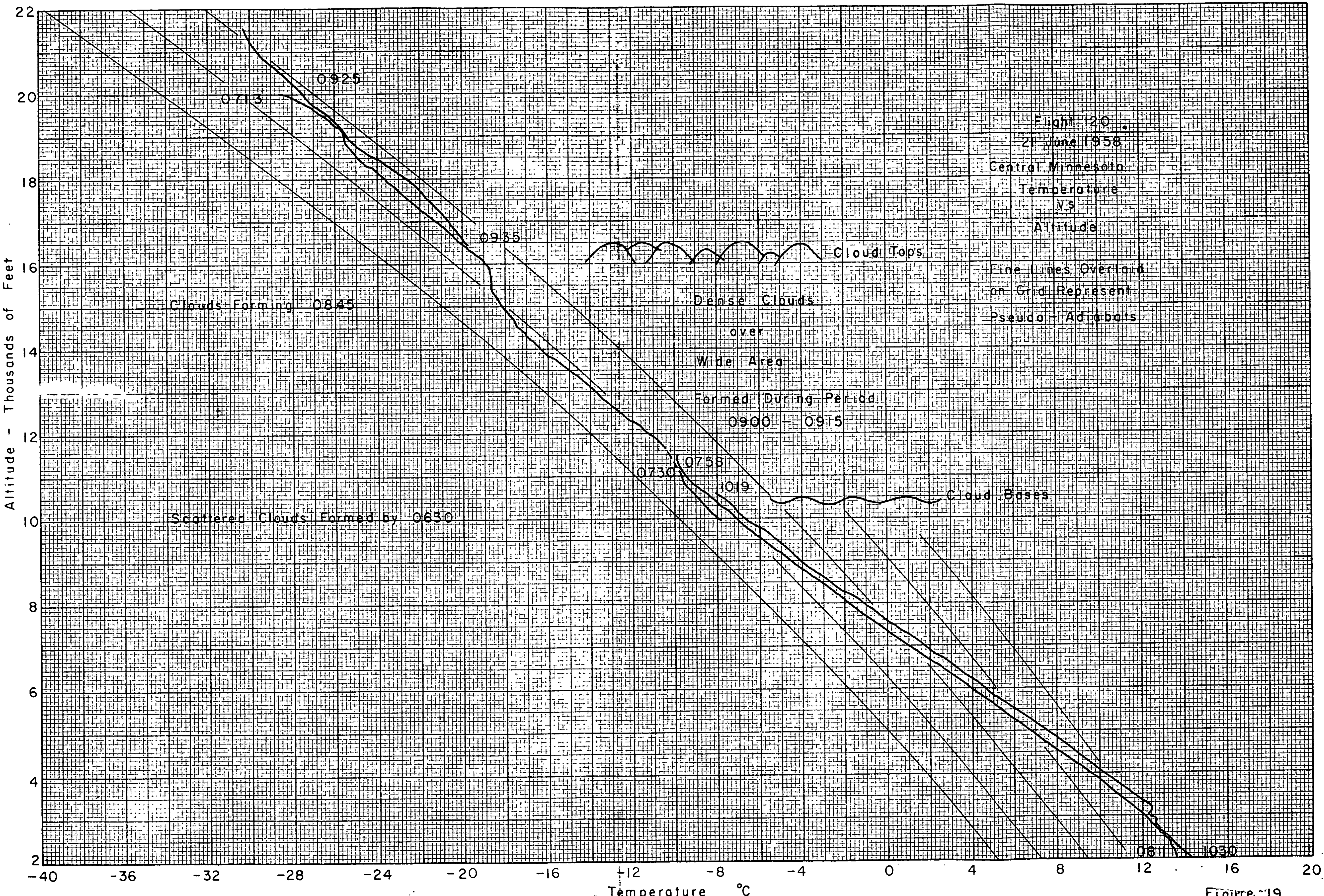
Flight 120
21 June 1958
Central Minnesota
Temperature
vs
Altitude
Fine Lines Overlaid
on Grid Represent
Pseudo-Adiabats
Cloud Tops
Dense Clouds
over
Wide Area
Formed During Period
0900 - 0915
Cloud Bases
Clouds Forming 0845
Scattered Clouds Formed by 0630
0925
0713
0935
0758
0730
1019
0811
1030
Altitude - Thousands of Feet
Temperature °C
22
20
18
16
14
12
10
8
6
4
2
-40
-36
-32
-28
-24
-20
-16
-12
-8
-4
0
4
8
12
16
20

Figure 19

Azimuth and zenith angles of the sun computed for a position at 46° North Latitude and 94° West Longitude, are shown in Figure 20. This position was selected because the balloons ranged from approximately 93° to 95° West Longitude in the vicinity of the 46° North Latitude parallel. These angles are plotted for the period of 0600 to 1100 Central Daylight Saving Time. The ordinates of the lower graph are shown as zenith angle values on the left side of the graph and as elevation angle on the right side of the graph, these angles being complementary.

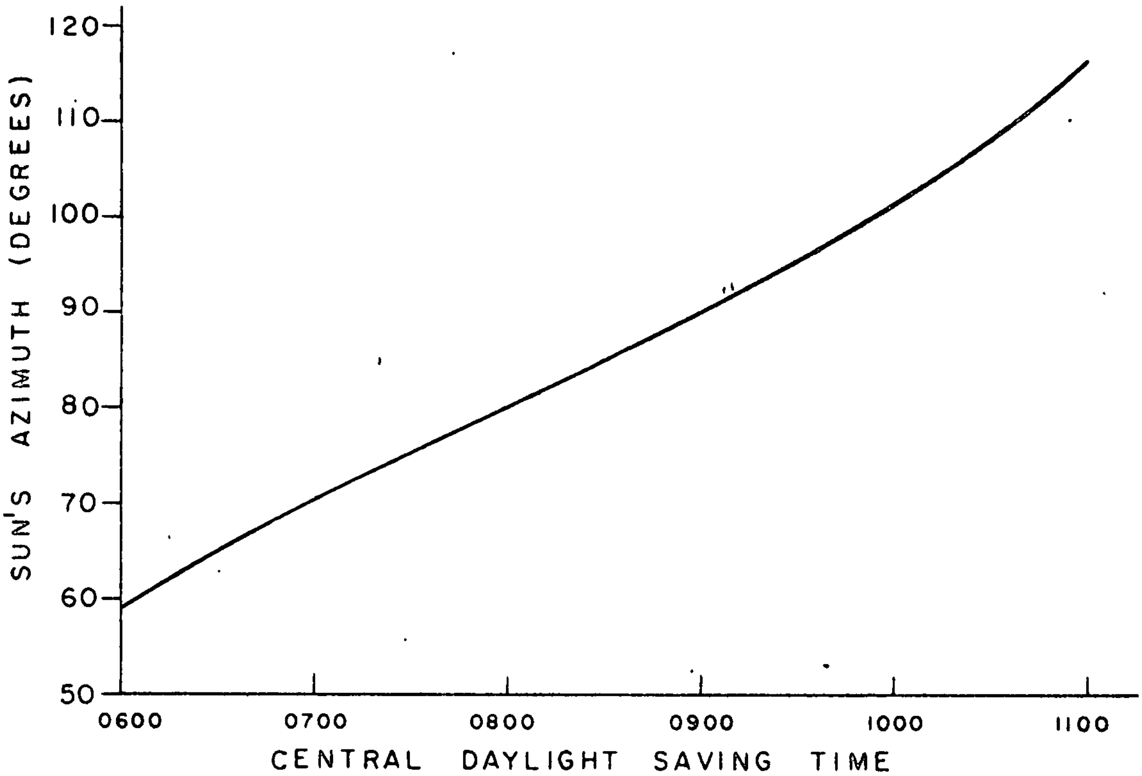

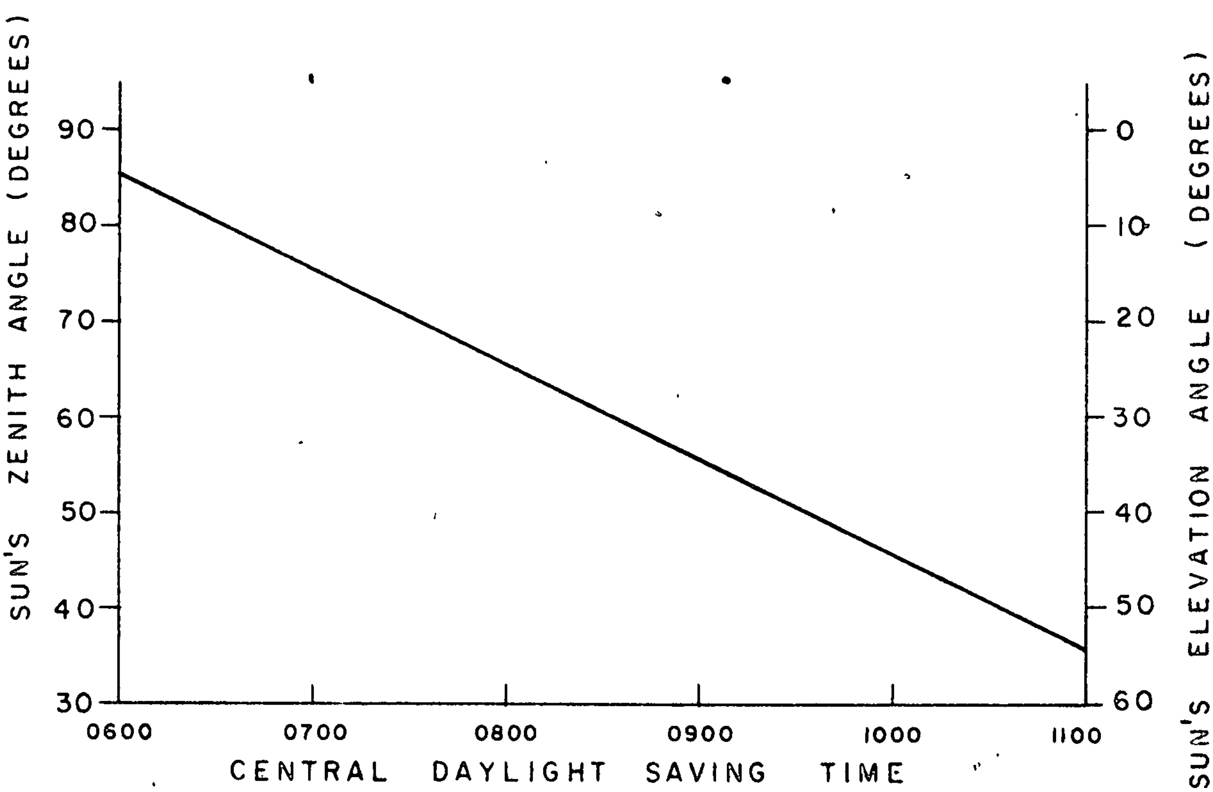

AZIMUTH AND ZENITH ANGLE OF SUN DURING FLIGHT 120, COMPUTED FOR POSITION 46° N. LAT., 94° W. LONG.

FIGURE 20
FLIGHT NO. 120
JUNE 21, 1958
CENTRAL MINNESOTA

PRESENTATION OF DATA

The data recorded during Flight 120 are presented herewith as a catalogue of graphs, each measured quantity being shown as it varied with altitude and time or as it varied with azimuth at a constant altitude. The computed apparent attenuation length, $L_A(z)$, is similarly presented.

The purpose of this report is to make available the data which were recorded and, in the case of apparent attenuation length, computed. Interpretation and discussion of applications of these data are reserved for subsequent reports.

The following notes concerning the graphs are pertinent:

1. The broken lines in Figures 23 and 27 indicate that data points are lacking.

2. Figures 39, 40 and 41, nadir luminance and radiance, show large random oscillations of values. This is due to the type of terrain beneath the airplane, i.e., lakes, fields, and wooded areas. The graphs shown cover the time of flight from start at 0713 until 0935. The balance of the material up to 1030 is so similar that no useful purpose would be served in including it.

3. Records of horizontal luminance and radiance, Figures 42 and 43, are incomplete due to failure of the heating system on that telephotometer. This permitted condensation of moisture on the optics when airplane descended from cold altitude into a warmer, moist altitude. After being in warmer altitude a sufficiently long time the moisture evaporated and records were again good. This condition accounts for the incomplete apparent attenuation length data, Figures 54 and 55, and the incomplete set of polar plots, Figures 56 to 79.

Catalogue of Graphs

Atmospheric Optical Measurements vs Altitude and Time

Quantity	Symbol	Figure	Page
Illuminance, Downwelling	$E(z,-)$	21-23	31-33
Irradiance, Downwelling	$H(z,-)$	24-29	34-39
Illuminance, Upwelling	$E(z,+)$	30-31	40-41
Irradiance, Upwelling	$H(z,+)$	32-34	42-44
Luminance, Zenith	$B(z,0,0)$	35	45
Radiance, Zenith	$N(z,0,0)$	36-38	46-48
Luminance, Nadir	$B(z,180^\circ,0)$	39	49
Radiance, Nadir	$N(z,180^\circ,0)$	40-41	50-51
Luminance, Horizontal	$B(z,90^\circ,90^\circ)$	42	52
Radiance, Horizontal	$N(z,90^\circ,90^\circ)$	43	53
Path Function, Luminous, Horizontal	$B_*(z,90^\circ,90^\circ)$	44-46	54-56
Path Function, Luminous, Horizontal	$B_*(z,90^\circ,60^\circ)$	47	57
Path Function, Radiant, Horizontal	$B_*(z,90^\circ,90^\circ)$	48-49, 51-52	58-59, 61-62
Path Function, Radiant, Horizontal	$B_*(z,90^\circ,60^\circ)$	50, 53	60, 63
Apparent Attenuation Length	$L_A(z)$	54-55	64-65

Atmospheric Optical Measurements

by Azimuthal Distribution at Constant Altitude

Time	Altitude	Figure	Page
0700	21000 feet	56-61	66-71
0751	11000 feet	62-63	72-73
0820	2000 feet	64-67	74-77
0916	22000 feet	68-73	78-83
0945	17200 feet	74-79	84-89

At each of the station altitudes listed above the upper and lower sky luminance and radiance values were recorded. These will be the subject of Part II of this report.

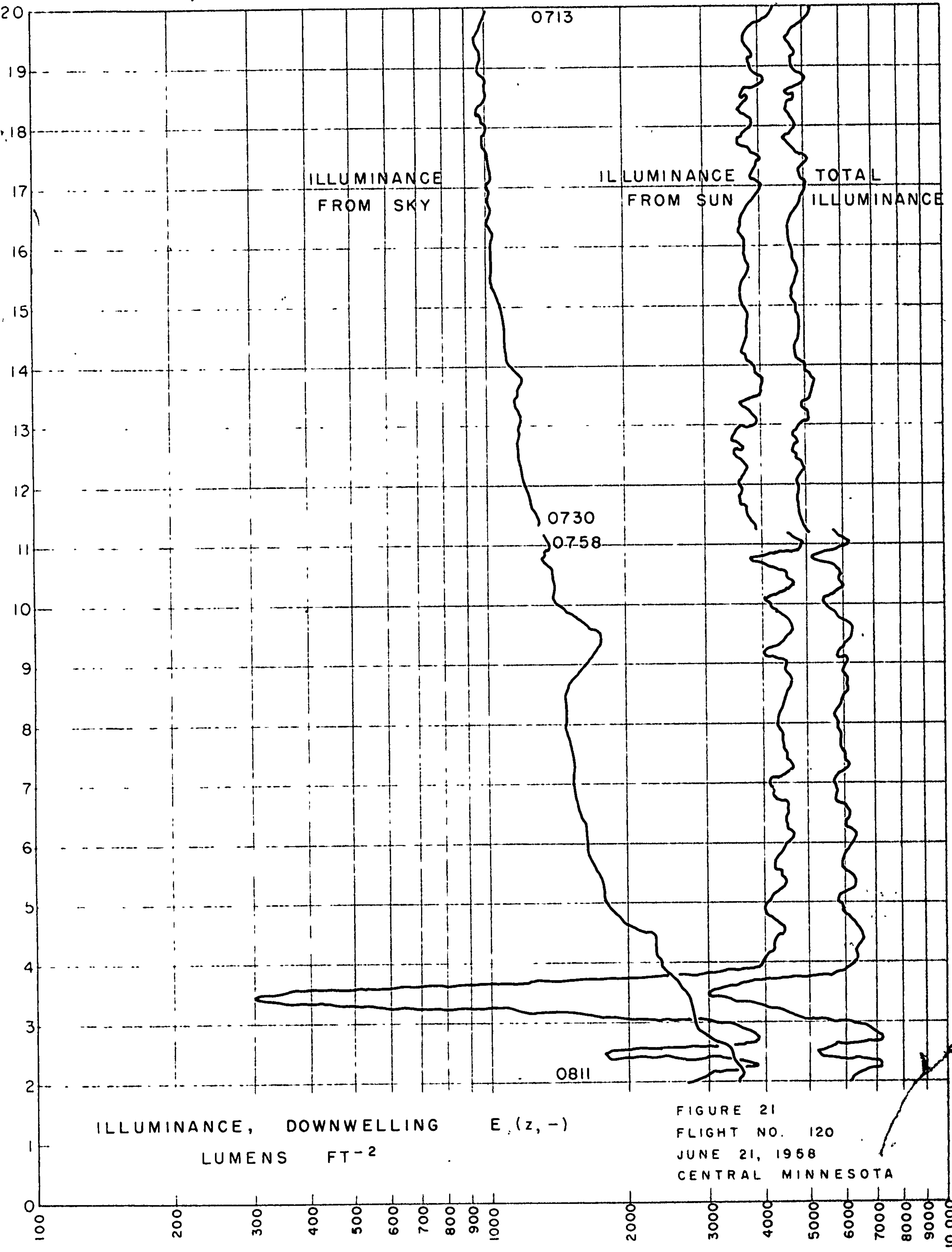

FIGURE 21
FLIGHT NO. 120
JUNE 21, 1958
CENTRAL MINNESOTA

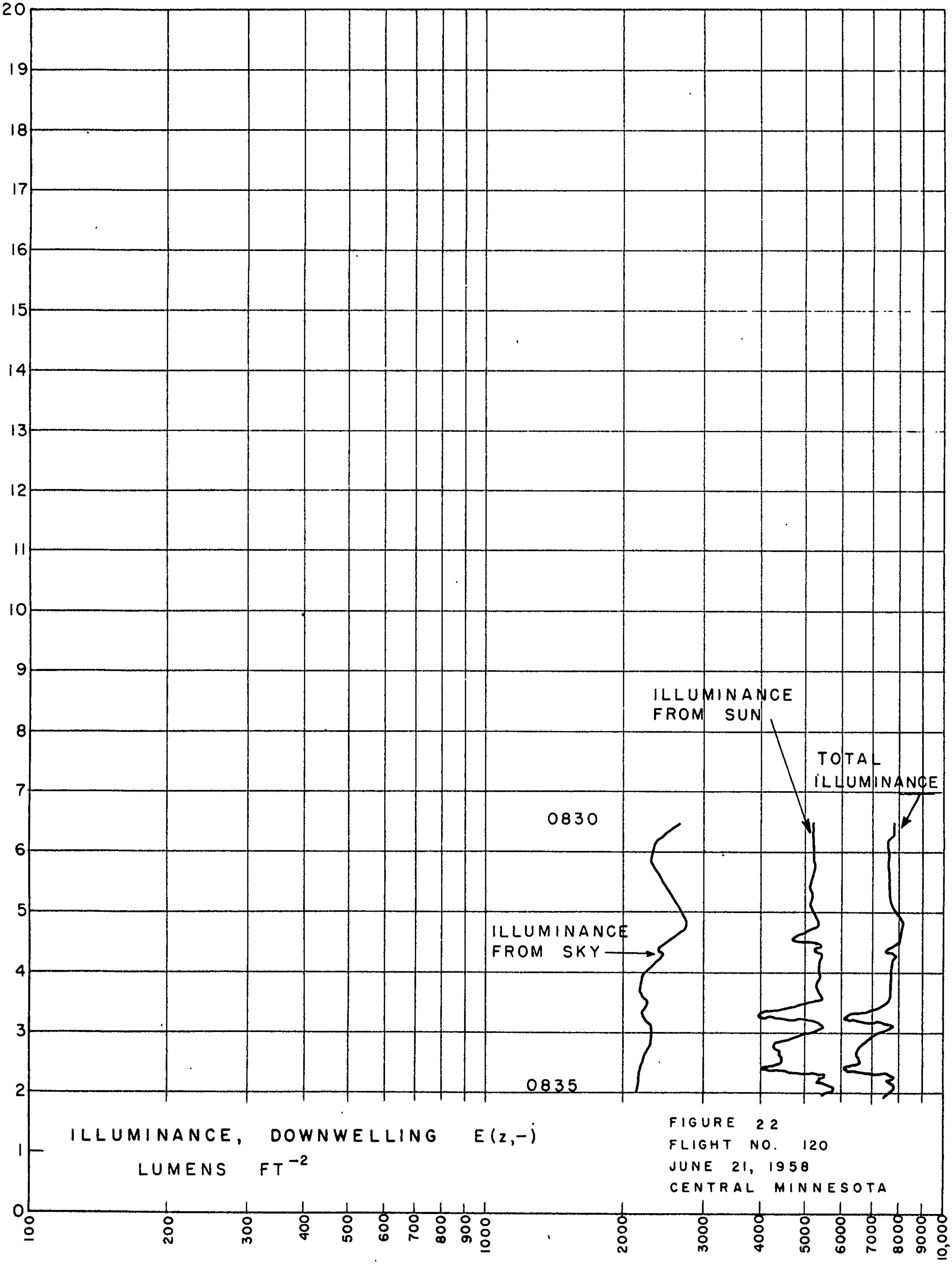

FIGURE 22
FLIGHT NO. 120
JUNE 21, 1958
CENTRAL MINNESOTA

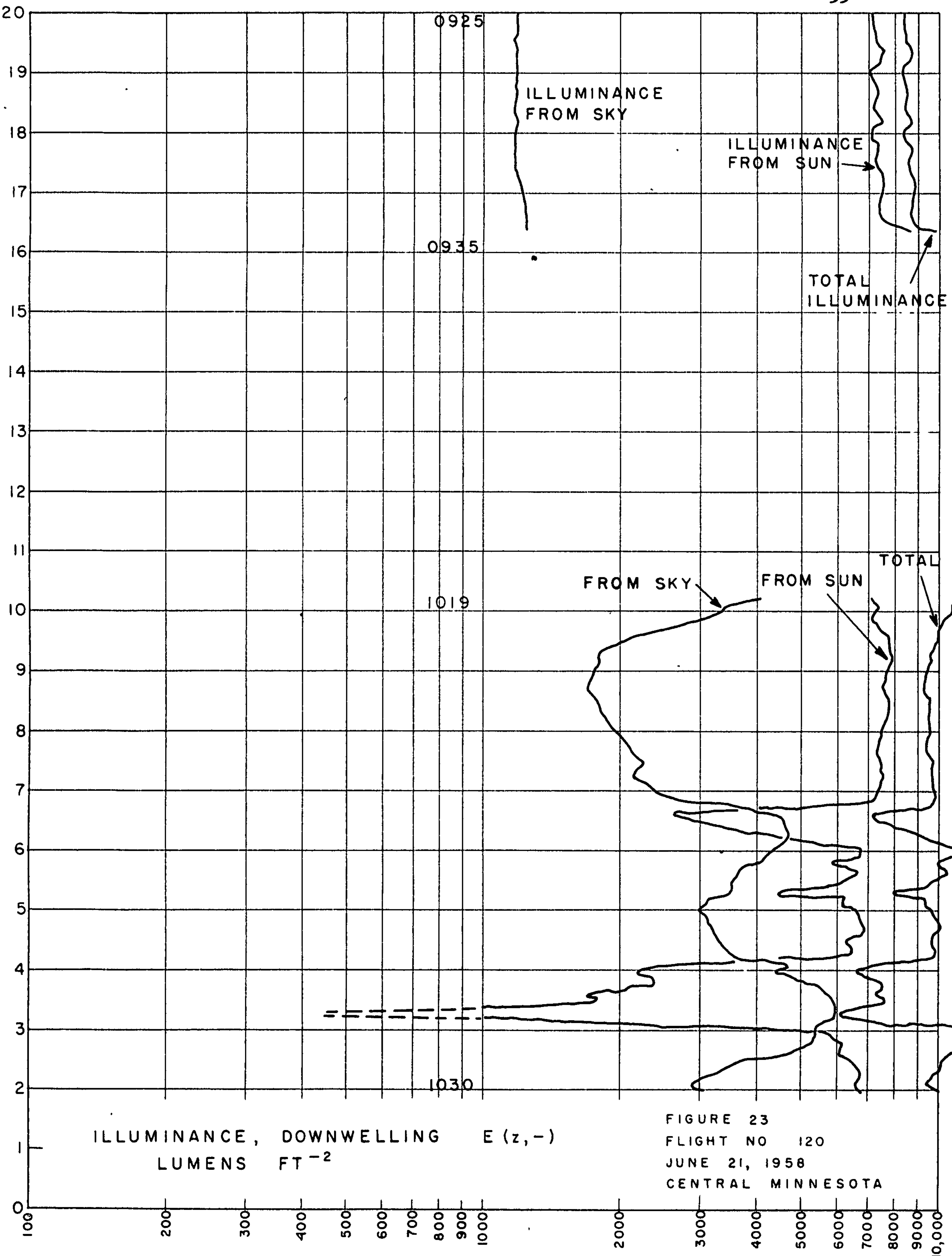

FIGURE 23
FLIGHT NO 120
JUNE 21, 1958
CENTRAL MINNESOTA

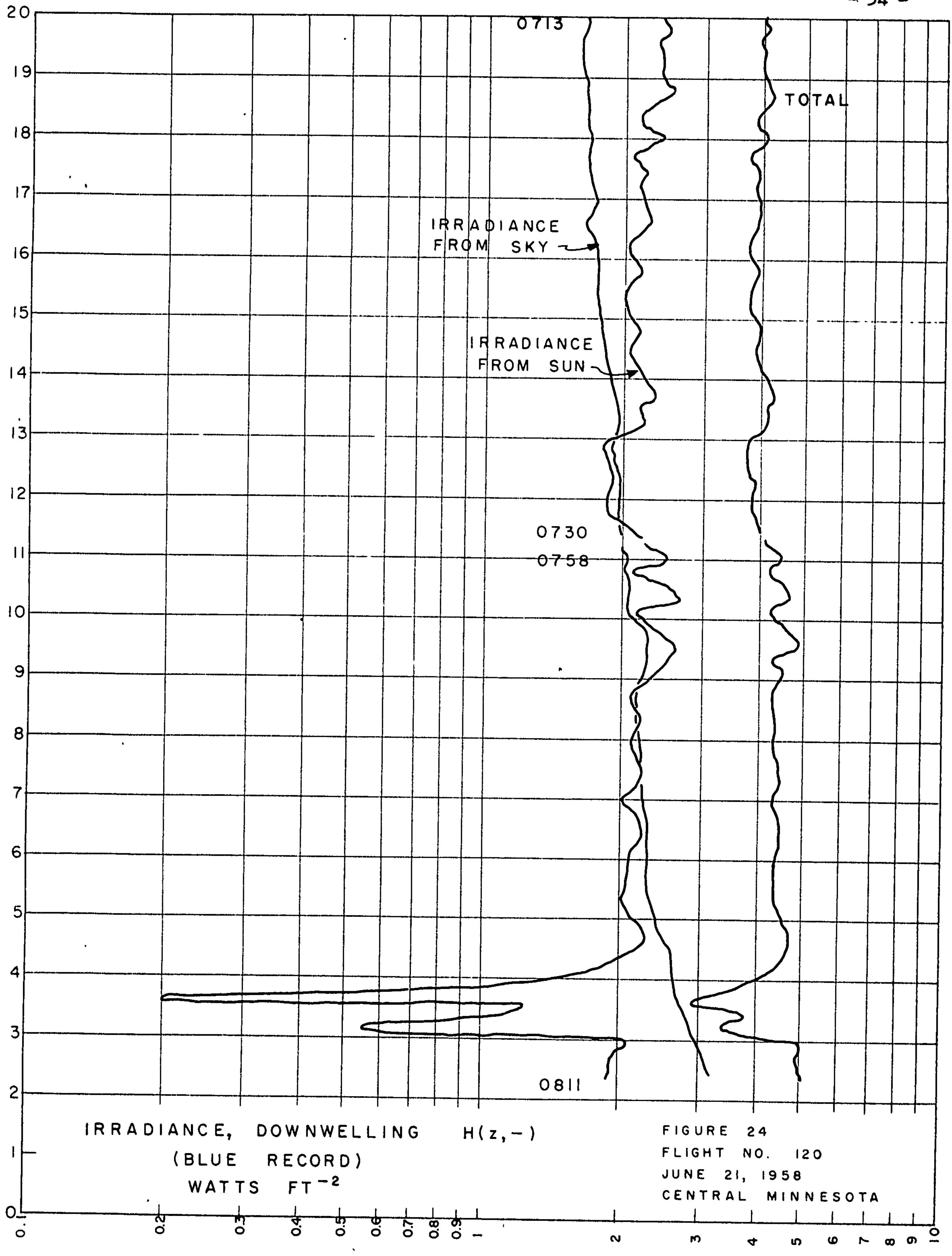

IRRADIANCE, DOWNWELLING H(z,-)
(BLUE RECORD)
WATTS FT^{-2}

FIGURE 24
FLIGHT NO. 120
JUNE 21, 1958
CENTRAL MINNESOTA

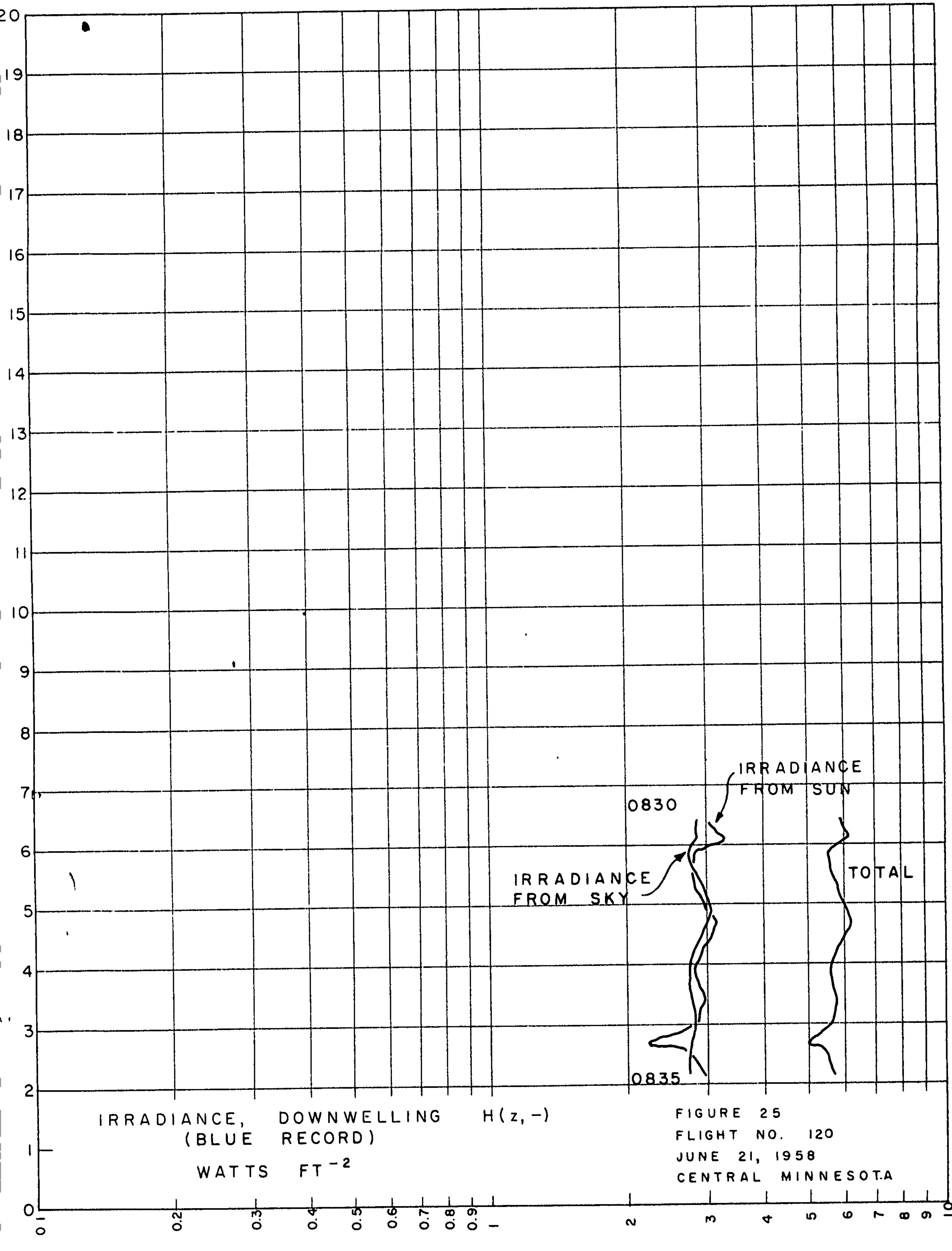

FIGURE 25
FLIGHT NO. 120
JUNE 21, 1958
CENTRAL MINNESOTA

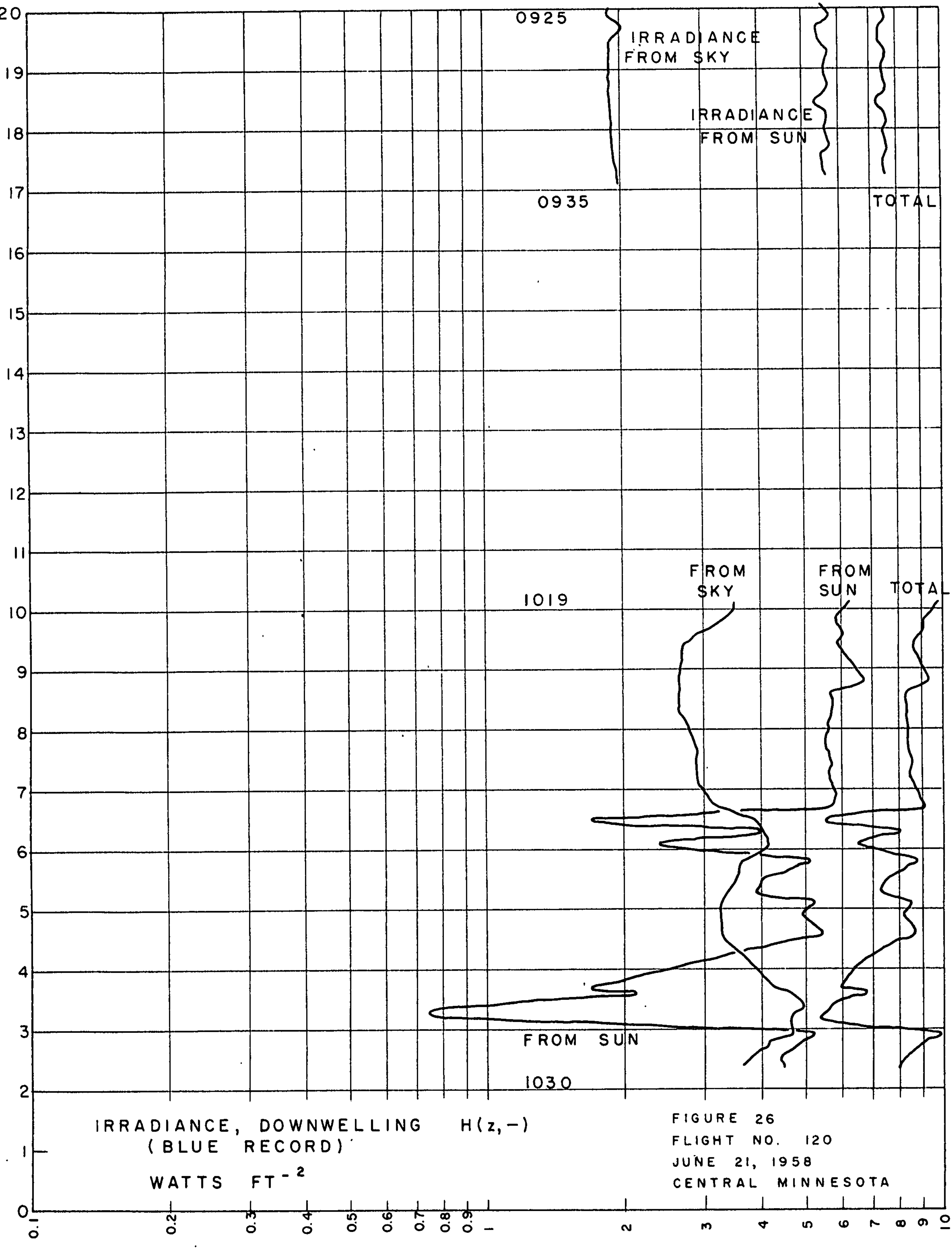

FIGURE 26
FLIGHT NO. 120
JUNE 21, 1958
CENTRAL MINNESOTA

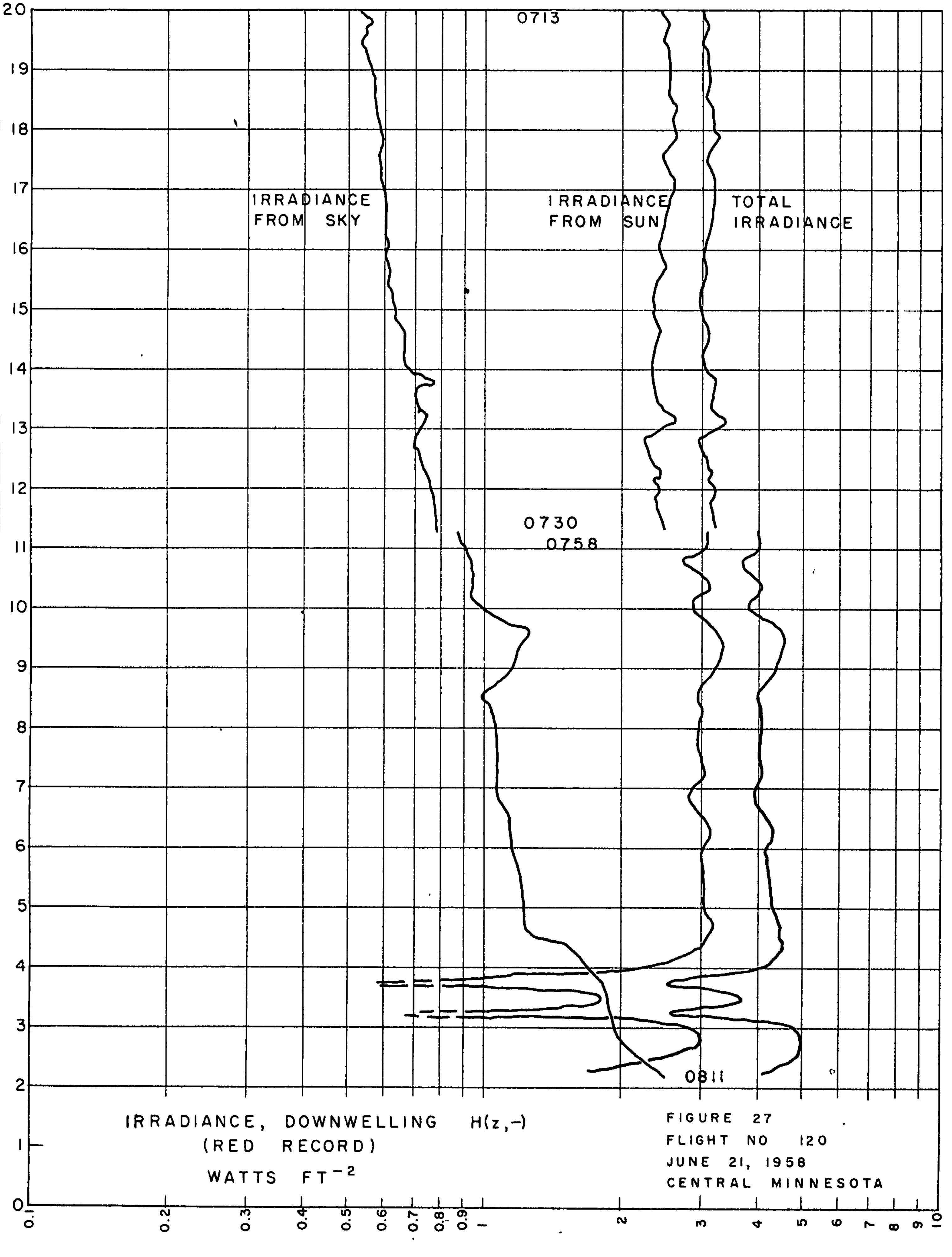

FIGURE 27
FLIGHT NO 120
JUNE 21, 1958
CENTRAL MINNESOTA

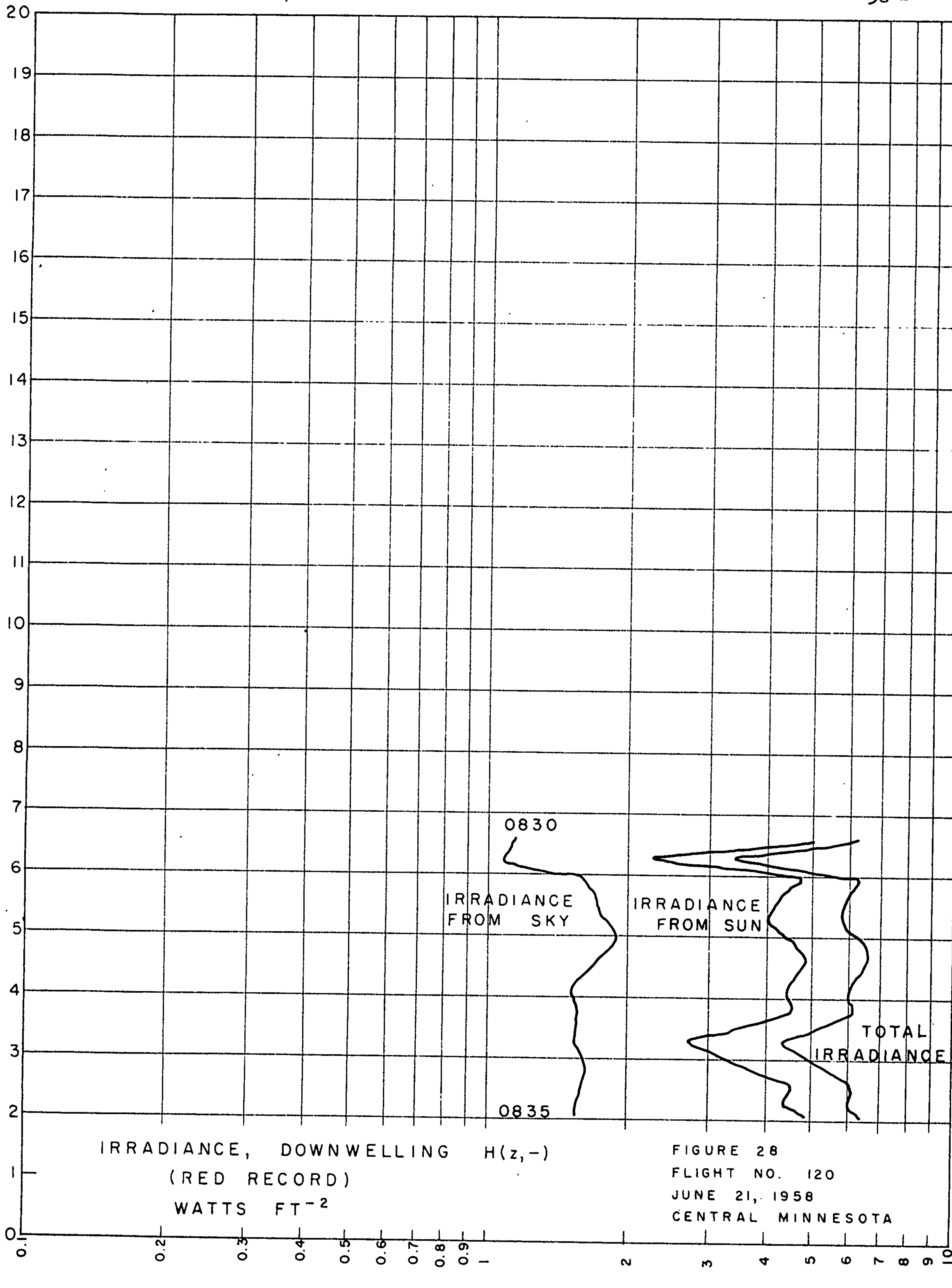

IRRADIANCE, DOWNWELLING H(z,−)
(RED RECORD)
WATTS FT^{-2}

FIGURE 28
FLIGHT NO. 120
JUNE 21, 1958
CENTRAL MINNESOTA

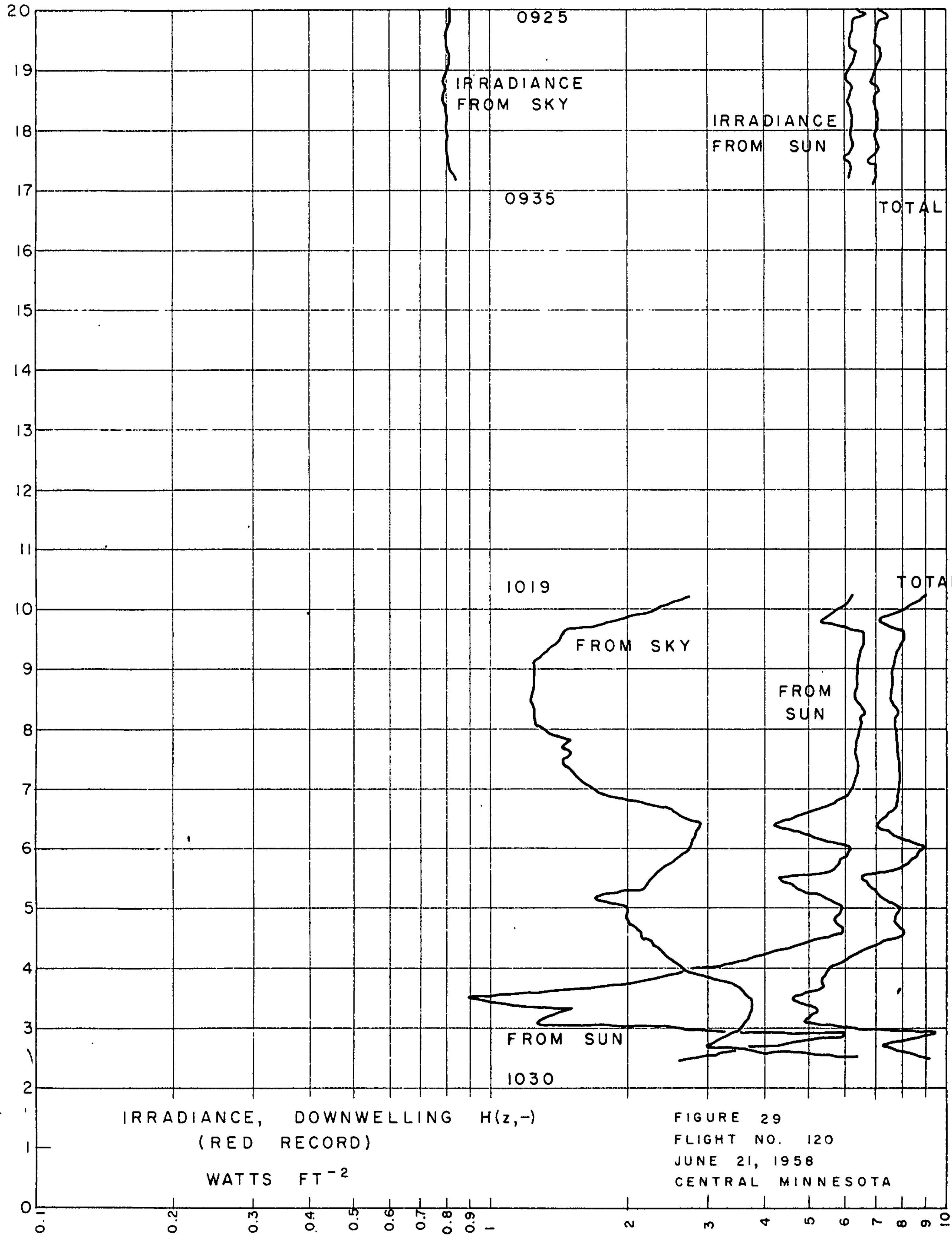

FIGURE 29
FLIGHT NO. 120
JUNE 21, 1958
CENTRAL MINNESOTA

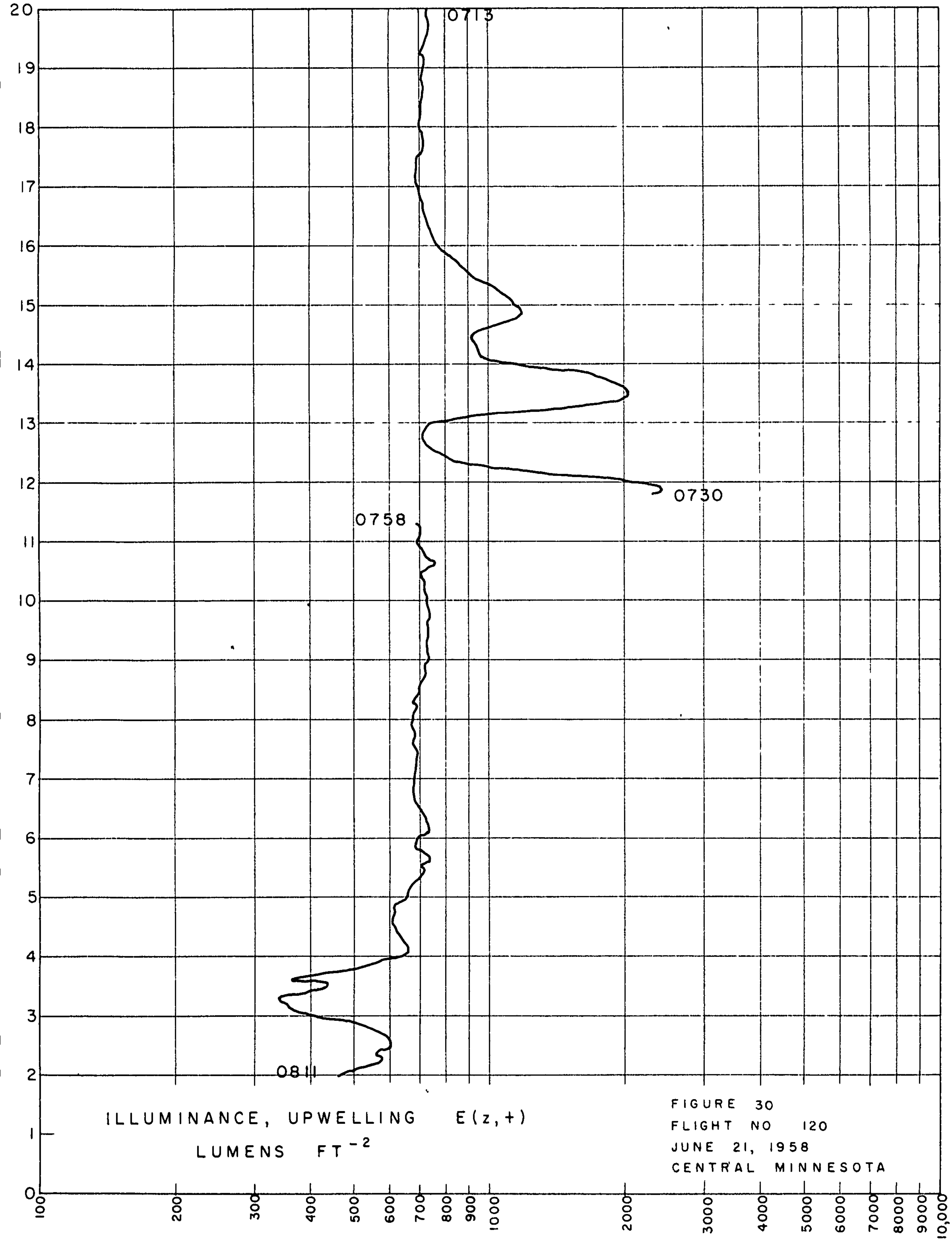

FIGURE 30
FLIGHT NO 120
JUNE 21, 1958
CENTRAL MINNESOTA

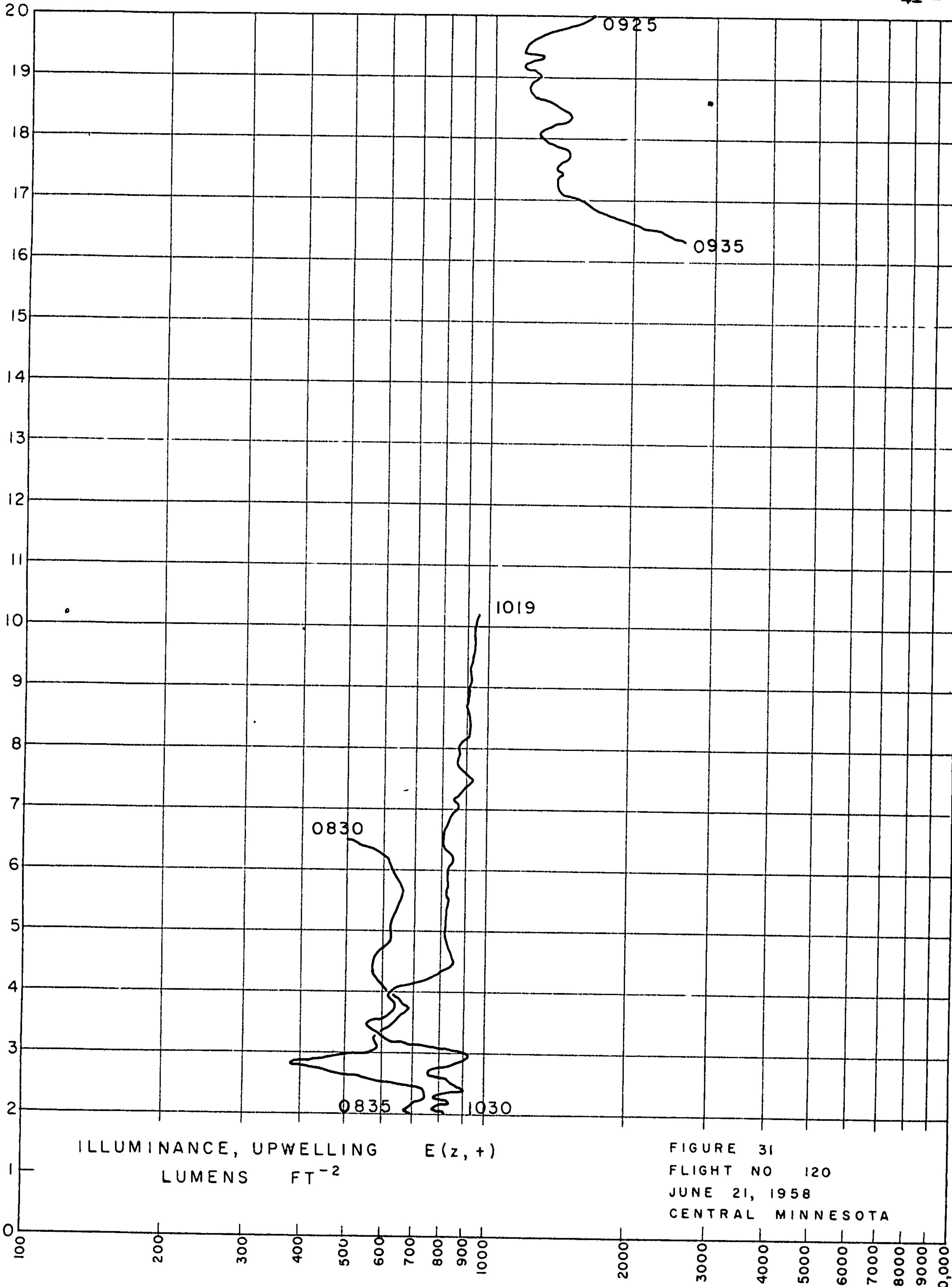

ILLUMINANCE, UPWELLING $E(z,+)$

LUMENS FT^{-2}

FIGURE 31

FLIGHT NO 120

JUNE 21, 1958

CENTRAL MINNESOTA

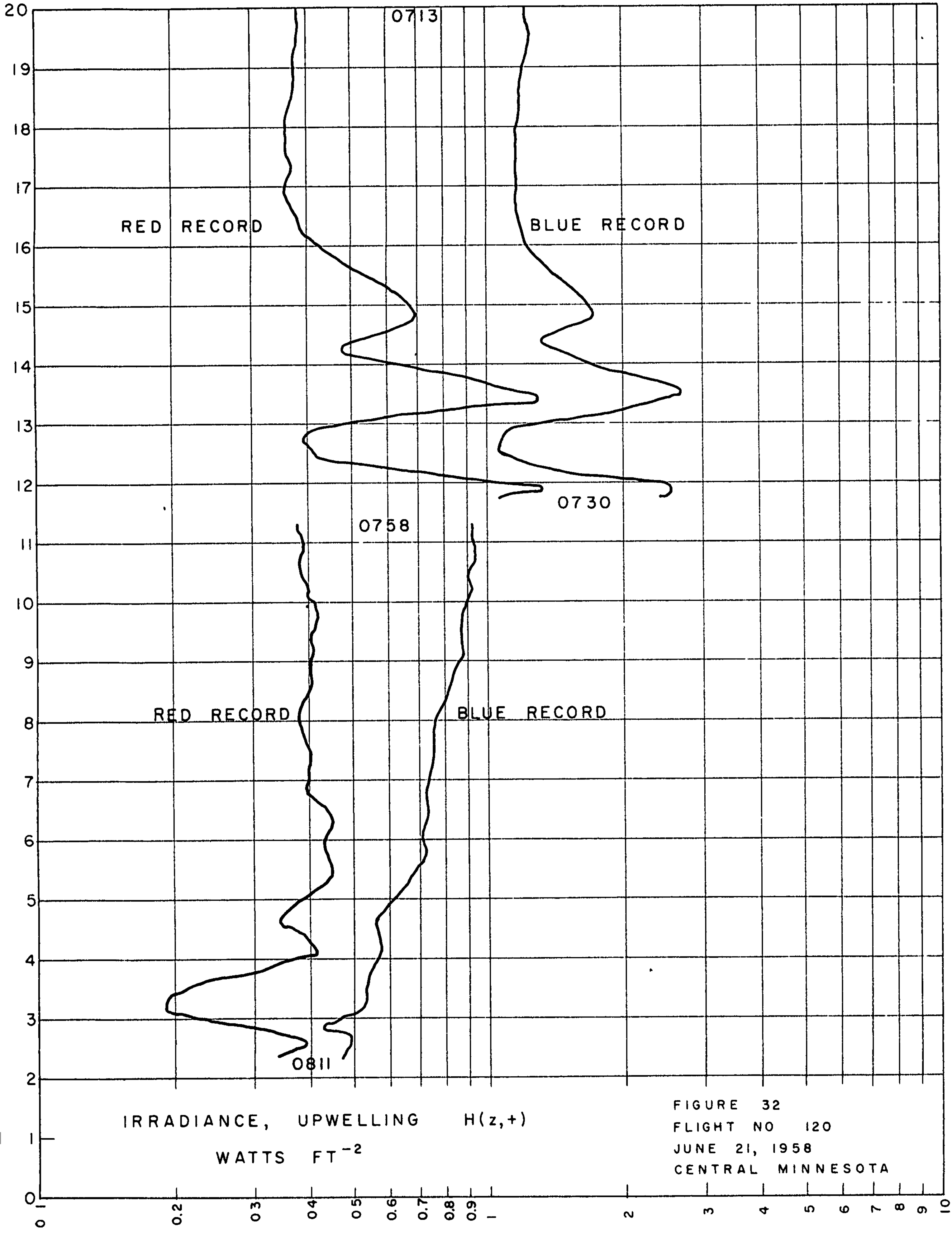

FIGURE 32
FLIGHT NO 120
JUNE 21, 1958
CENTRAL MINNESOTA

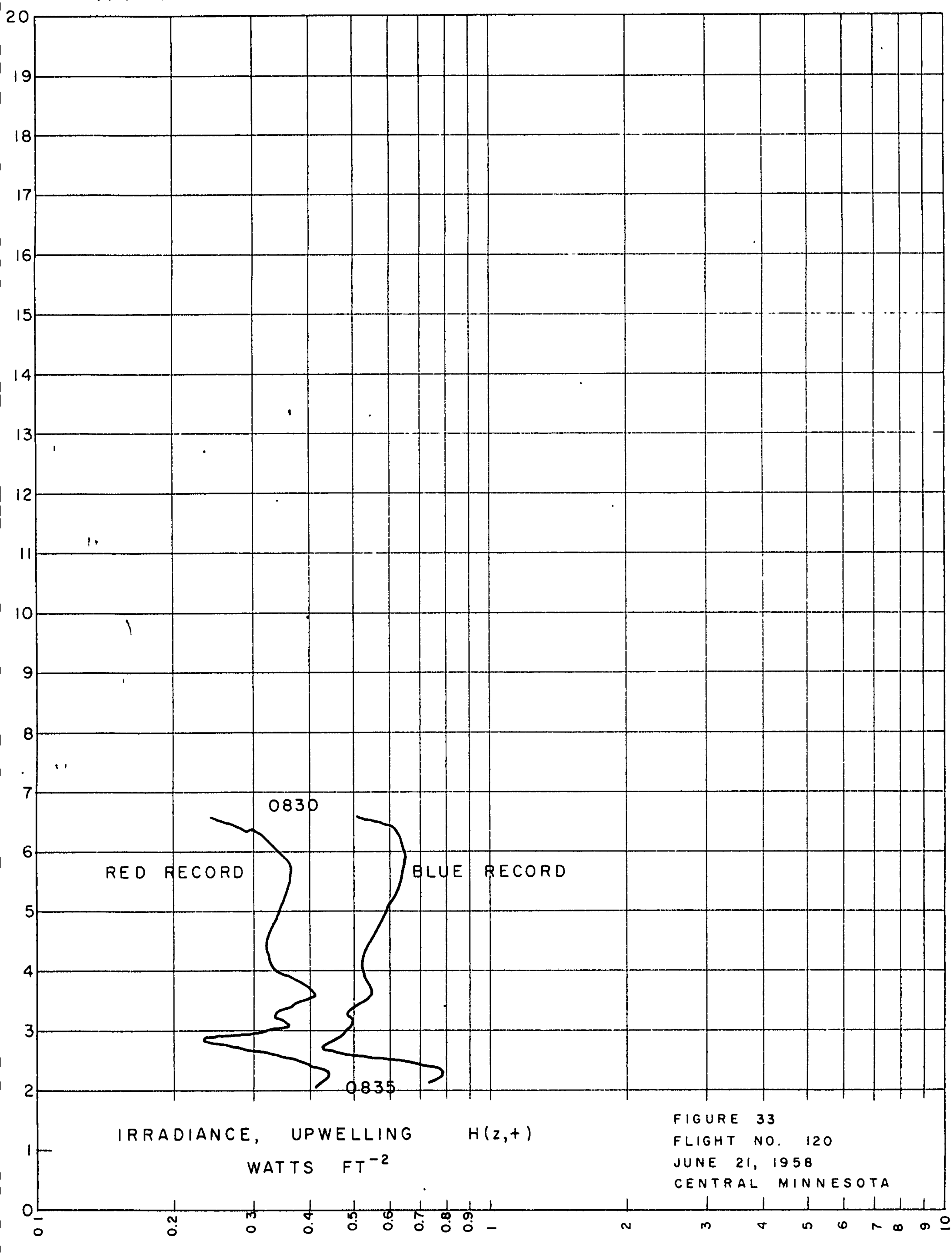

FIGURE 33
FLIGHT NO. 120
JUNE 21, 1958
CENTRAL MINNESOTA

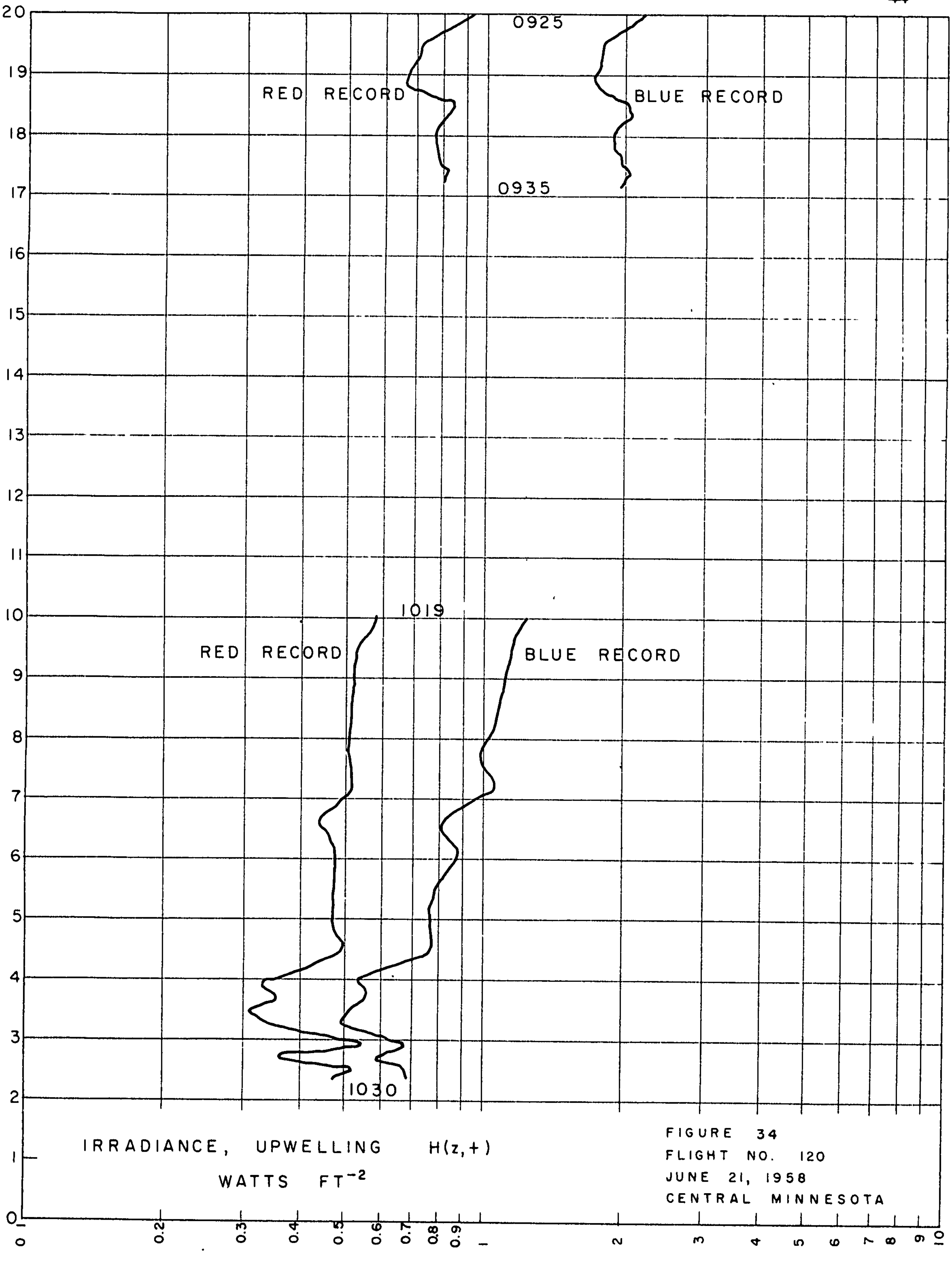

FIGURE 34
FLIGHT NO. 120
JUNE 21, 1958
CENTRAL MINNESOTA

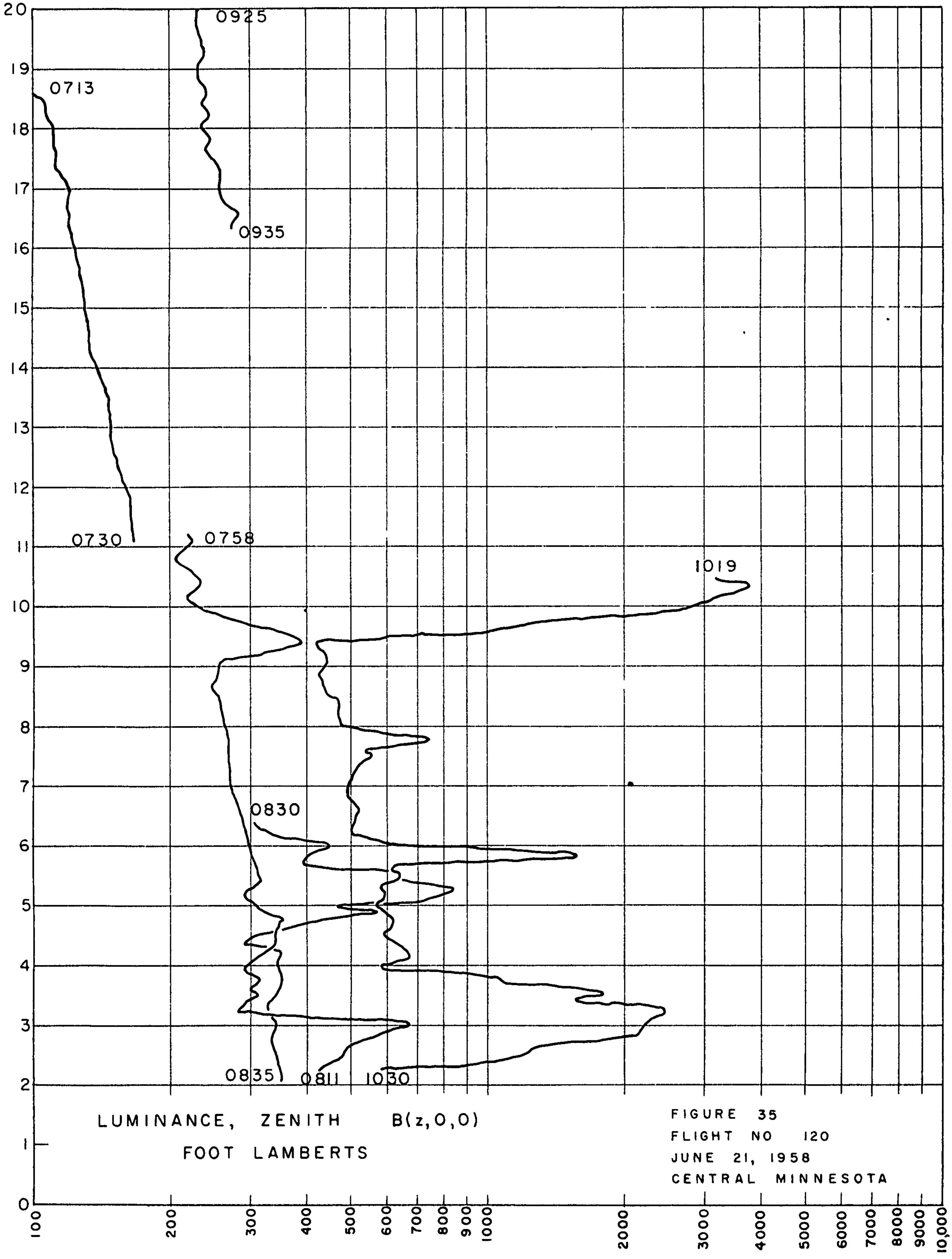

LUMINANCE, ZENITH B(z,0,0)
FOOT LAMBERTS

FIGURE 35
FLIGHT NO 120
JUNE 21, 1958
CENTRAL MINNESOTA

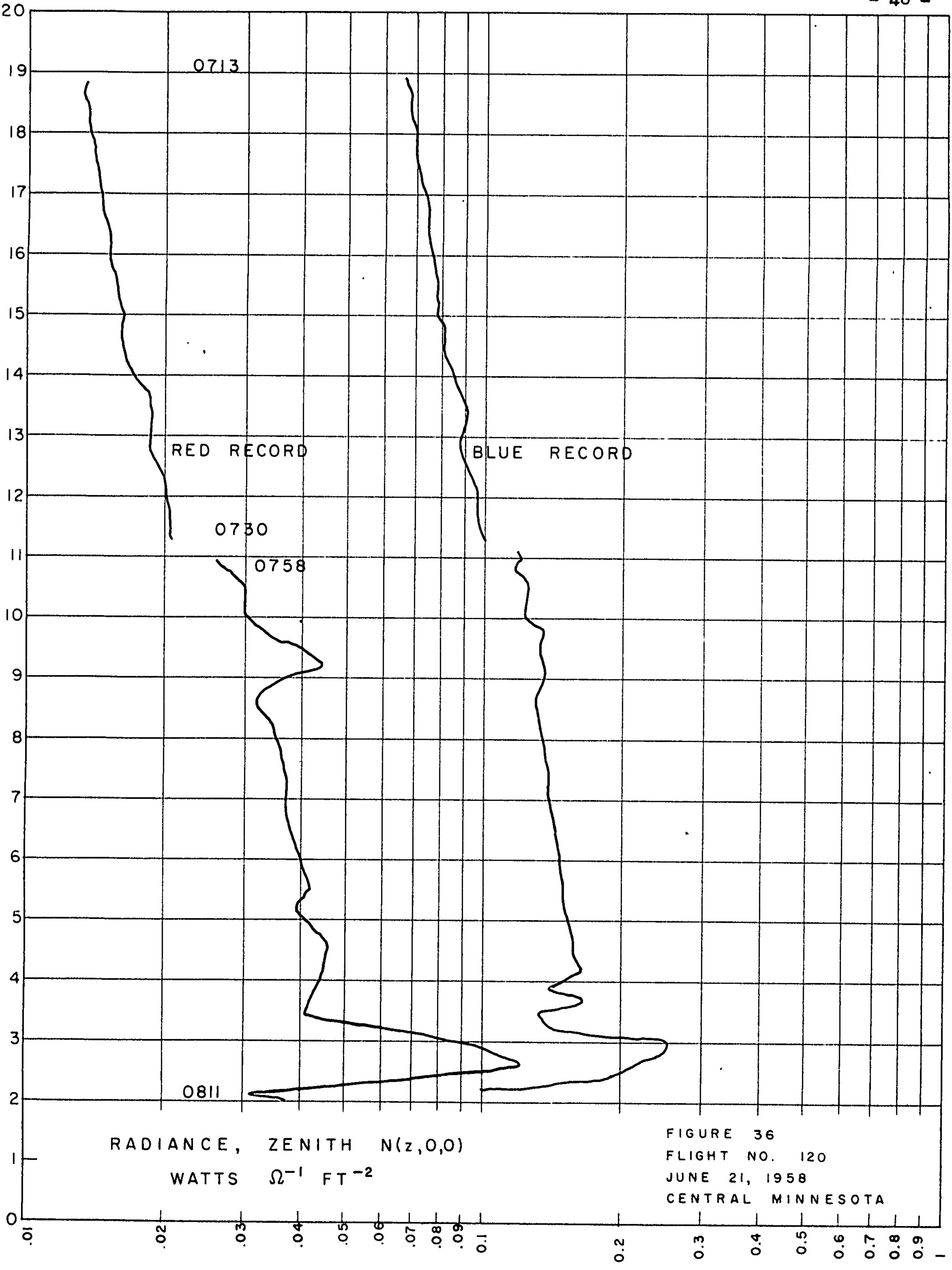

FIGURE 36
FLIGHT NO. 120
JUNE 21, 1958
CENTRAL MINNESOTA

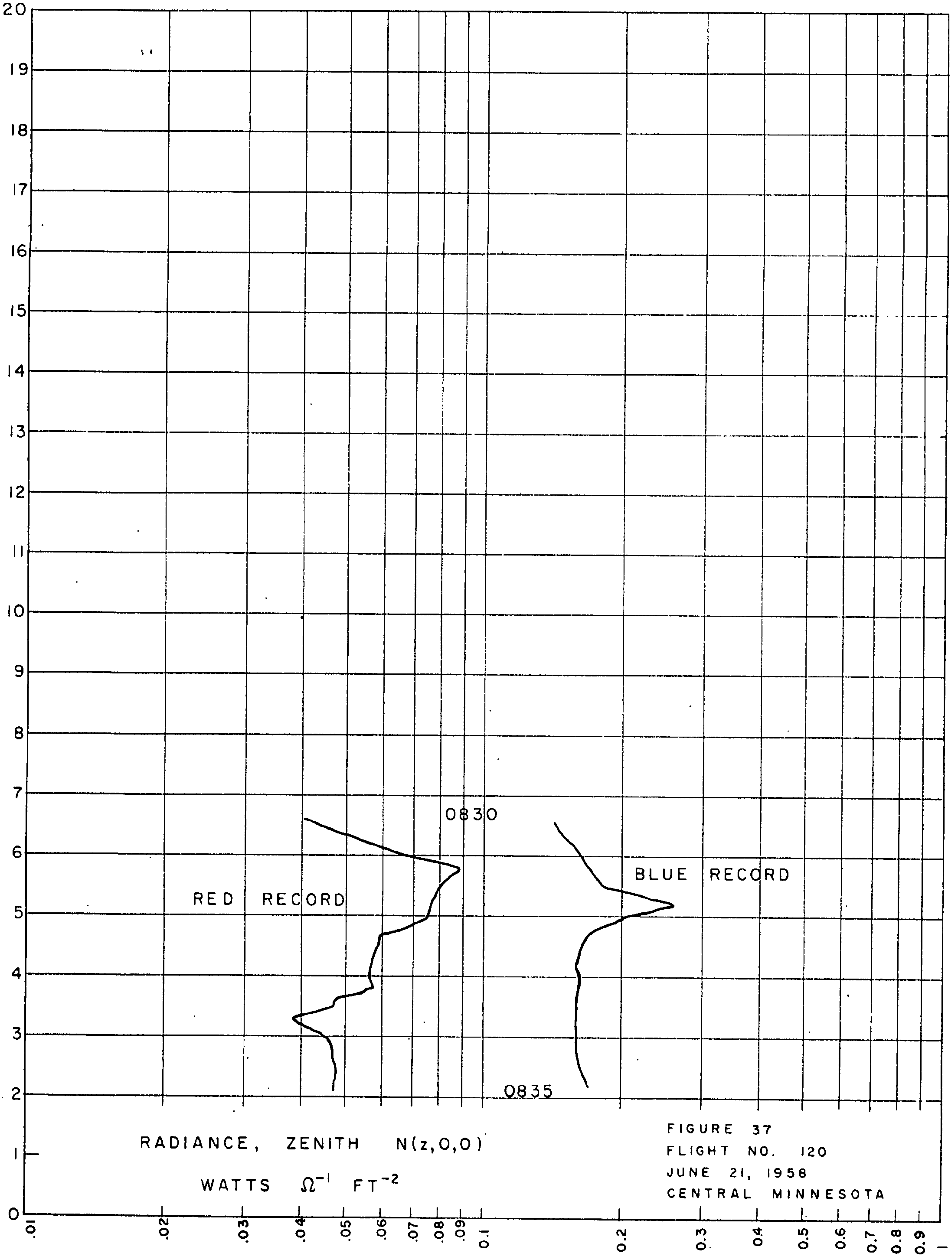

FIGURE 37
FLIGHT NO. 120
JUNE 21, 1958
CENTRAL MINNESOTA

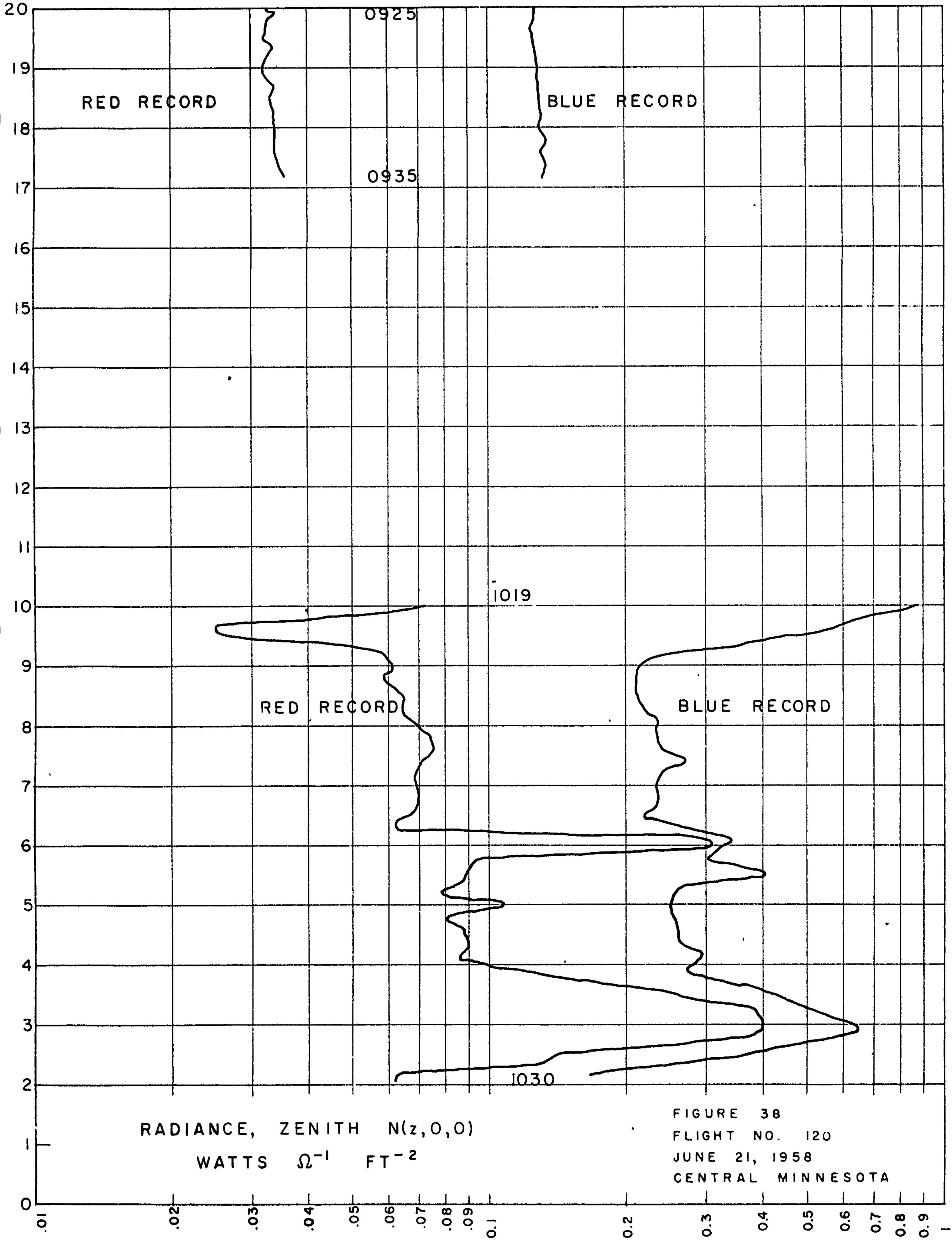

FIGURE 38
FLIGHT NO. 120
JUNE 21, 1958
CENTRAL MINNESOTA

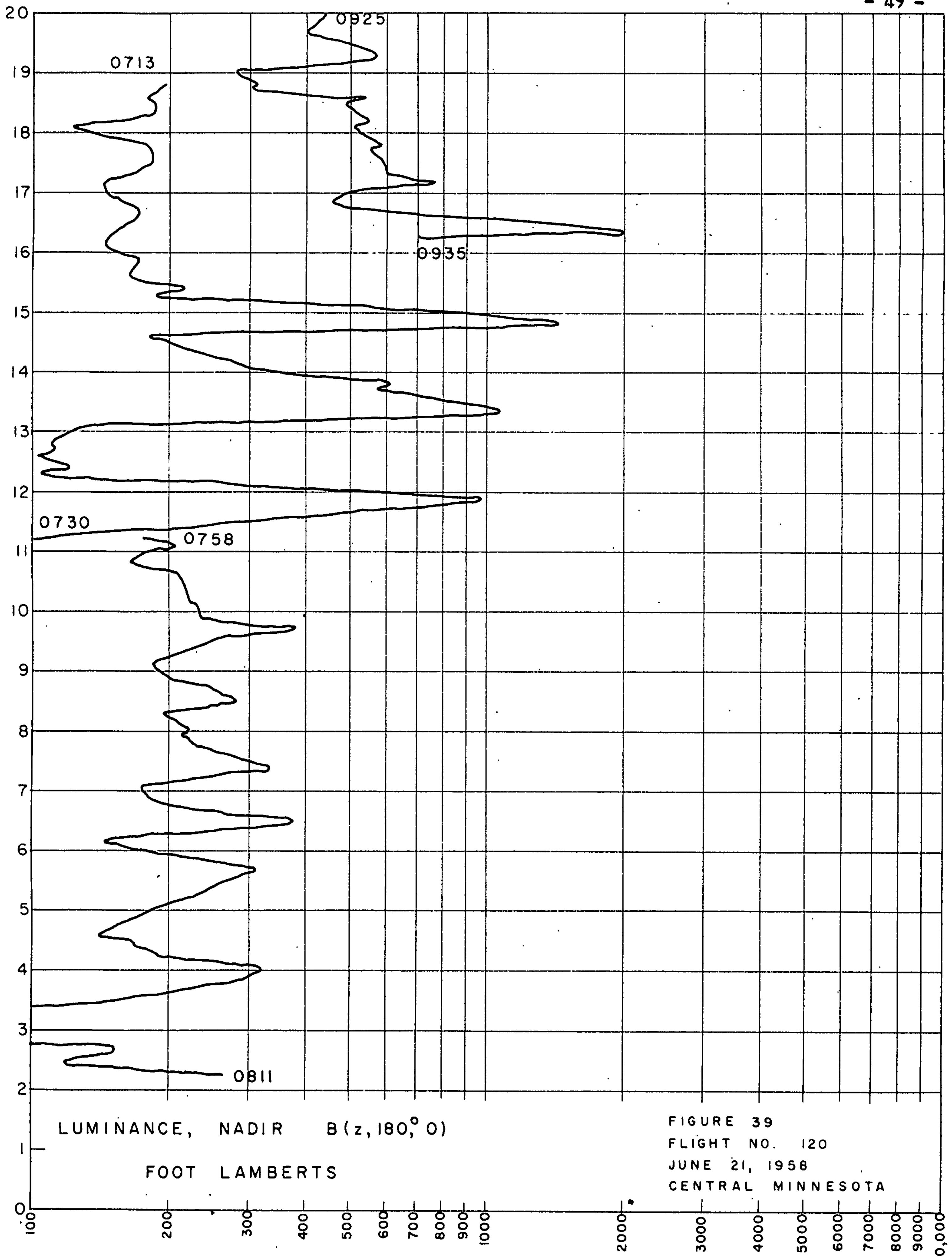

FIGURE 39
FLIGHT NO. 120
JUNE 21, 1958
CENTRAL MINNESOTA

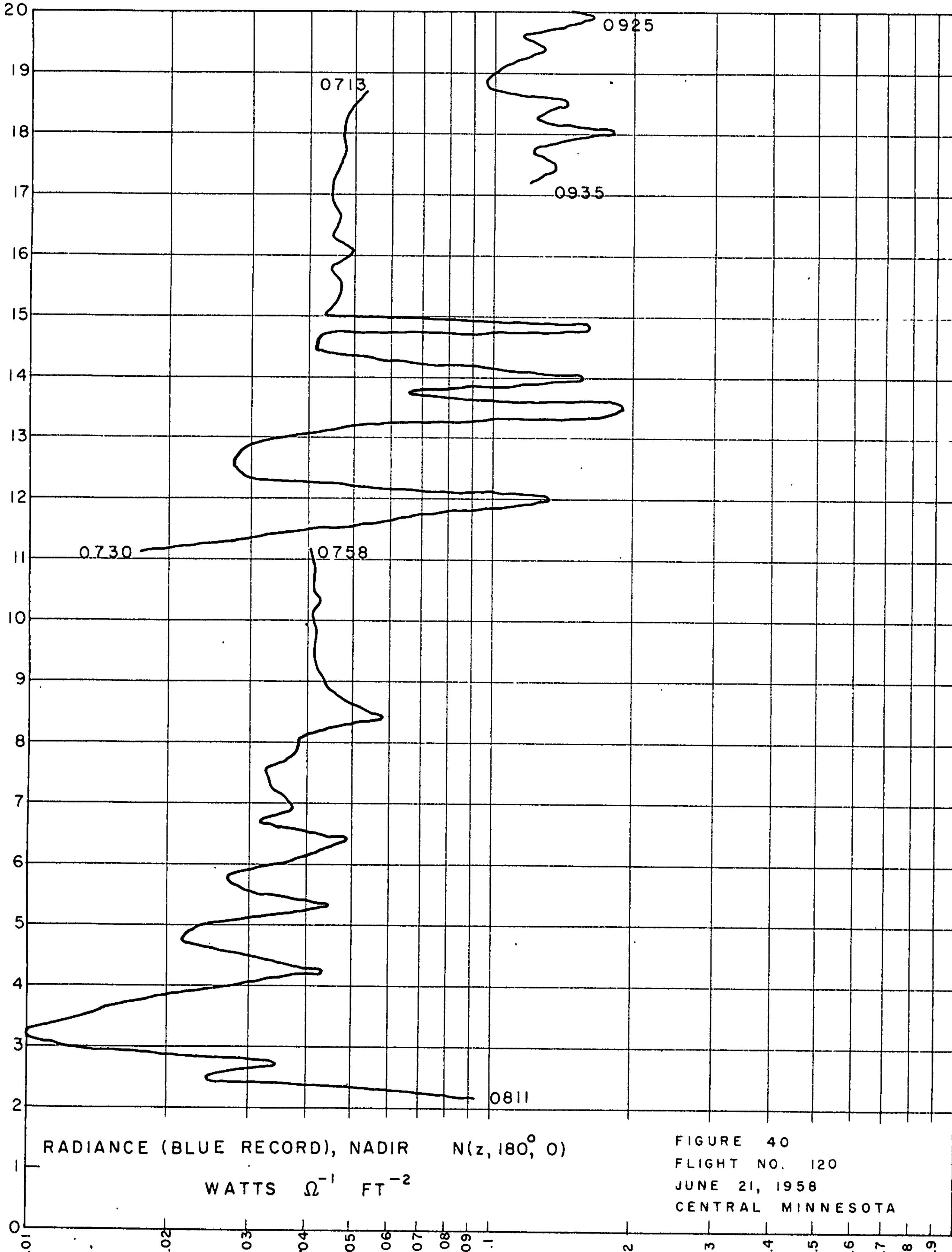

RADIANCE (BLUE RECORD), NADIR $N(z, 180^\circ, 0)$

WATTS Ω^{-1} FT^{-2}

FIGURE 40
FLIGHT NO. 120
JUNE 21, 1958
CENTRAL MINNESOTA

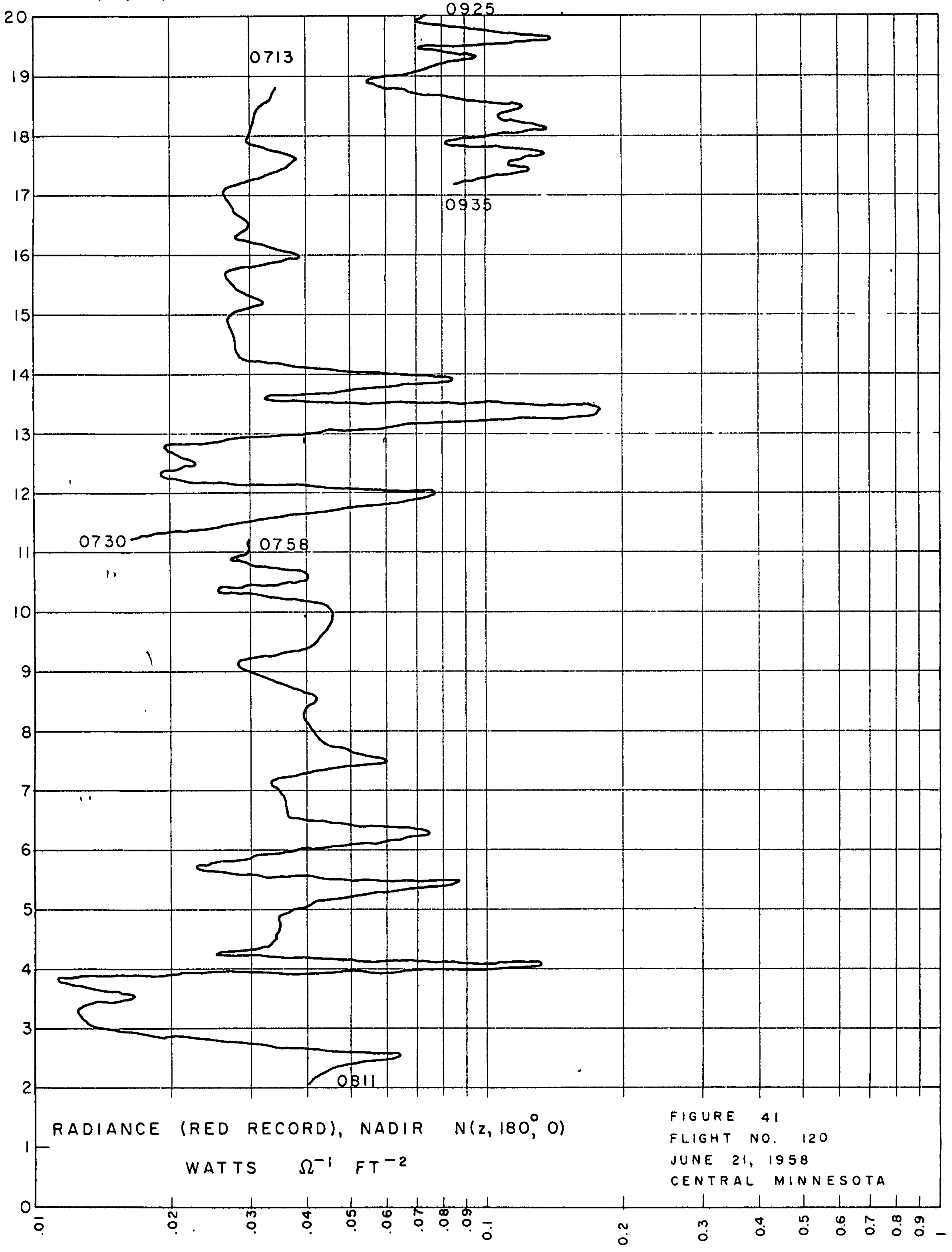

RADIANCE (RED RECORD), NADIR $N(z, 180^\circ, 0)$

WATTS Ω^{-1} FT^{-2}

FIGURE 41
FLIGHT NO. 120
JUNE 21, 1958
CENTRAL MINNESOTA

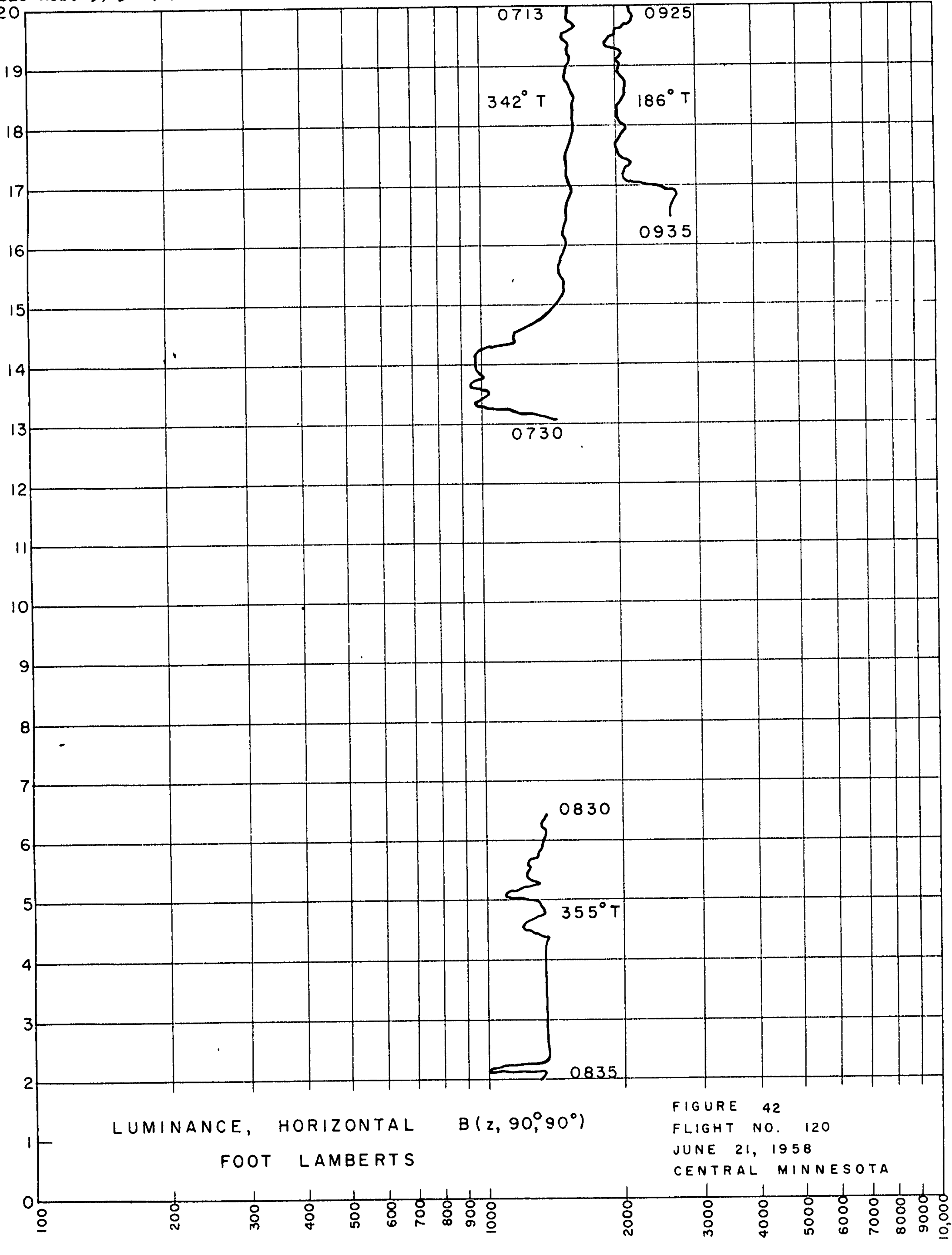

FIGURE 42
FLIGHT NO. 120
JUNE 21, 1958
CENTRAL MINNESOTA

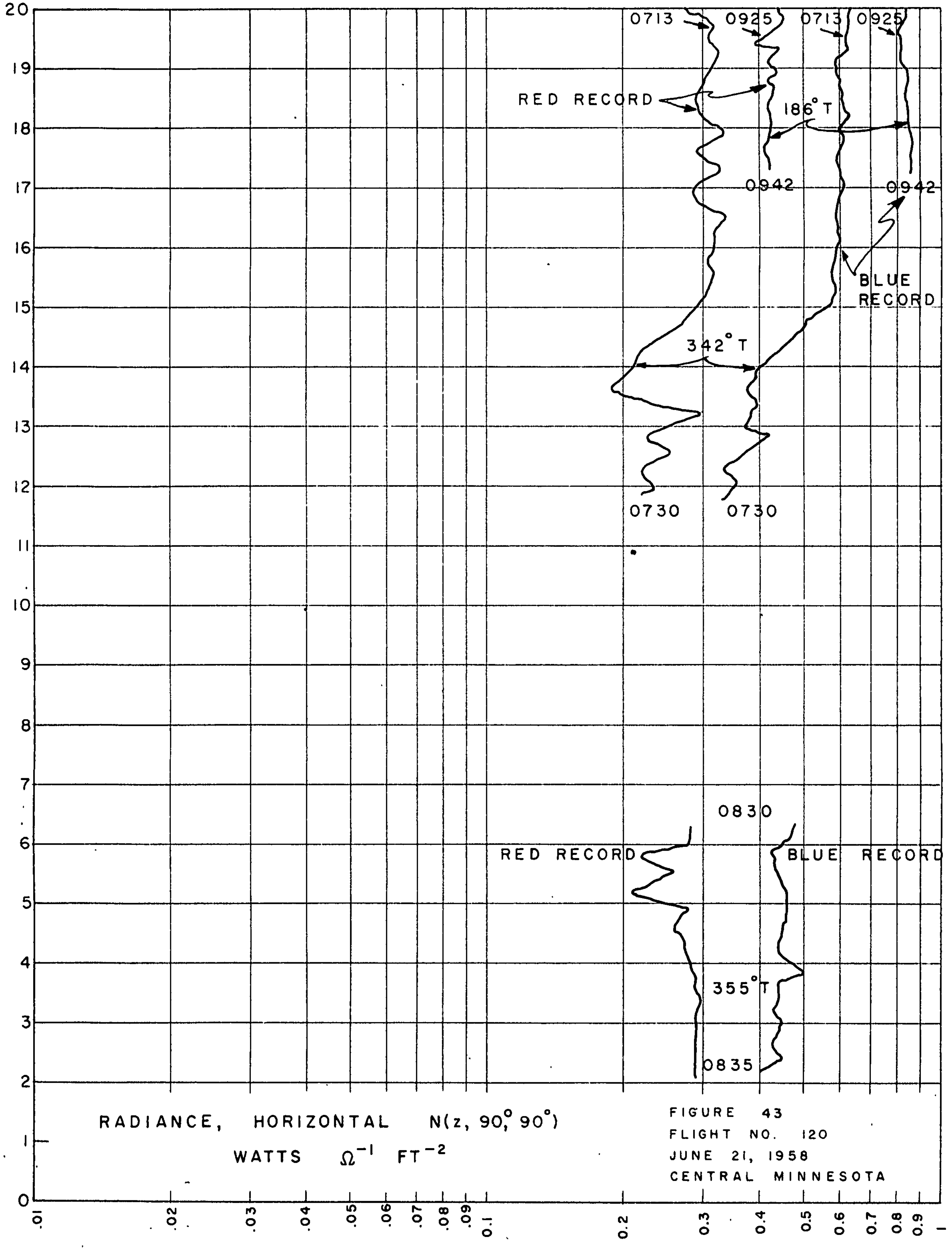
0713
0925
0713
0925
RED RECORD
186° T
0942
0942
BLUE RECORD
342° T
0730
0730
0830
RED RECORD
BLUE RECORD
355° T
0835
20
19
18
17
16
15
14
13
12
11
10
9
8
7
6
5
4
3
2
1
0
.01
.02
.03
.04
.05
.06
.07
.08
.09
0.1
0.2
0.3
0.4
0.5
0.6
0.7
0.8
0.9
RADIANCE, HORIZONTAL N(z, 90°, 90°)
WATTS Ω^{-1} FT^{-2}
FIGURE 43
FLIGHT NO. 120
JUNE 21, 1958
CENTRAL MINNESOTA

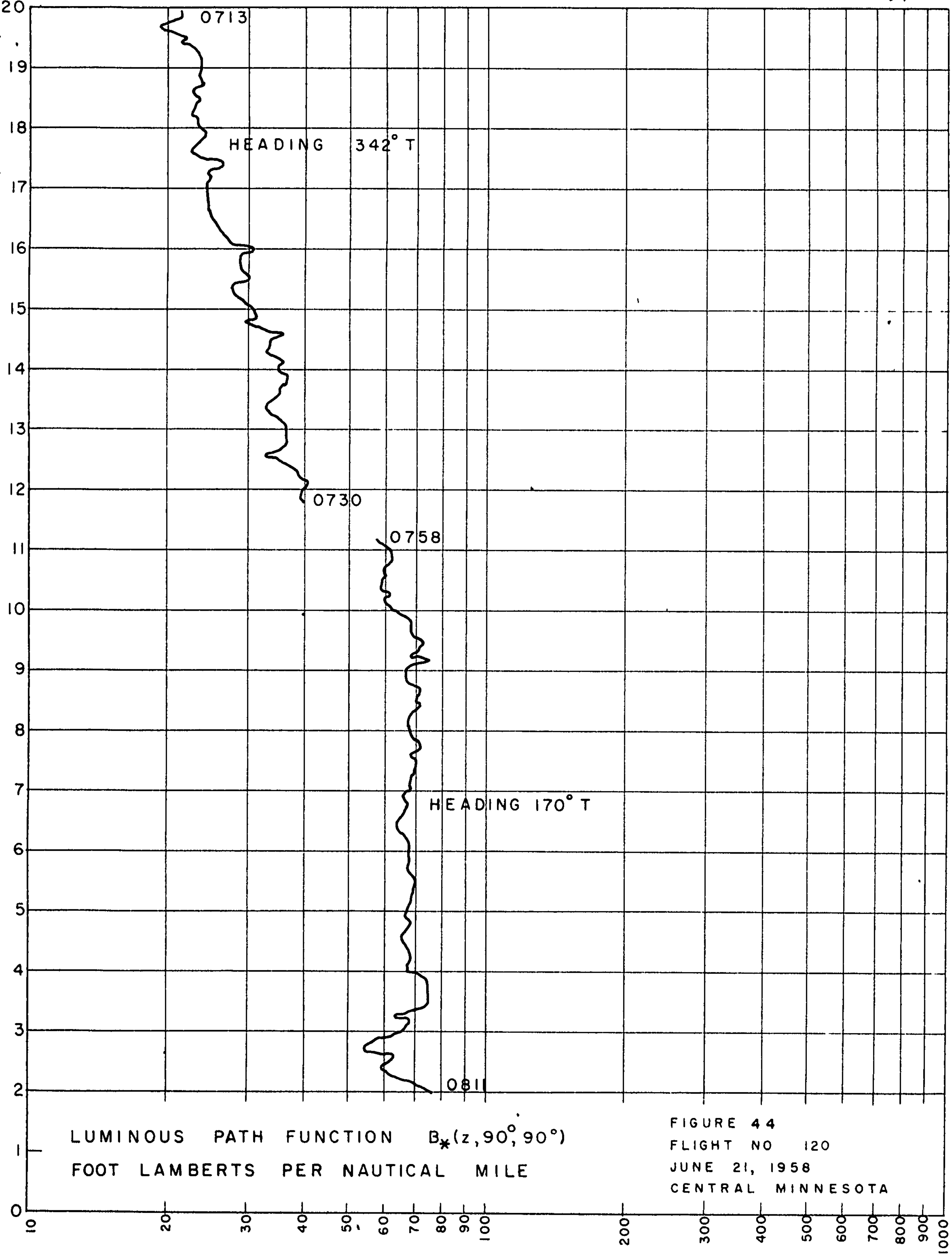

LUMINOUS PATH FUNCTION $B_*(z, 90°, 90°)$
FOOT LAMBERTS PER NAUTICAL MILE

FIGURE 44
FLIGHT NO 120
JUNE 21, 1958
CENTRAL MINNESOTA

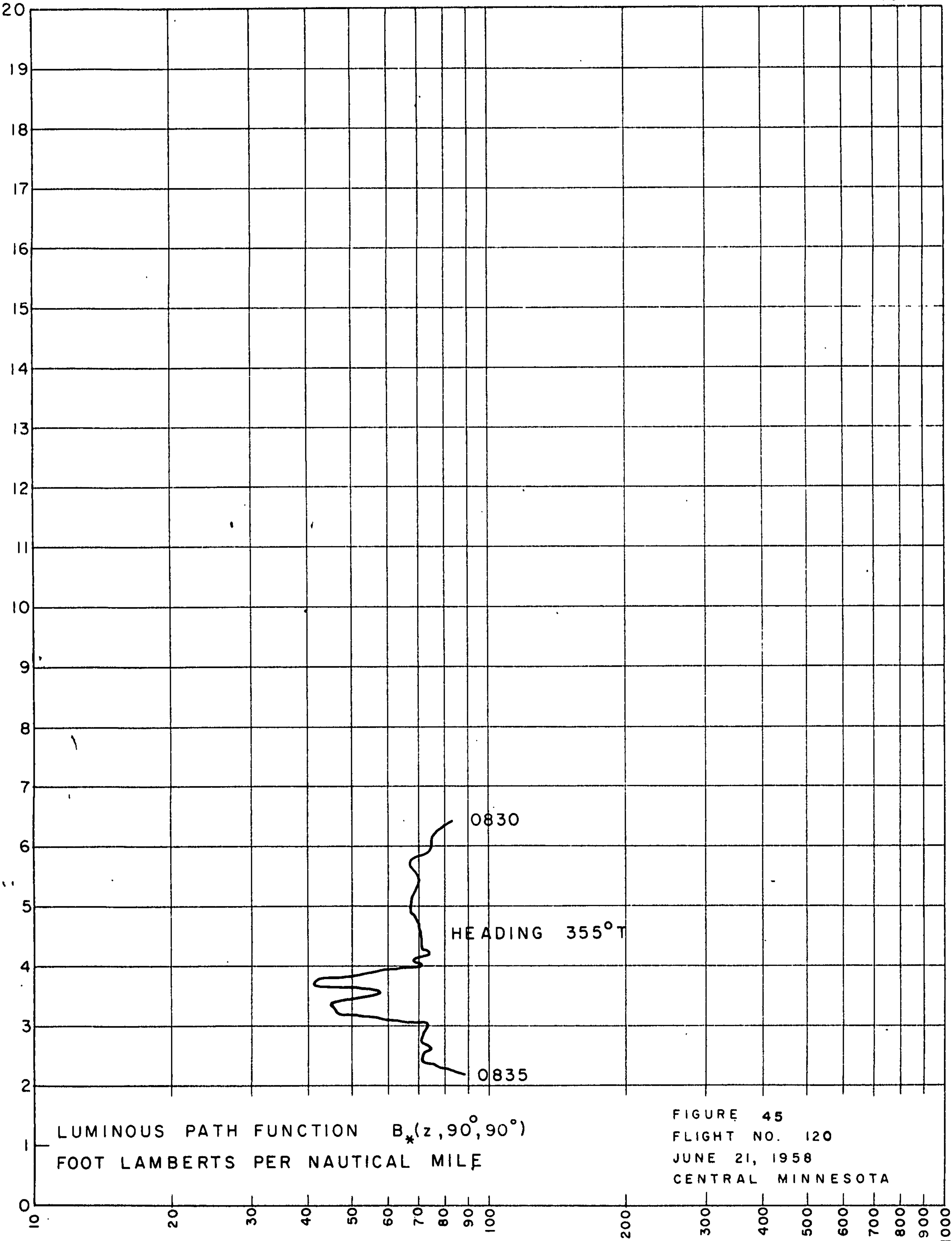

FIGURE 45
FLIGHT NO. 120
JUNE 21, 1958
CENTRAL MINNESOTA

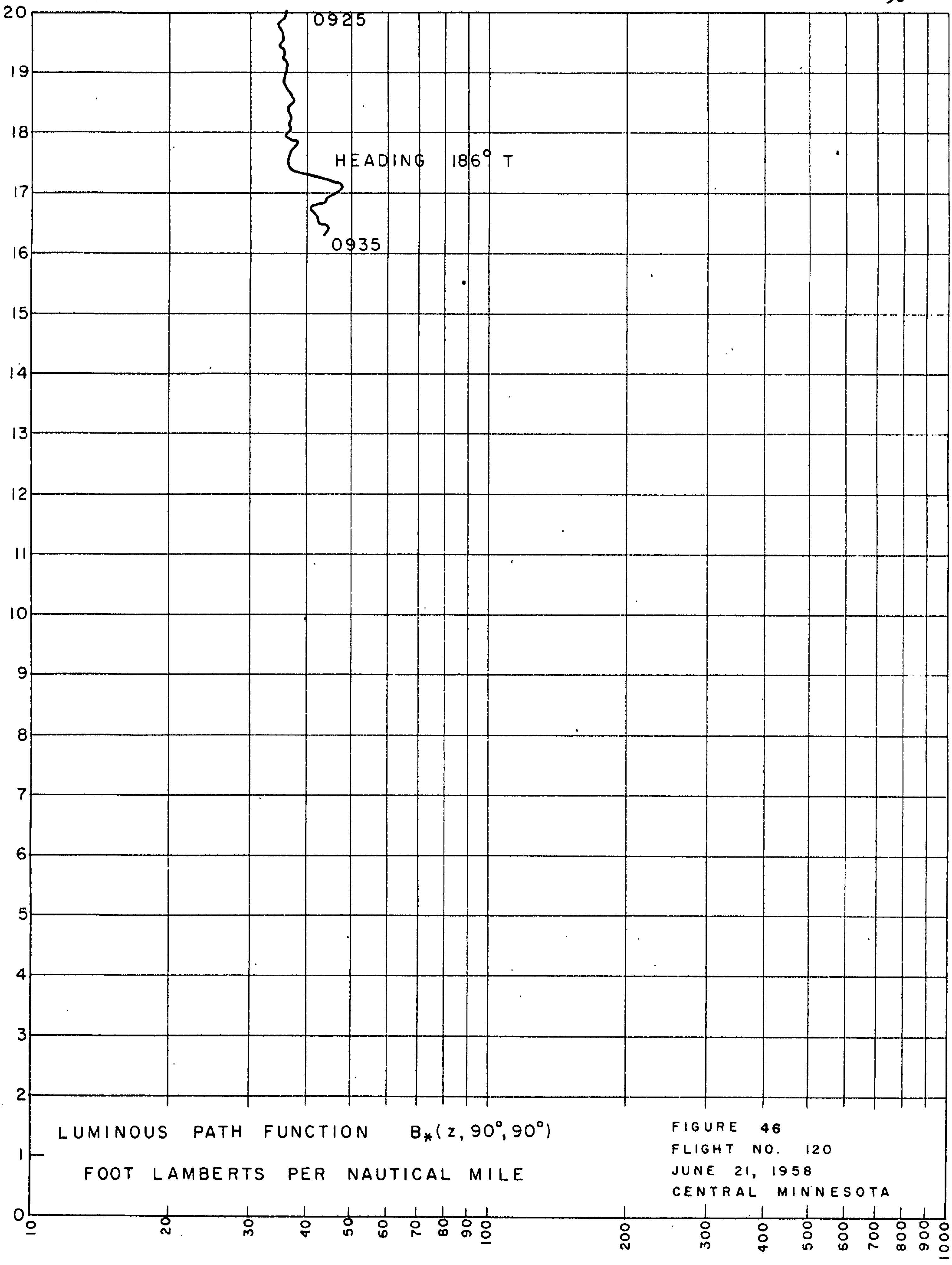

LUMINOUS PATH FUNCTION $B_*(z, 90°, 90°)$

FOOT LAMBERTS PER NAUTICAL MILE

FIGURE 46
FLIGHT NO. 120
JUNE 21, 1958
CENTRAL MINNESOTA

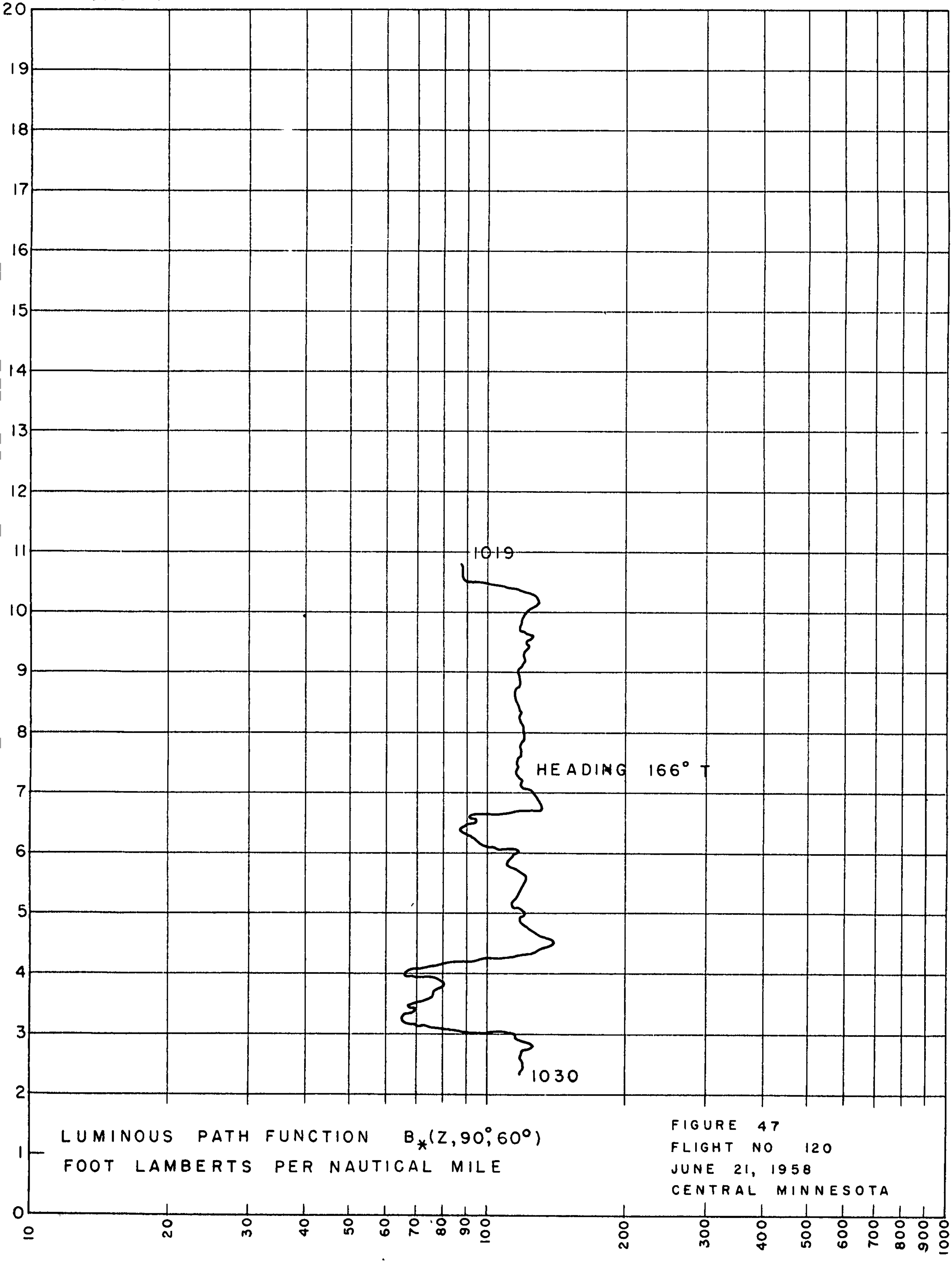

FIGURE 47
FLIGHT NO 120
JUNE 21, 1958
CENTRAL MINNESOTA

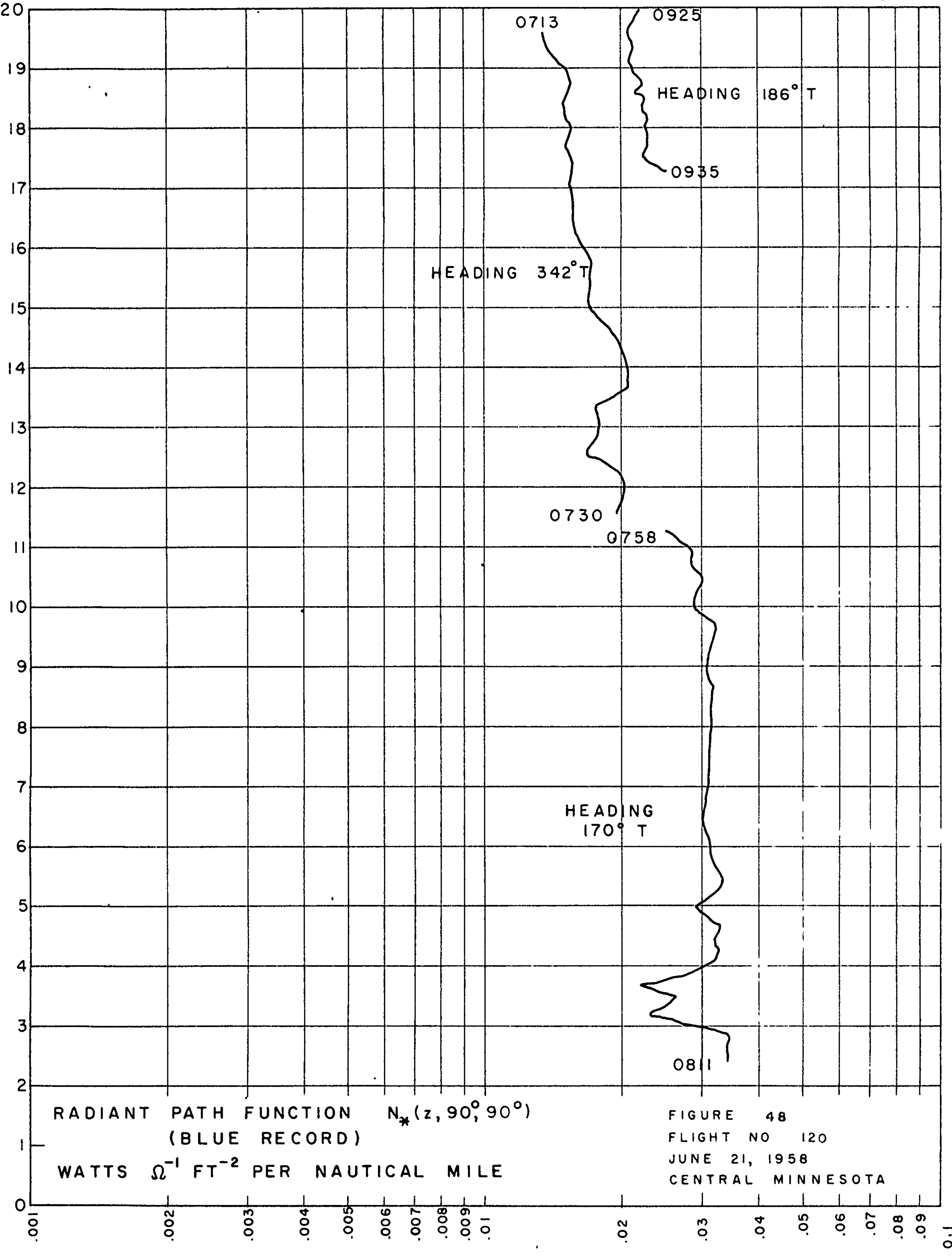
0713
0925
HEADING 186° T
0935
HEADING 342° T
0730
0758
HEADING
170° T
0811
RADIANT PATH FUNCTION $N_*(z, 90°, 90°)$
(BLUE RECORD)
WATTS Ω^{-1} FT^{-2} PER NAUTICAL MILE
FIGURE 48
FLIGHT NO 120
JUNE 21, 1958
CENTRAL MINNESOTA
20
19
18
17
16
15
14
13
12
11
10
9
8
7
6
5
4
3
2
1
0
.001
.002
.003
.004
.005
.006
.007
.008
.009
.01
.02
.03
.04
.05
.06
.07
.08
.09
0.1

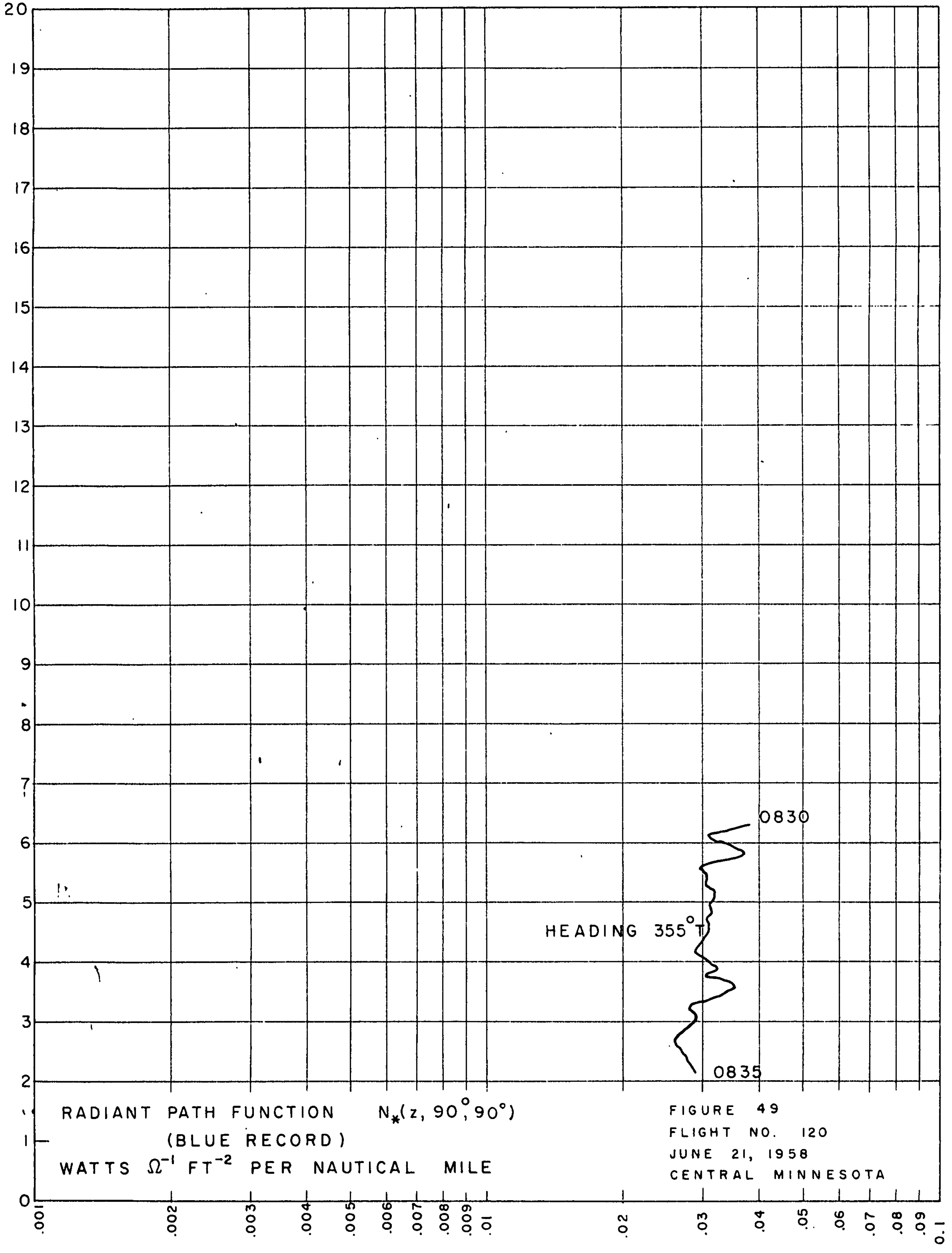

FIGURE 49
FLIGHT NO. 120
JUNE 21, 1958
CENTRAL MINNESOTA

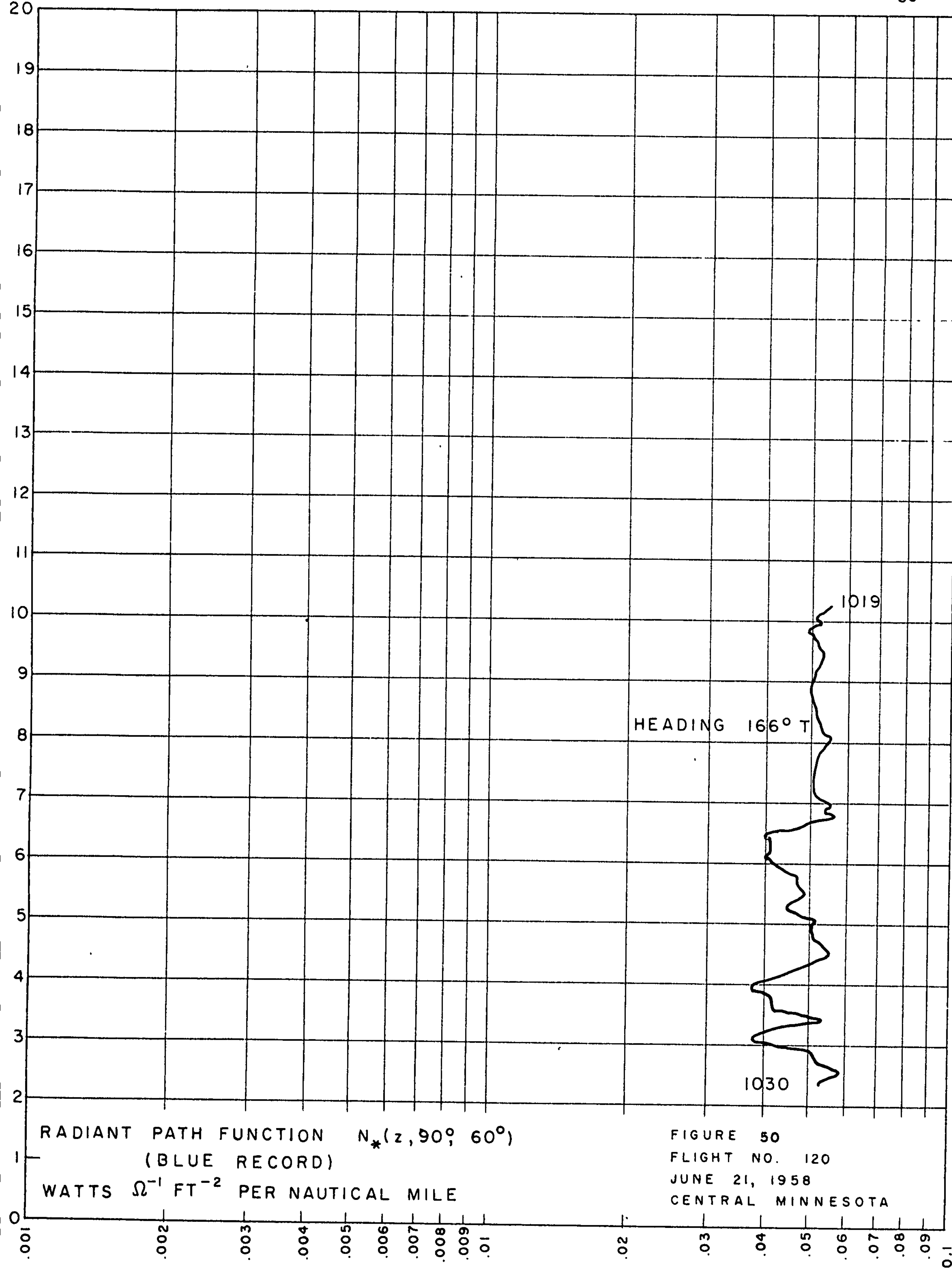

RADIANT PATH FUNCTION $N_*(z, 90°, 60°)$
(BLUE RECORD)
WATTS Ω^{-1} FT^{-2} PER NAUTICAL MILE

FIGURE 50
FLIGHT NO. 120
JUNE 21, 1958
CENTRAL MINNESOTA

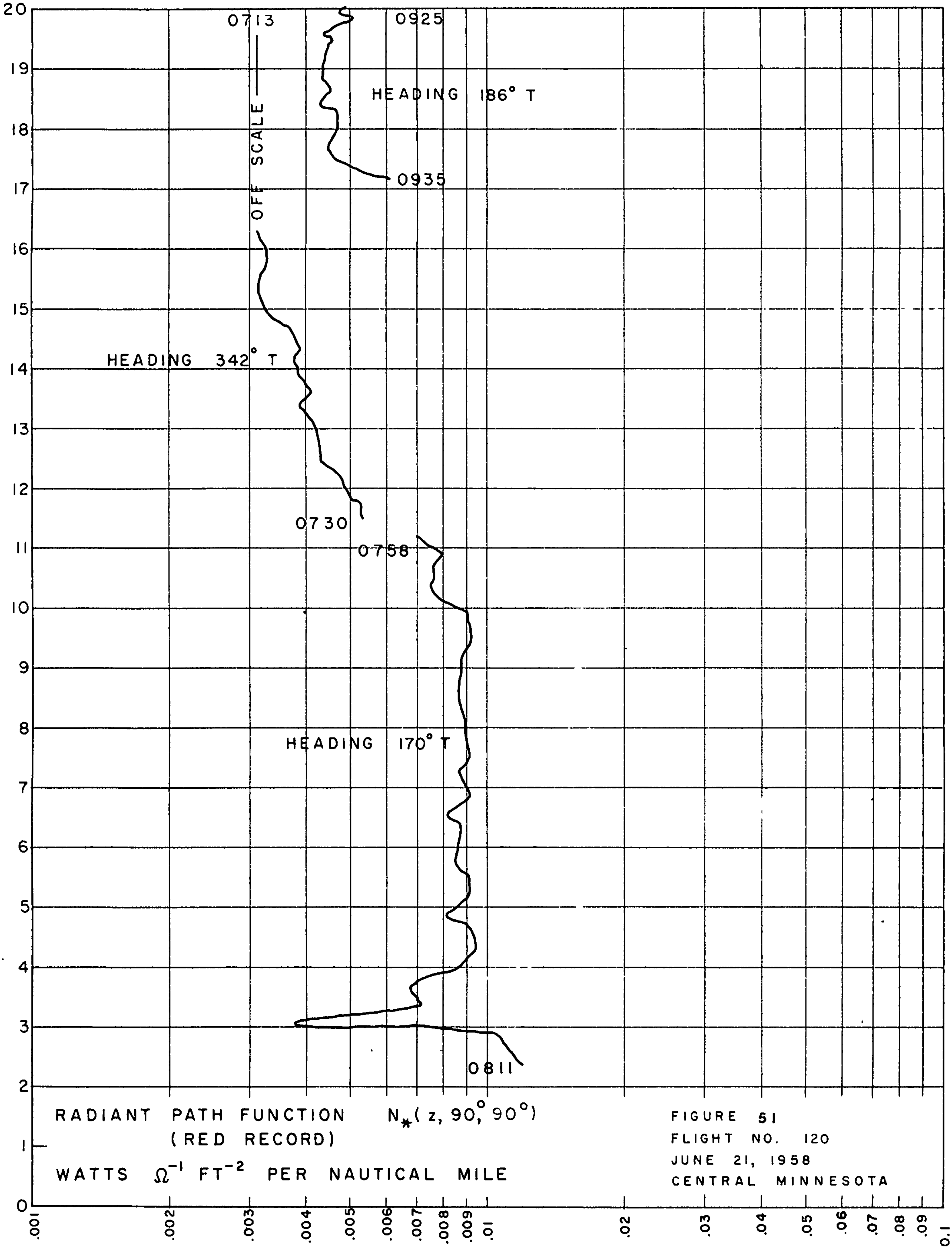

RADIANT PATH FUNCTION $N_*(z, 90°, 90°)$
(RED RECORD)

WATTS Ω^{-1} FT^{-2} PER NAUTICAL MILE

FIGURE 51
FLIGHT NO. 120
JUNE 21, 1958
CENTRAL MINNESOTA

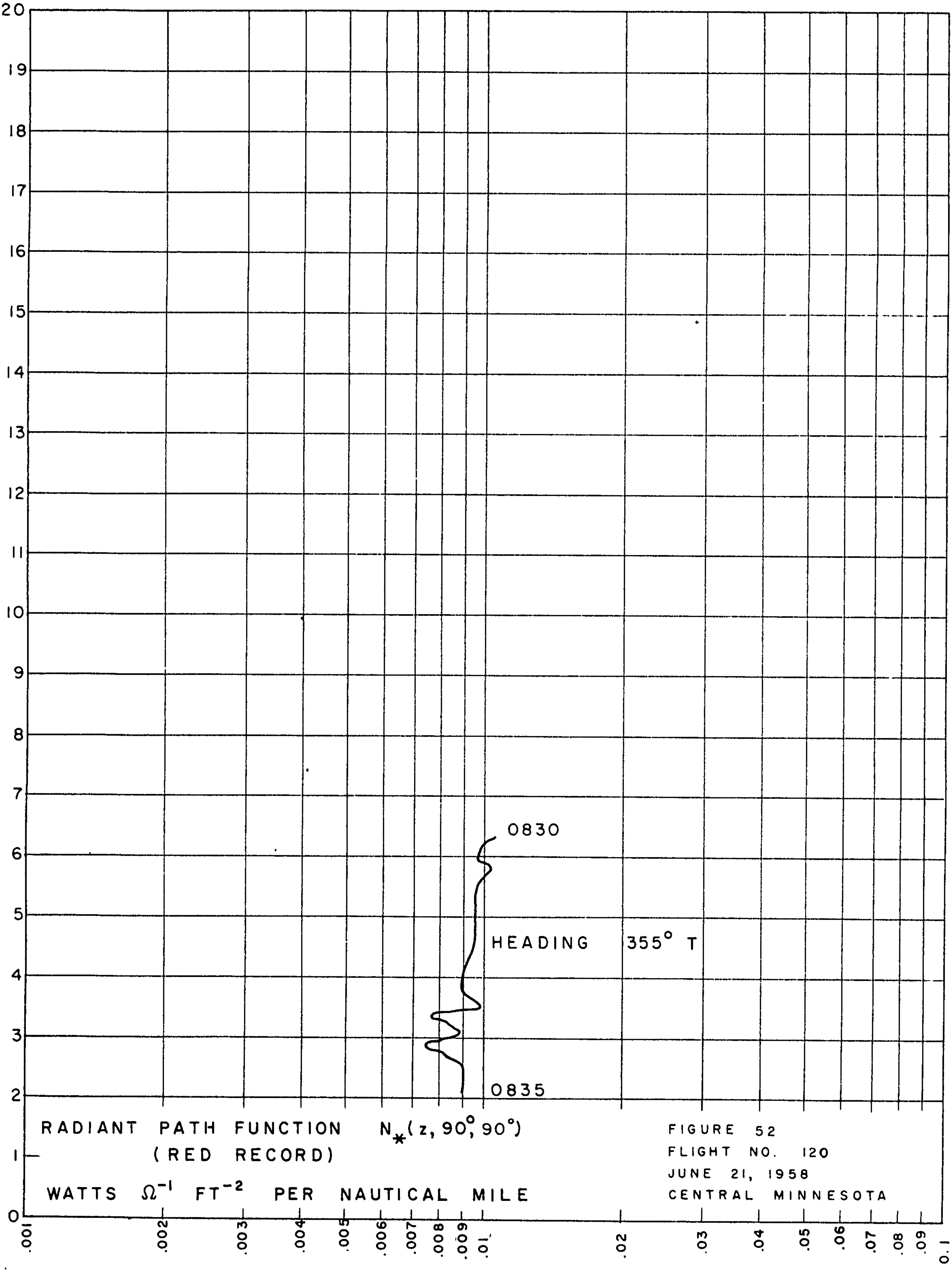

20
19
18
17
16
15
14
13
12
11
10
9
8
7
6
5
4
3
2
1
0
0830
HEADING 355° T
0835
RADIANT PATH FUNCTION N*(z, 90°, 90°)
(RED RECORD)
WATTS Ω⁻¹ FT⁻² PER NAUTICAL MILE
FIGURE 52
FLIGHT NO. 120
JUNE 21, 1958
CENTRAL MINNESOTA
.001
.002
.003
.004
.005
.006
.007
.008
.009
.01
.02
.03
.04
.05
.06
.07
.08
.09
0.1

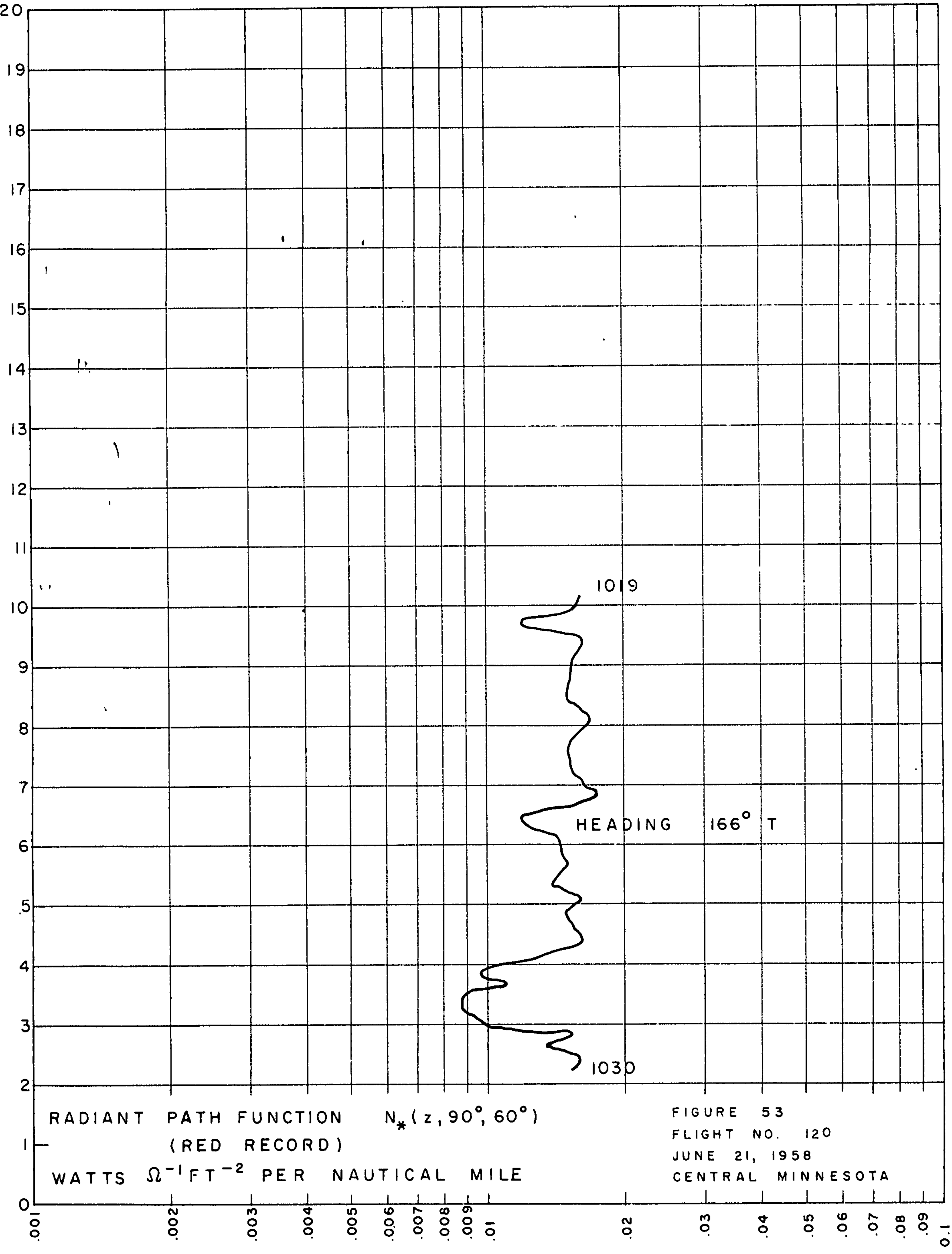

RADIANT PATH FUNCTION $N_*(z, 90°, 60°)$
(RED RECORD)
WATTS $\Omega^{-1}FT^{-2}$ PER NAUTICAL MILE

FIGURE 53
FLIGHT NO. 120
JUNE 21, 1958
CENTRAL MINNESOTA

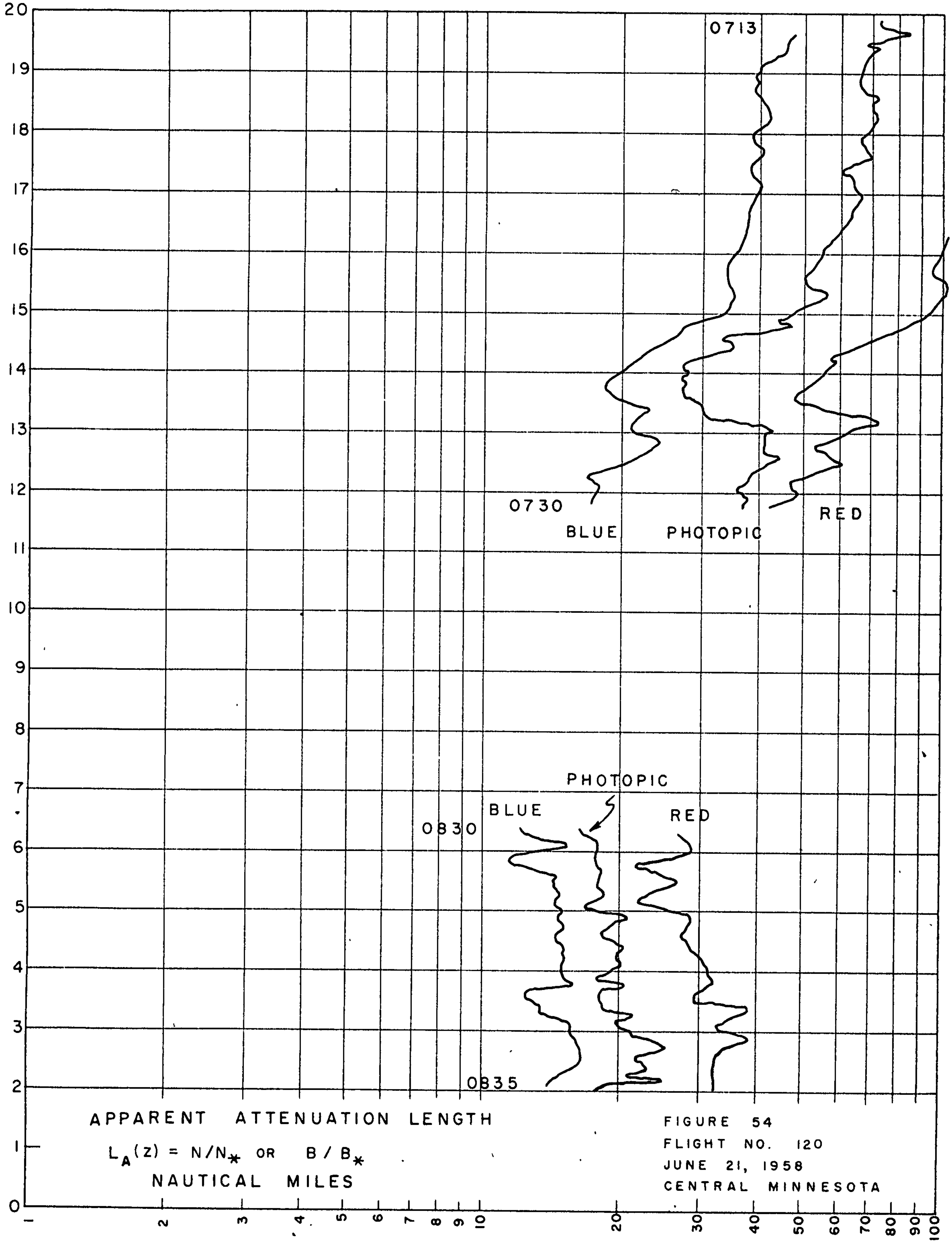
0713
0730
BLUE
PHOTOPIC
RED
PHOTOPIC
BLUE
0830
RED
0835
APPARENT ATTENUATION LENGTH
$L_A(z) = N/N_*$ OR B/B_*
NAUTICAL MILES
FIGURE 54
FLIGHT NO. 120
JUNE 21, 1958
CENTRAL MINNESOTA

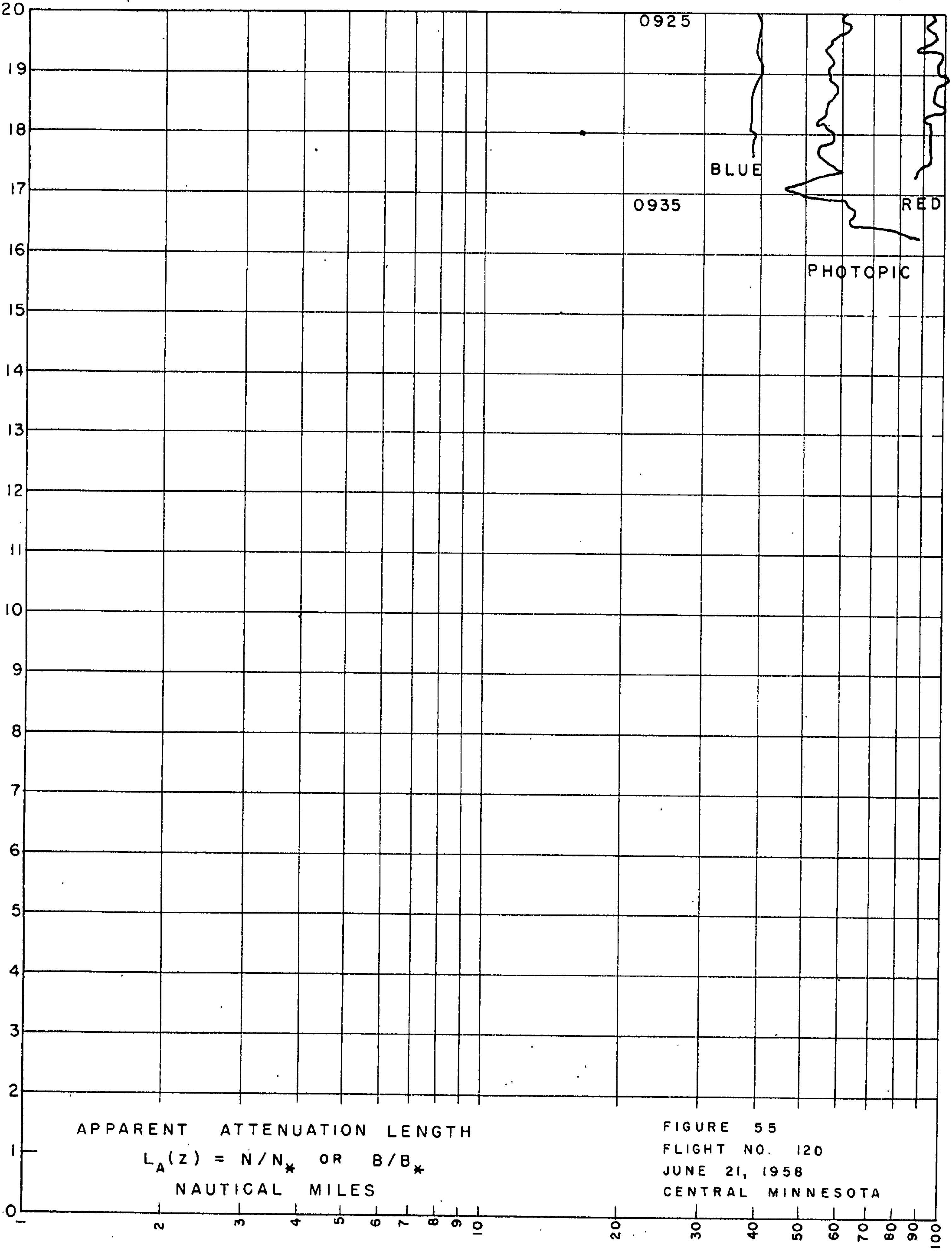

FIGURE 55
FLIGHT NO. 120
JUNE 21, 1958
CENTRAL MINNESOTA

Ⓢ

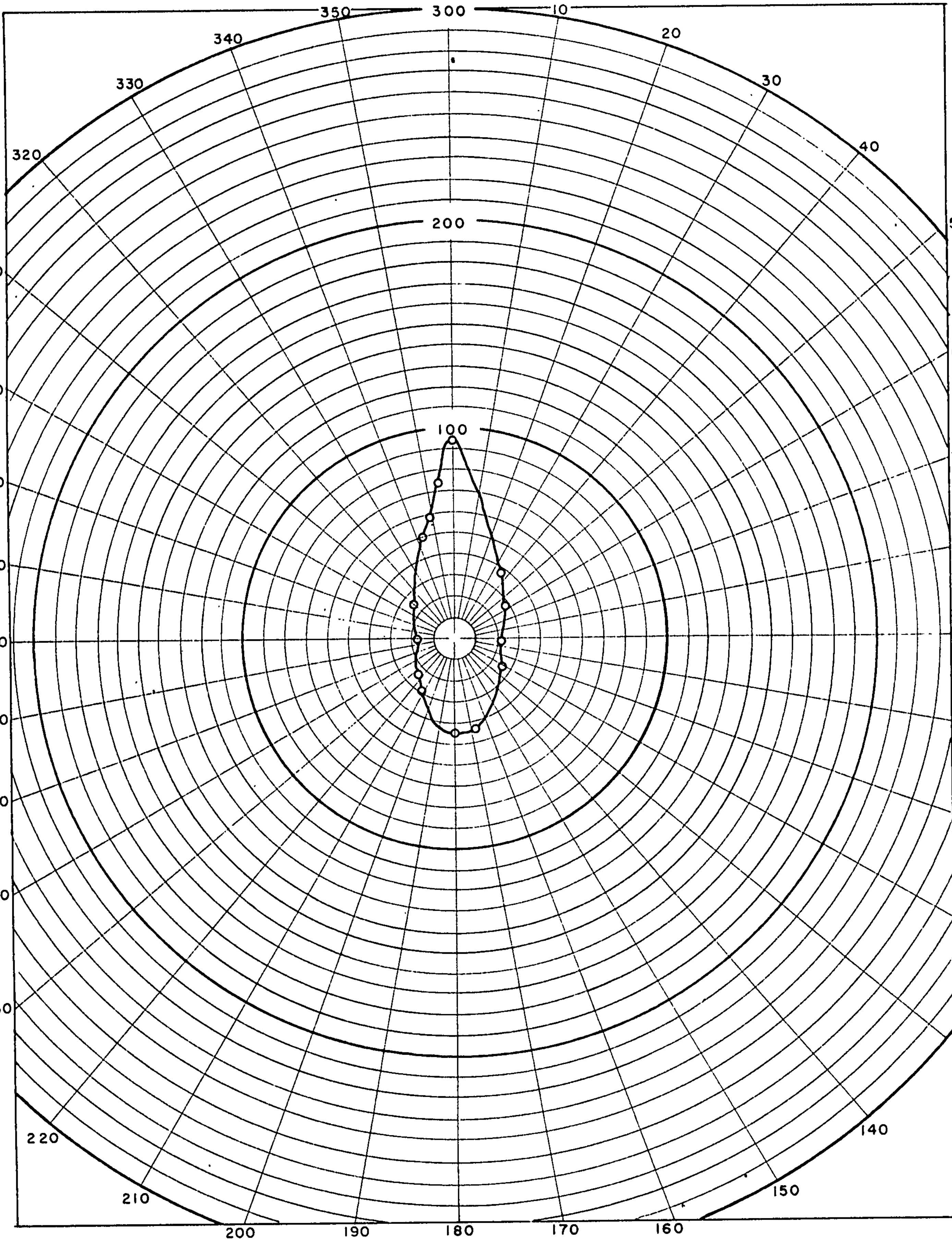

LUMINOUS PATH FUNCTION $B_*(21000, 90^\circ, \phi)$

FOOT LAMBERTS PER NAUTICAL MILE

PHOTOPIC RECORD, 21000 FT. 0700 CDST

FIGURE 56
FLIGHT NO. 120
JUNE 21, 1958
CENTRAL MINNESOTA

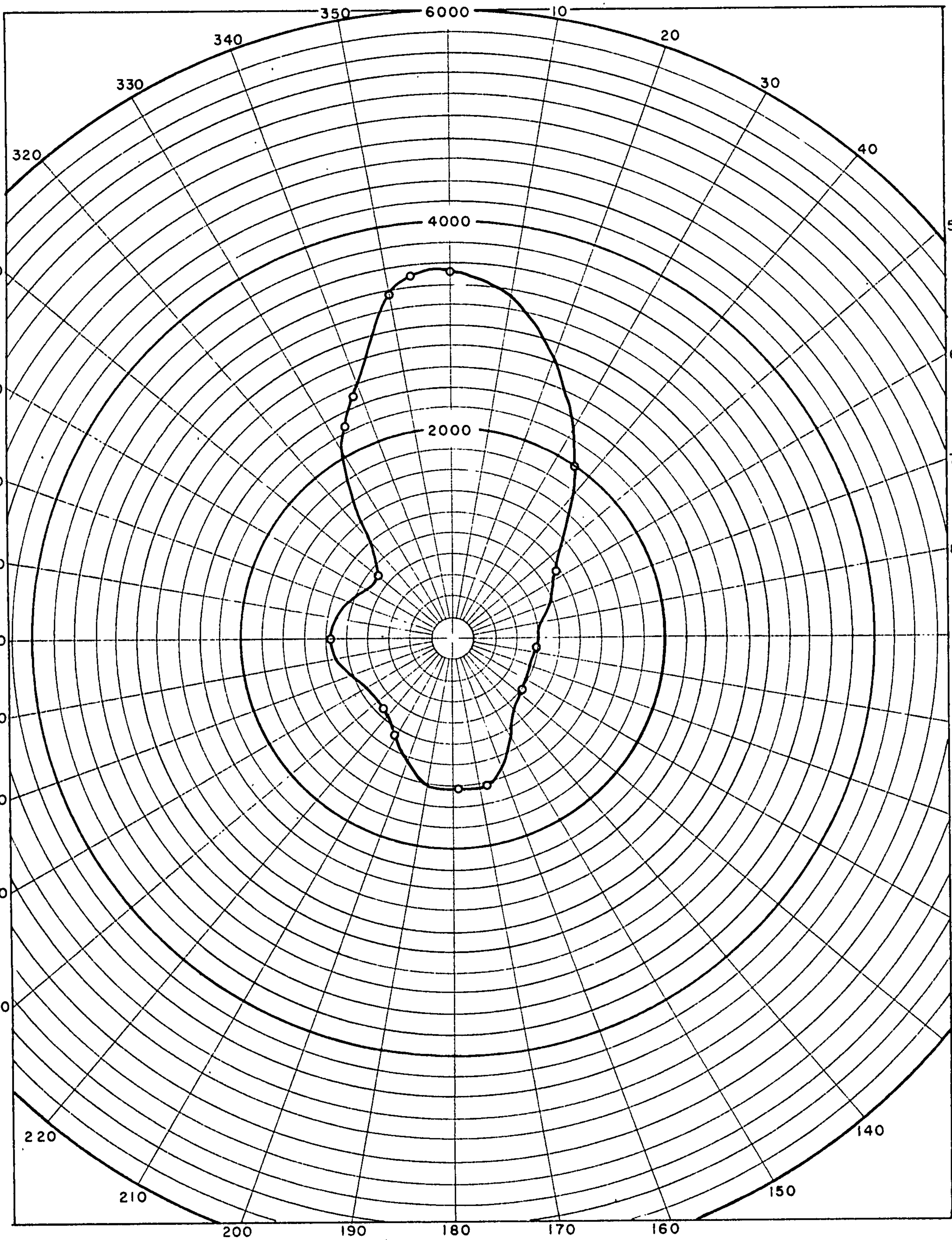

LUMINANCE, HORIZONTAL B (21000, 90°, ϕ)
FOOT-LAMBERTS

PHOTOPIC RECORD, 21 000 FT. 0700 CDST

FIGURE 57
FLIGHT NO. 120
JUNE 21, 1958
CENTRAL MINNESOTA

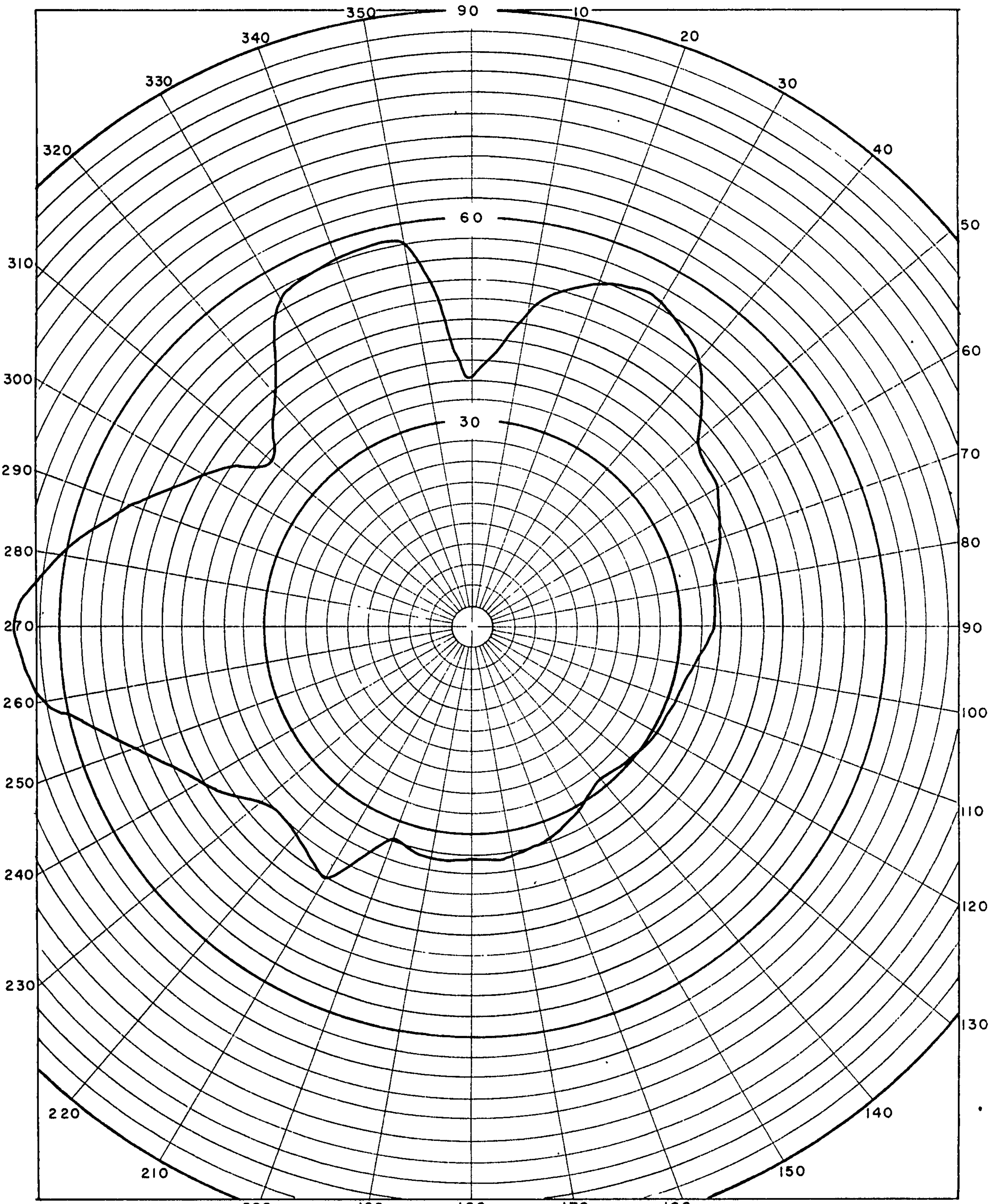

APPARENT ATTENUATION LENGTH $L_A(21000)$
NAUTICAL MILES
PHOTOPIC RECORD, 21000 FT. 0700 CDST

FIGURE 58
FLIGHT NO. 120
JUNE 21, 1958
CENTRAL MINNESOTA

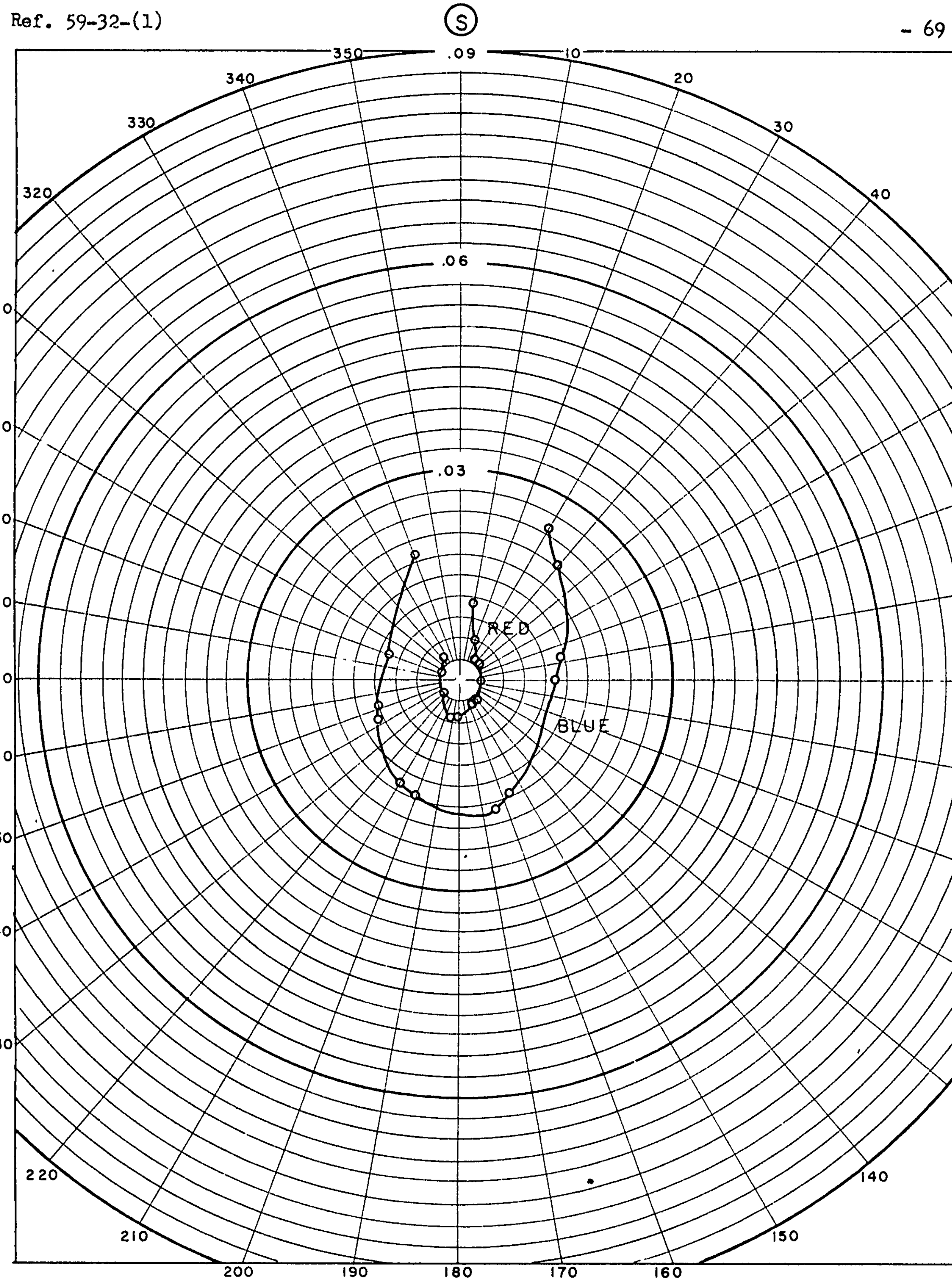

RADIANT PATH FUNCTION $N_*(21000, 90°, \phi)$
WATTS Ω^{-1} FT^{-2} PER NAUTICAL MILE
BLUE AND RED RECORDS, 21000 FT. 0700 CDST

FIGURE 59
FLIGHT NO. 120
JUNE 21, 1958
CENTRAL MINNESOTA

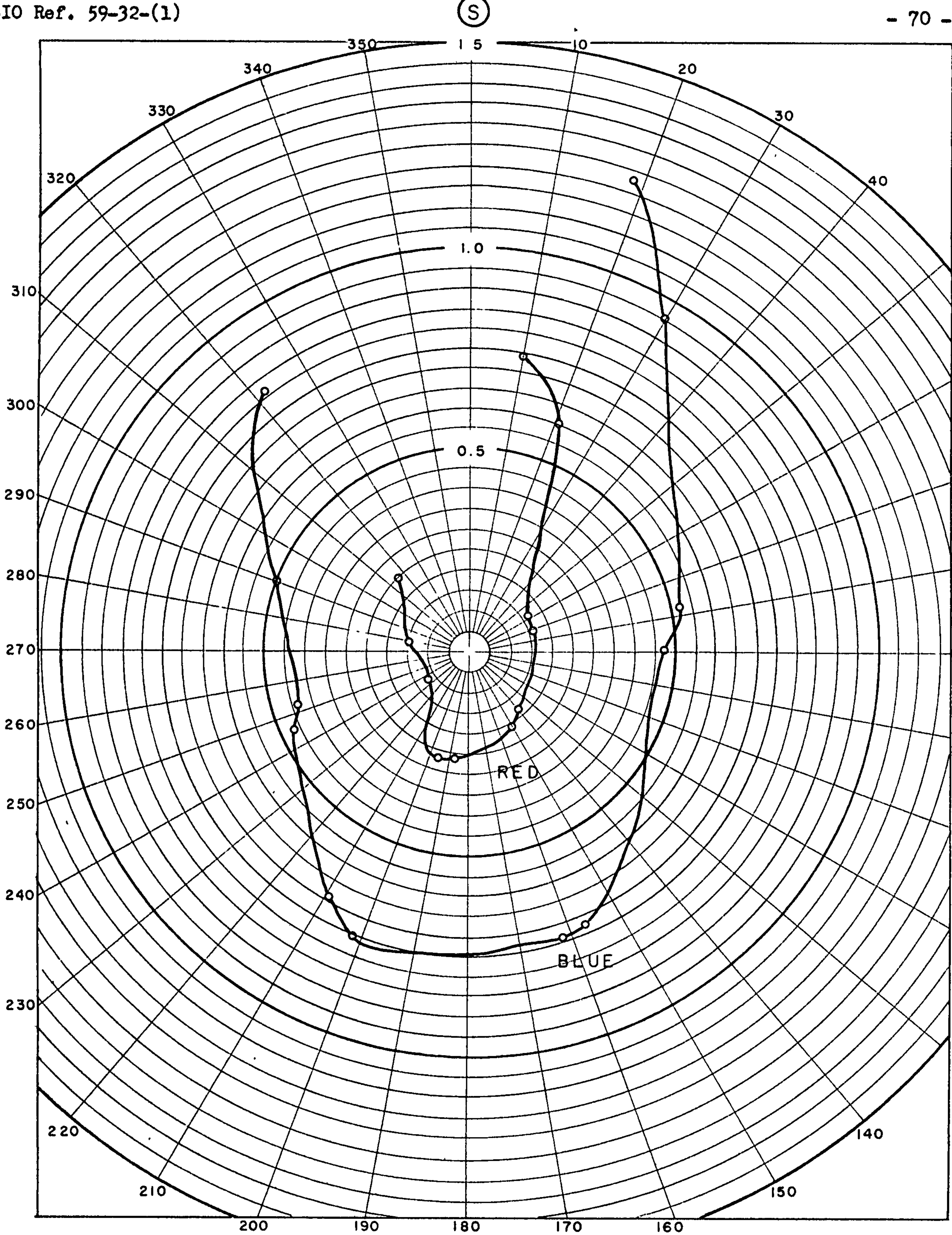

RADIANCE, HORIZONTAL N(21000, 90°, ϕ)
WATTS Ω^{-1} FT^{-2}
BLUE AND RED RECORDS 21000 FT 0700 EDST

FIGURE 60
FLIGHT NO. 120
JUNE 21, 1958
CENTRAL MINNESOTA

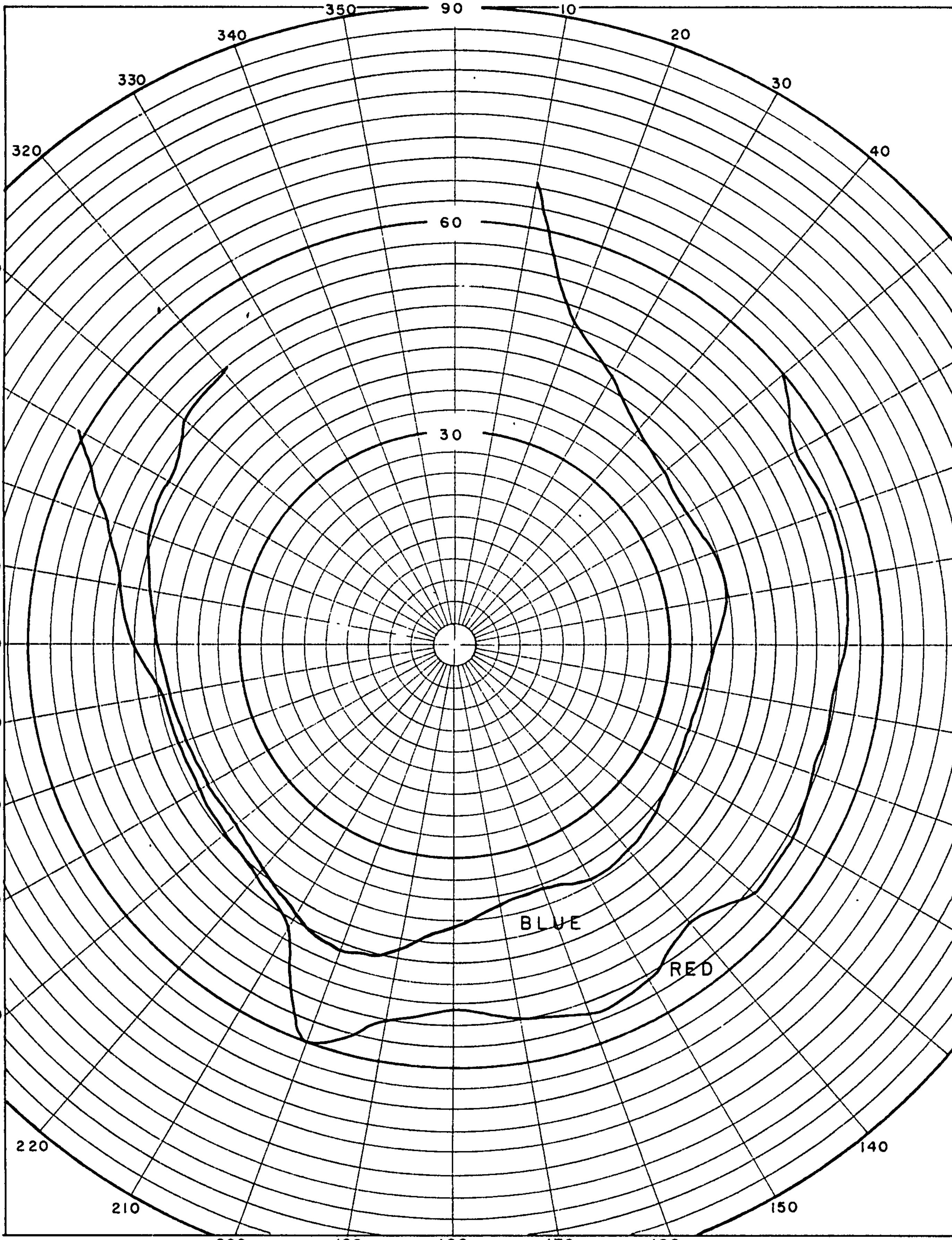

APPARENT ATTENUATION LENGTH $L_A(21000)$
NAUTICAL MILES
BLUE AND RED RECORDS 21000 FT. 0700 CDST

FIGURE 61
FLIGHT NO. 120
JUNE 21, 1958
CENTRAL MINNESOTA

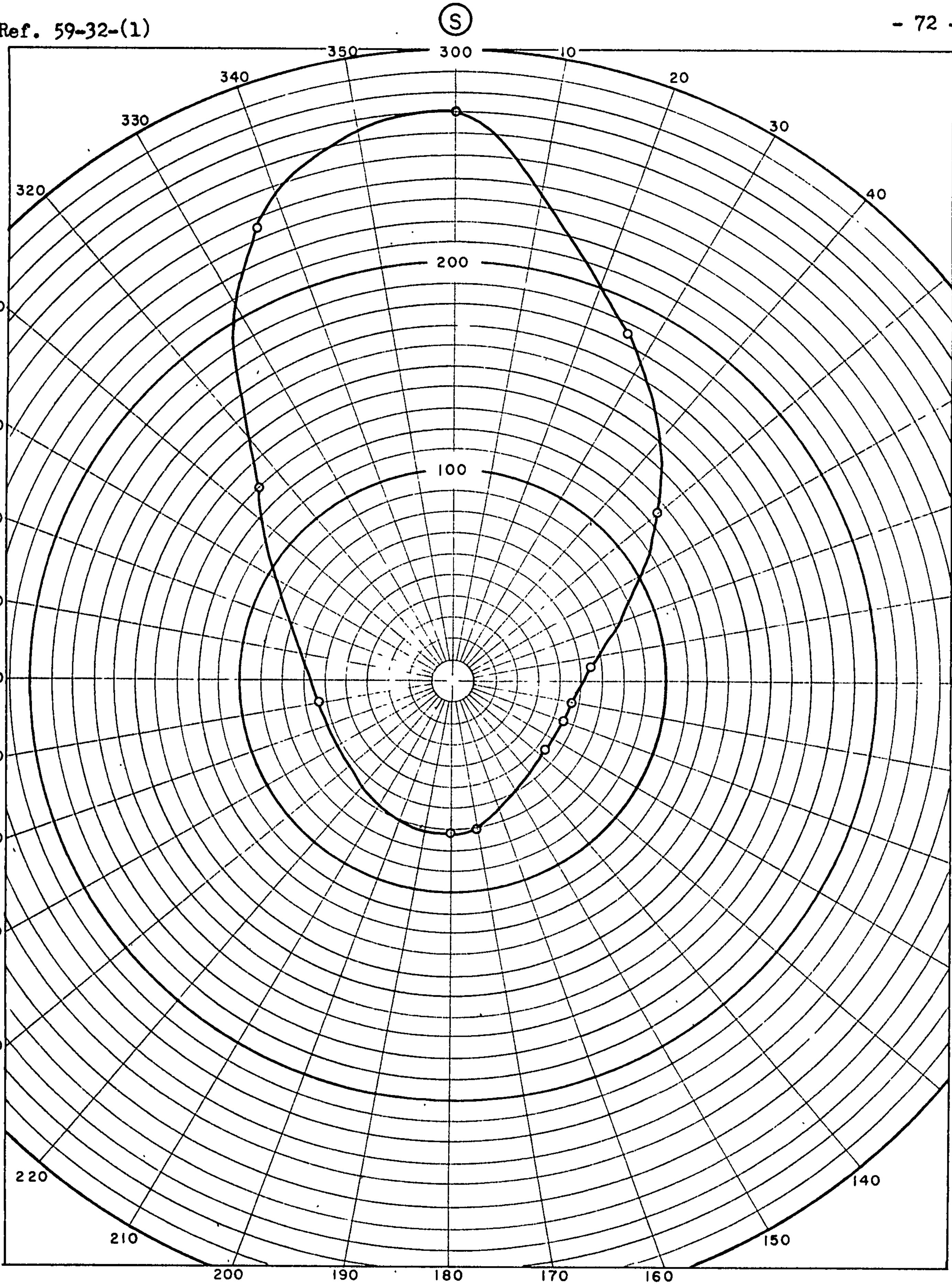

LUMINOUS PATH FUNCTION $B_*(11000, 90°, \phi)$
FOOT LAMBERTS PER NAUTICAL MILE
PHOTOPIC RECORD, 11000 FT. 0751 CDST

FIGURE 62
FLIGHT NO. 120
JUNE 21, 1958
CENTRAL MINNESOTA

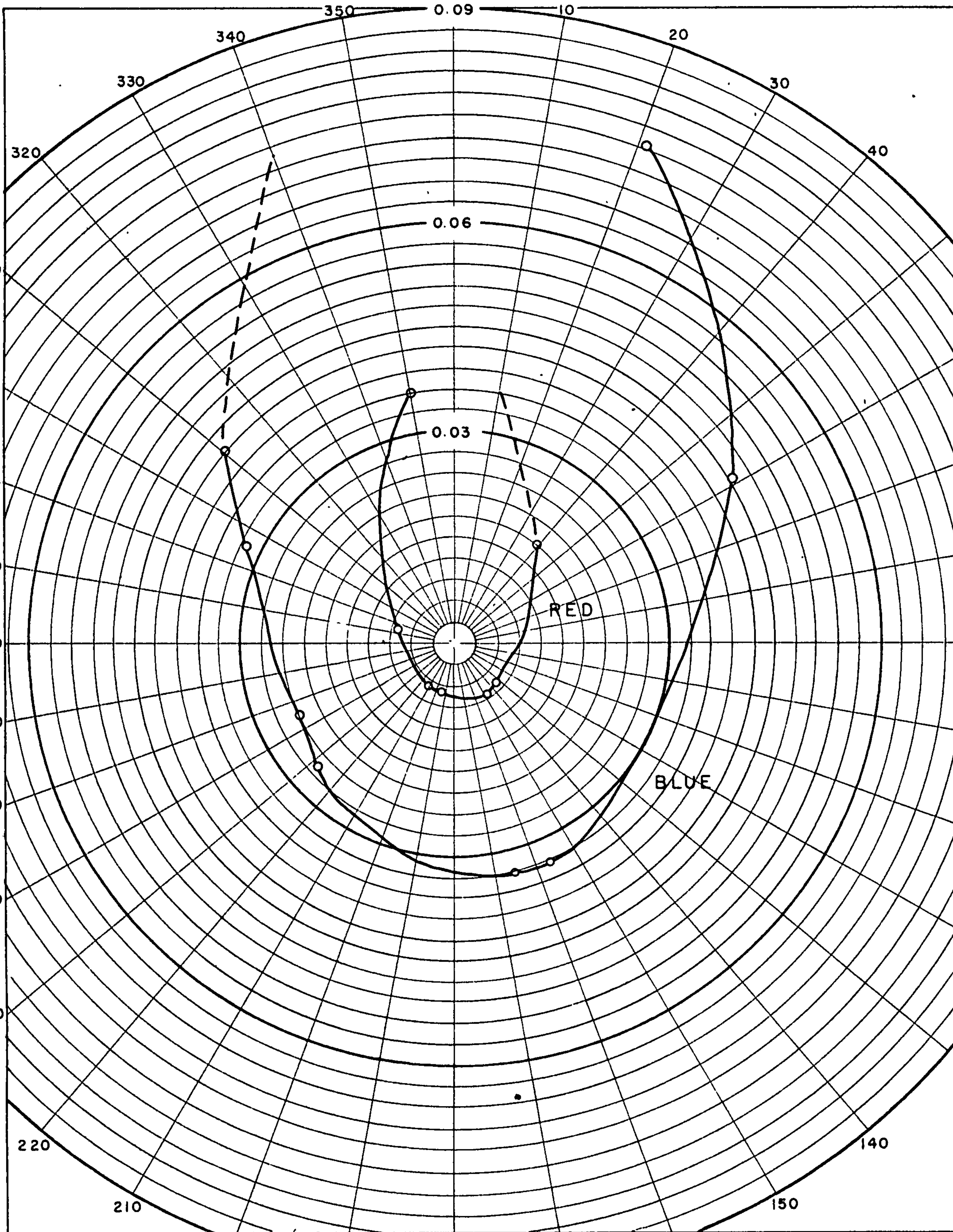

RADIANT PATH FUNCTION $N_*(11000, 90^\circ, \phi)$
WATTS Ω^{-1} FT^{-2} PER NAUTICAL MILE
BLUE AND RED RECORDS, 11000 FT 0751 CDST

FIGURE 63
FLIGHT NO. 120
JUNE 21, 1958
CENTRAL MINNESOTA

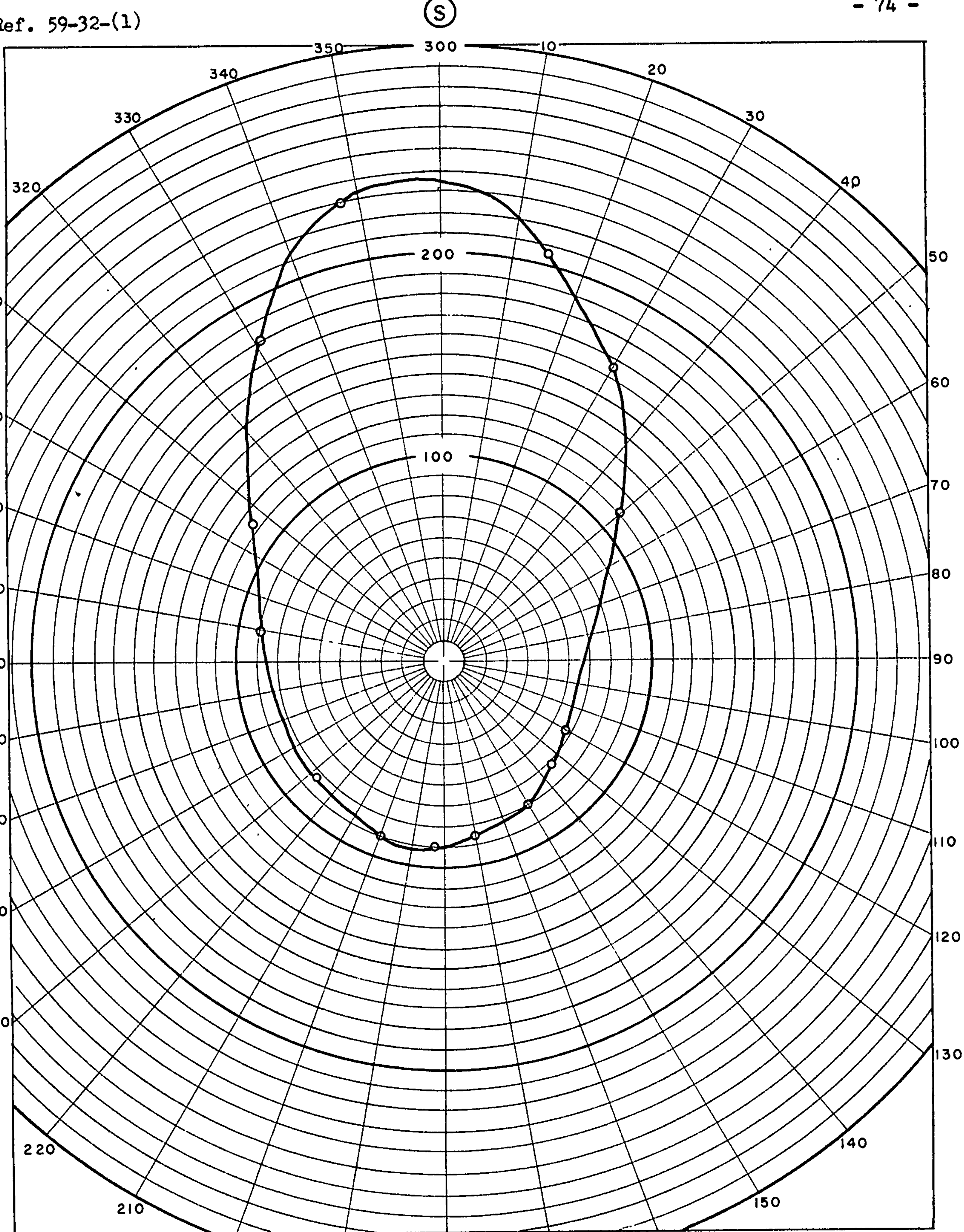

LUMINOUS PATH FUNCTION $B_*(2000, 90°, \phi)$

FOOT LAMBERTS PER NAUTICAL MILE

PHOTOPIC RECORD, 2000 FT 0820 CDST

FIGURE 64
FLIGHT NO. 120
JUNE 21, 1958
CENTRAL MINNESOTA

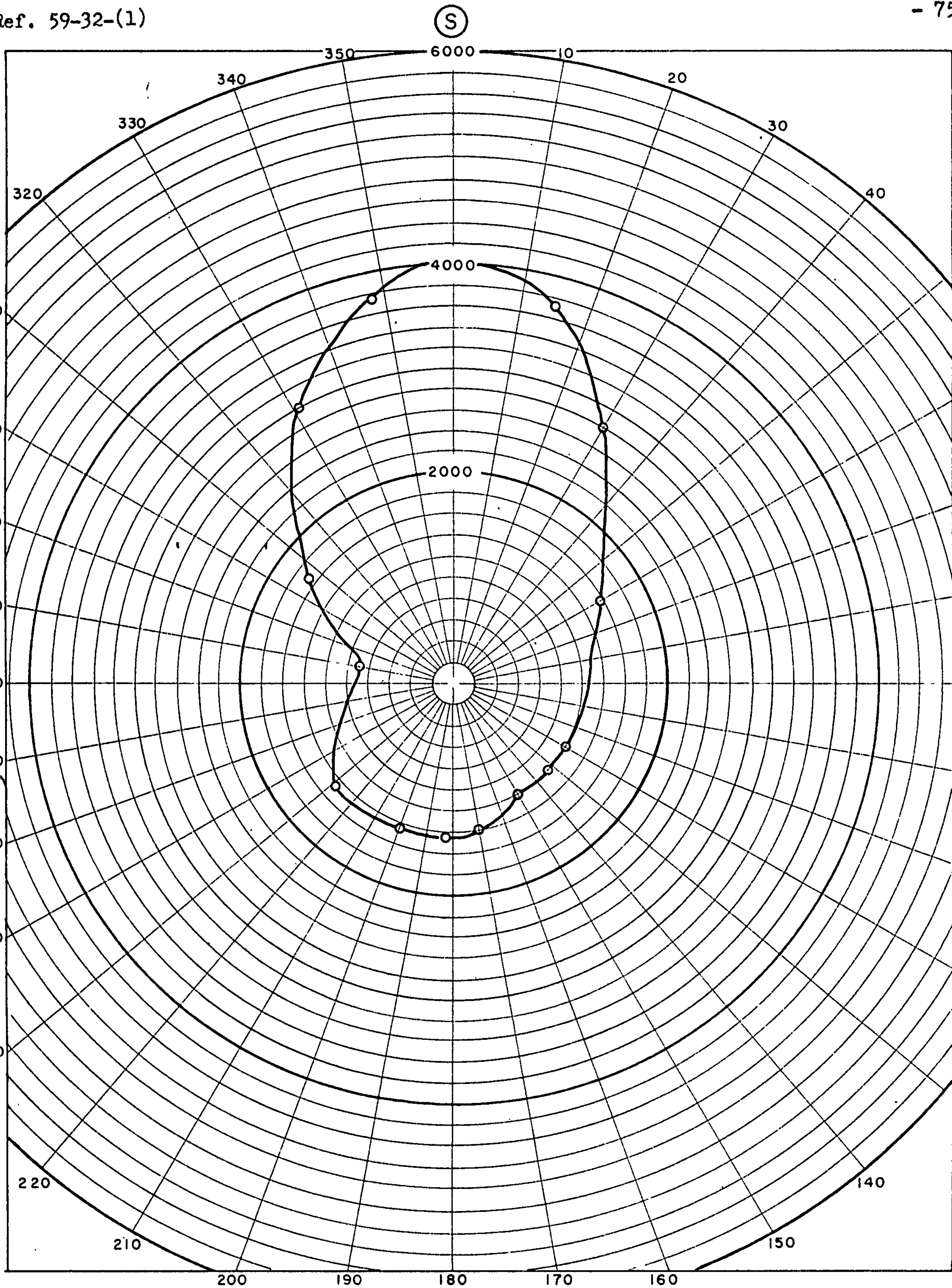

LUMINANCE, HORIZONTAL B(2000, 90°, ϕ)
FOOT LAMBERTS
PHOTOPIC RECORD, 2000 FT. 0820 CDST

FIGURE 65
FLIGHT NO. 120
JUNE 21, 1958
CENTRAL MINNESOTA

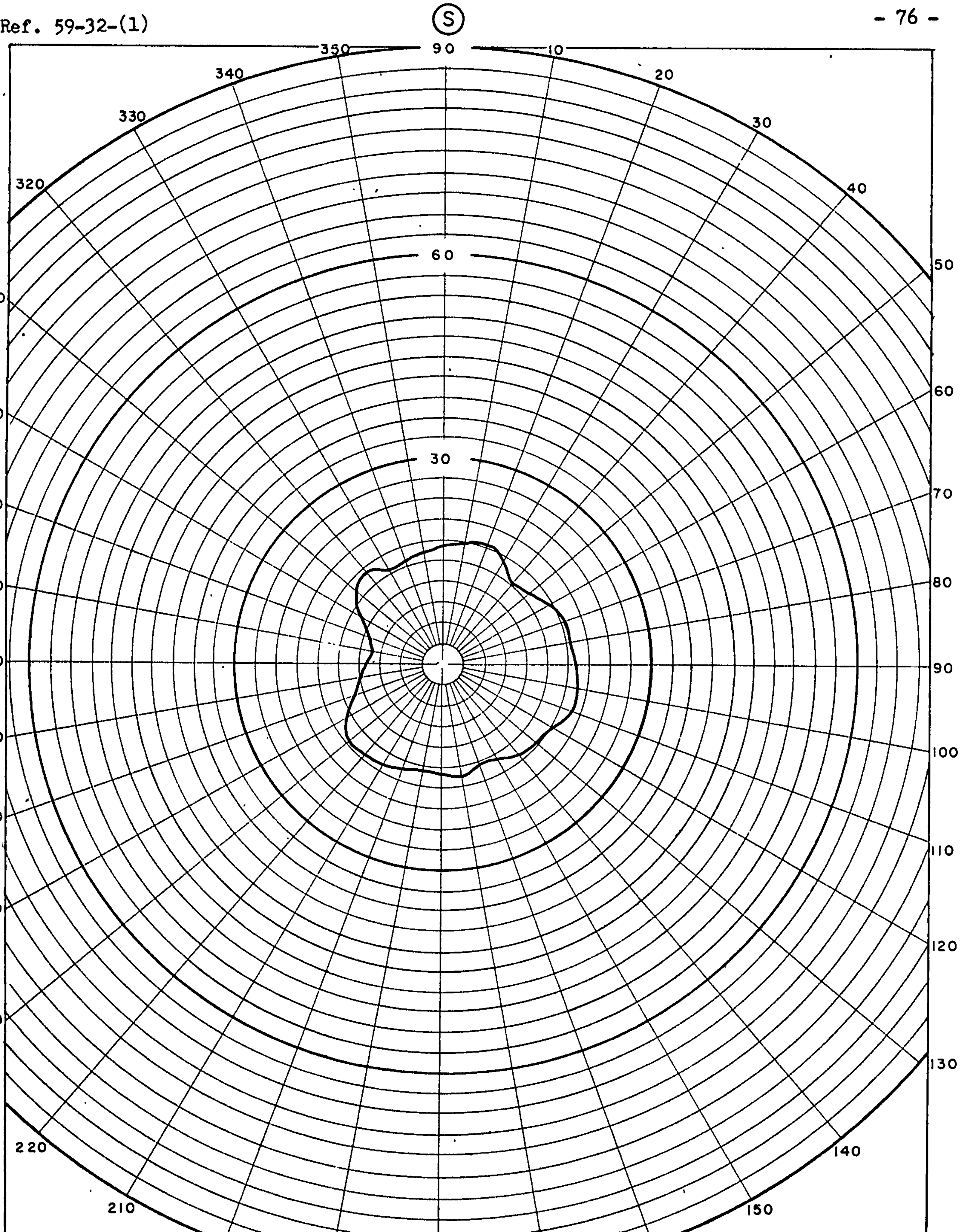

APPARENT ATTENUATION LENGTH $L_A(2000)$
NAUTICAL MILES
PHOTOPIC RECORD, 2000 FT. 0820 CDST

FIGURE 66
FLIGHT NO. 120
JUNE 21, 1958
CENTRAL MINNESOTA

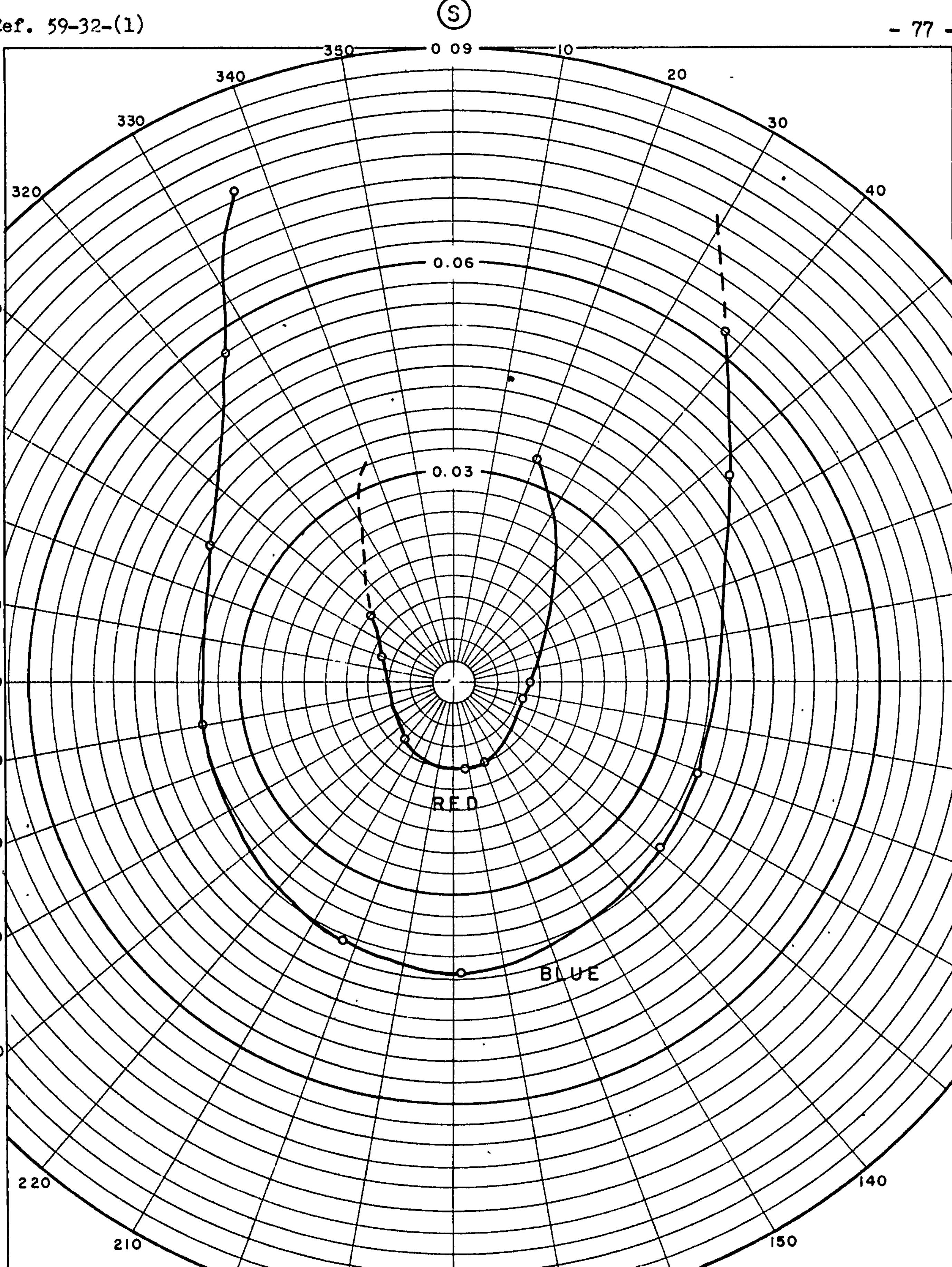

RADIANT PATH FUNCTION $N_{*}(2000, 90°, \phi)$

WATTS Ω^{-1} FT.$^{-2}$ PER NAUTICAL MILE

BLUE AND RED RECORDS, 2000 FT. 0820 CDST

FIGURE 67
FLIGHT NO. 120
JUNE 21, 1958
CENTRAL MINNESOTA

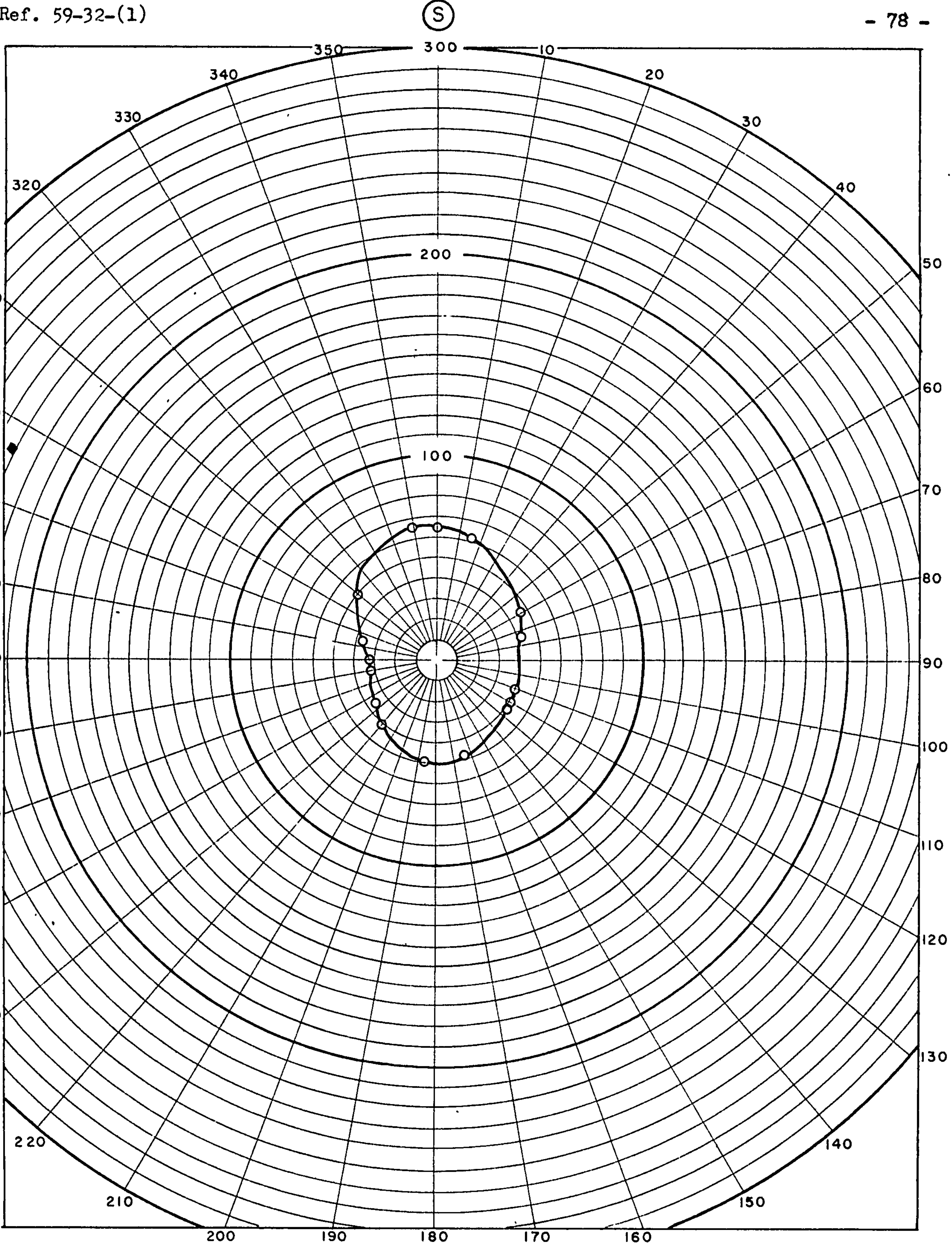

LUMINOUS PATH FUNCTION $B_*(22000, 90°, \phi)$
FOOT LAMBERTS PER NAUTICAL MILE
PHOTOPIC RECORD, 22000 FT. 0916 CDST

FIGURE 68
FLIGHT NO. 120
JUNE 21, 1958
CENTRAL MINNESOTA

Ⓢ

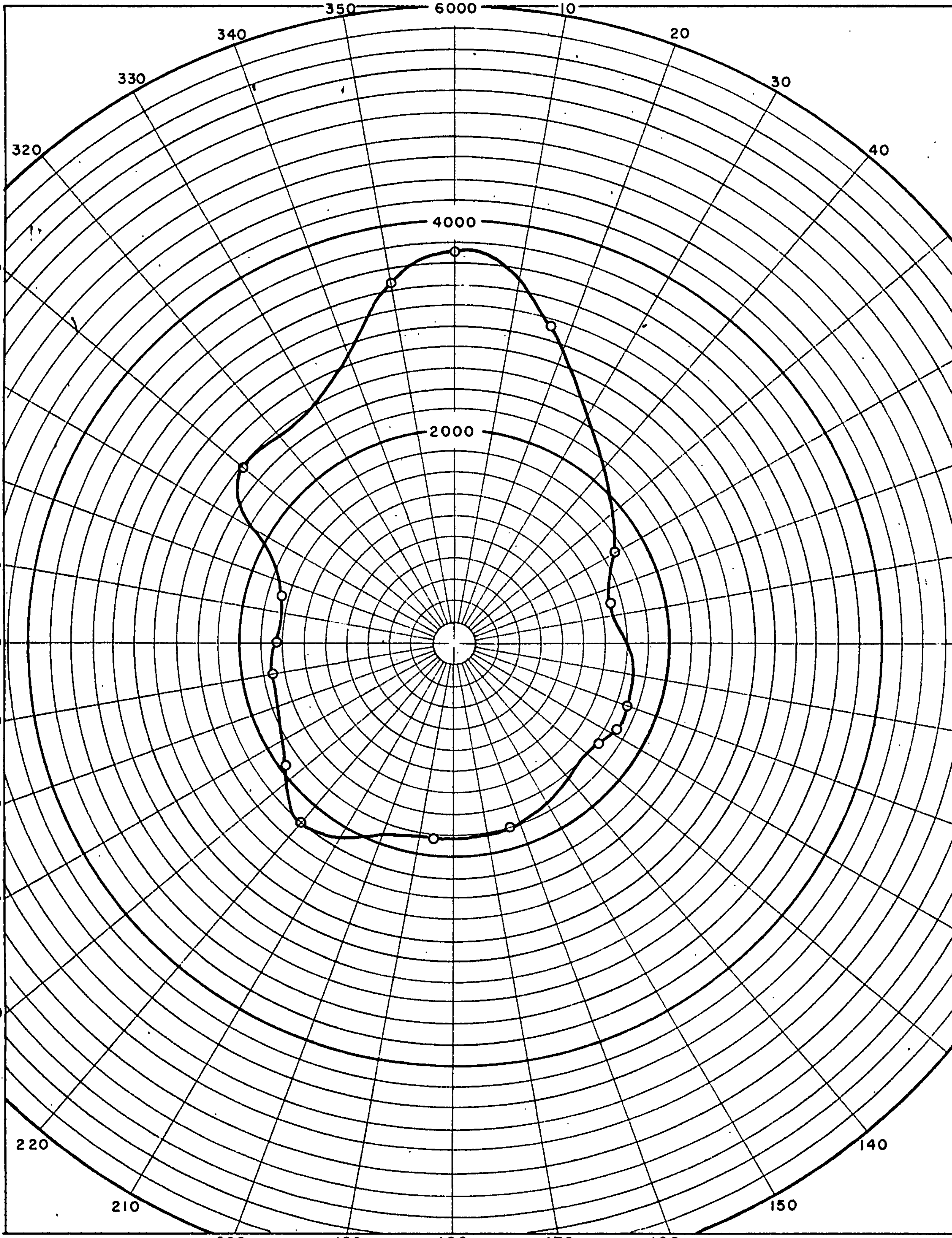

LUMINANCE, HORIZONTAL B(22000, 90°, ϕ)
FOOT LAMBERTS
PHOTOPIC RECORD, 22 000 FT. 0916 CDST

FIGURE 69
FLIGHT NO. 120
JUNE 21, 1958
CENTRAL MINNESOTA

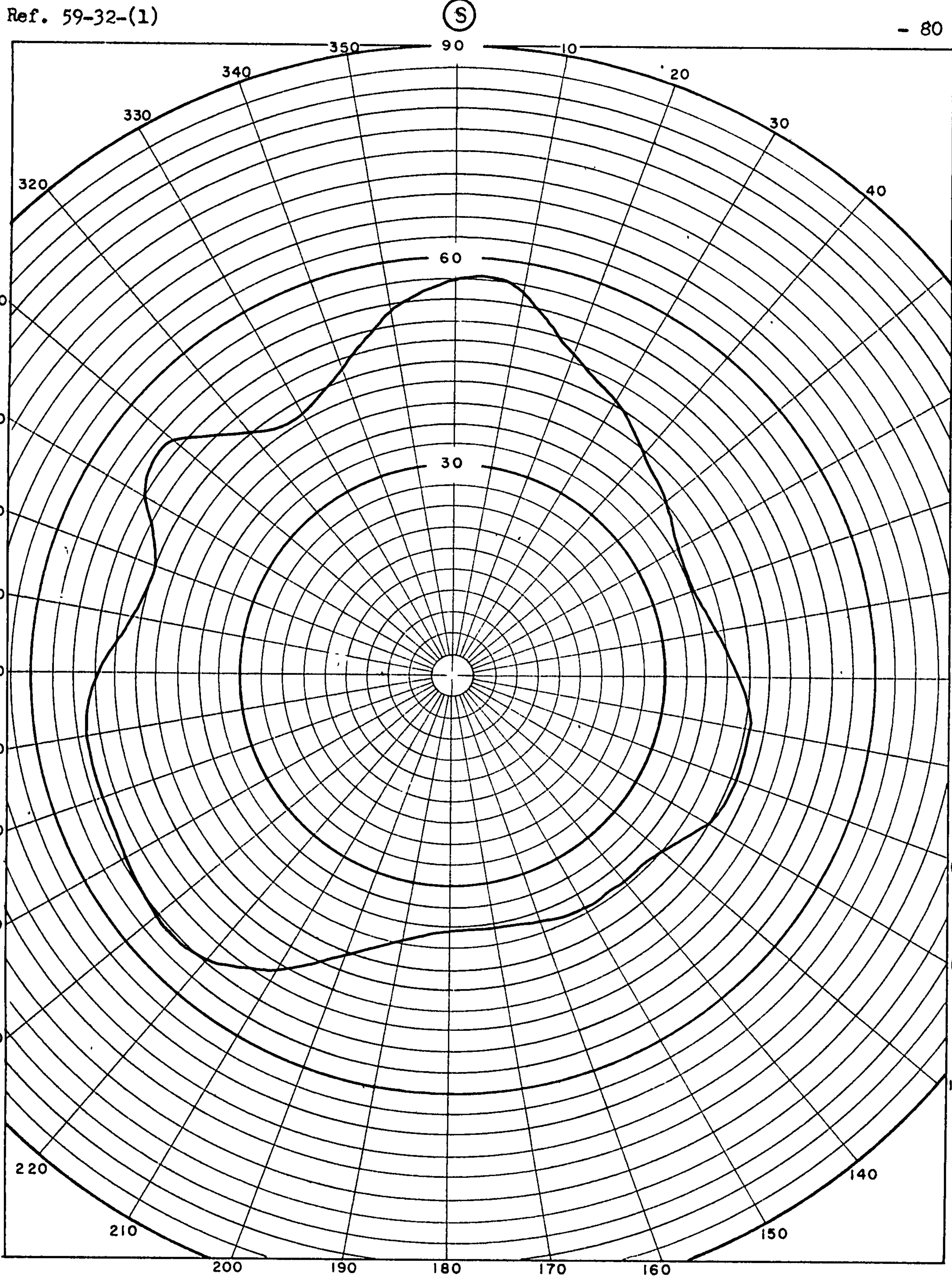

APPARENT ATTENUATION LENGTH $L_A(22000)$

NAUTICAL MILES

PHOTOPIC RECORD, 22000 FT. 0916 CDST

FIGURE 70
FLIGHT NO. 120
JUNE 21, 1958
CENTRAL MINNESOTA

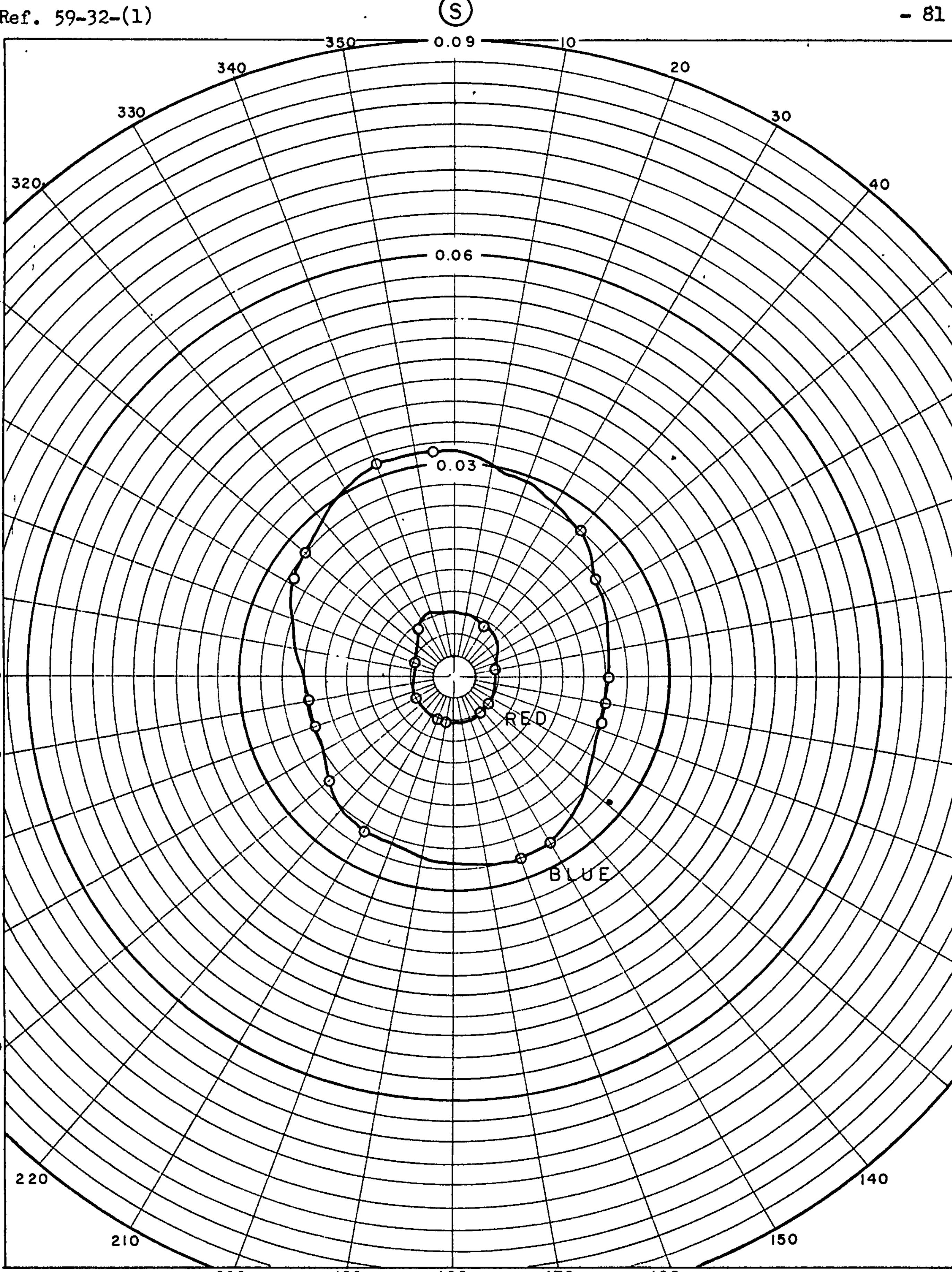

RADIANT PATH FUNCTION $N_*(22000, 90°, \phi)$
WATTS $\Omega^{-1}FT^{-2}$ PER NAUTICAL MILE
BLUE AND RED RECORDS, 22000 FT. 0916 CDST

FIGURE 71
FLIGHT NO. 120
JUNE 21, 1958
CENTRAL MINNESOTA

Ⓢ

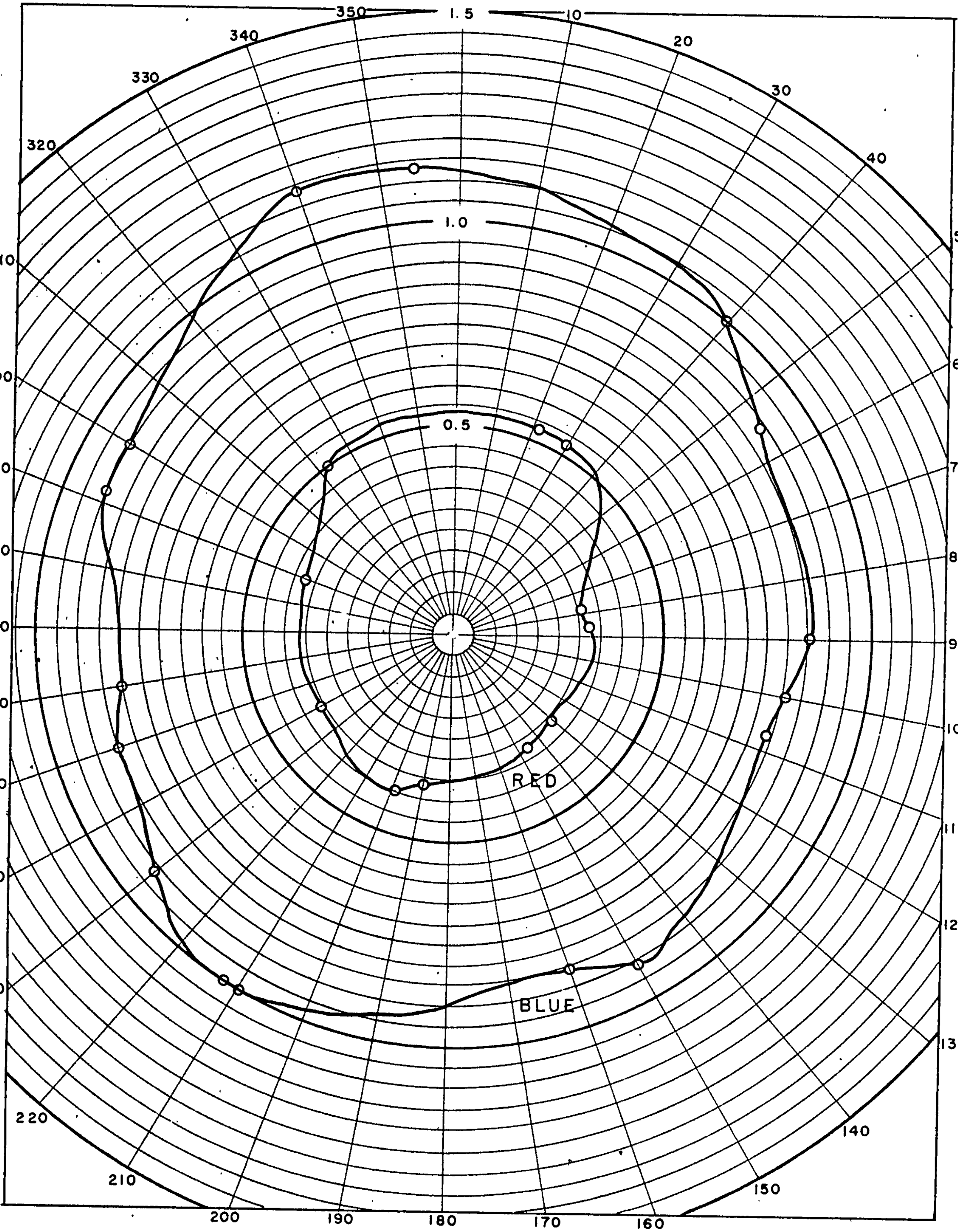

RADIANCE, HORIZONTAL N(22000, 90°, ϕ)
WATTS Ω^{-1} FT^{-2}
BLUE AND RED RECORDS, 22000 FT. 0916 CDST

FIGURE 72
FLIGHT NO. 120
JUNE 21, 1958
CENTRAL MINNESOTA

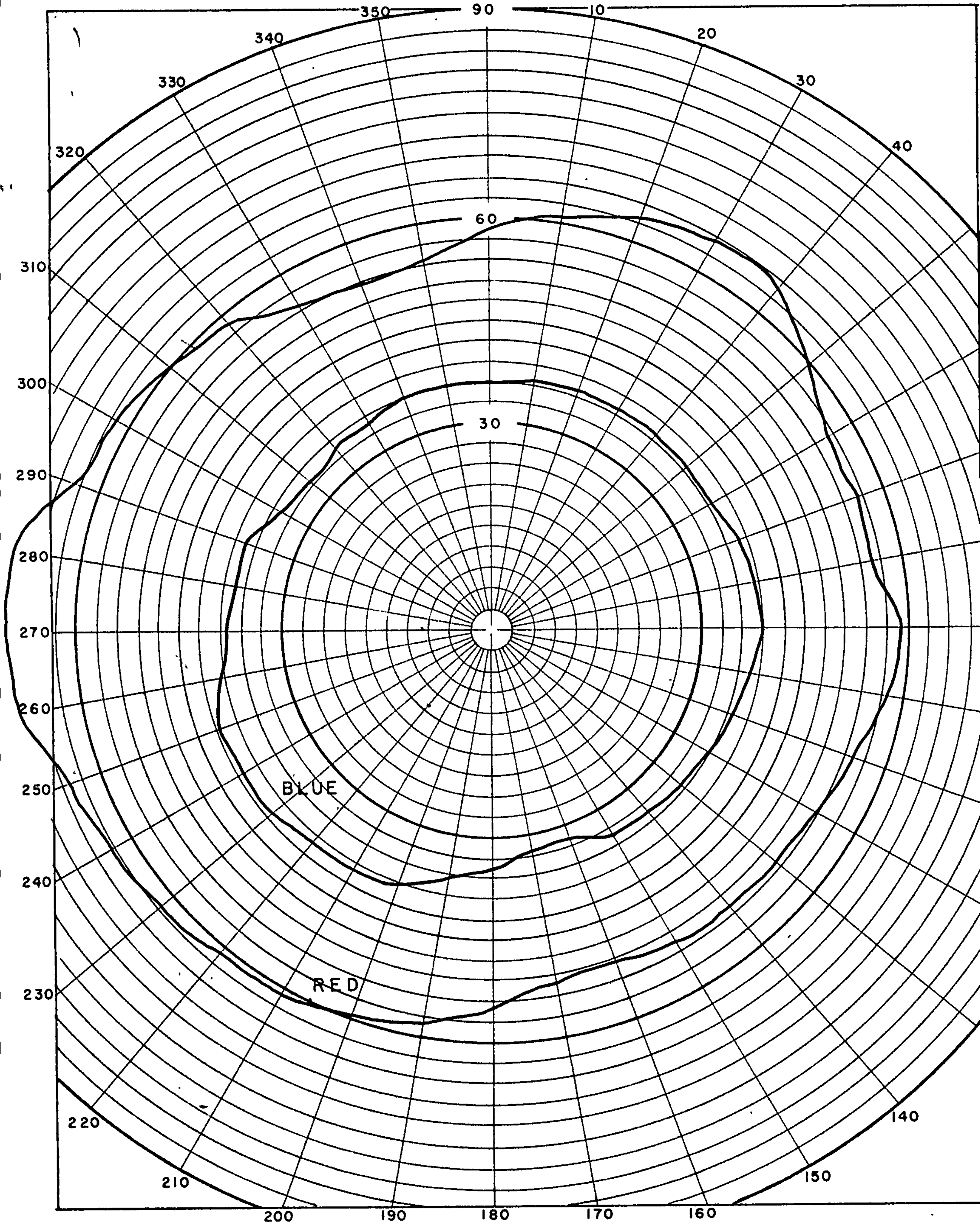

APPARENT ATTENUATION LENGTH $L_A(22000)$
NAUTICAL MILES
BLUE AND RED RECORDS, 22000 FT. 0916 CDST

FIGURE 73
FLIGHT NO. 120
JUNE 21, 1958
CENTRAL MINNESOTA

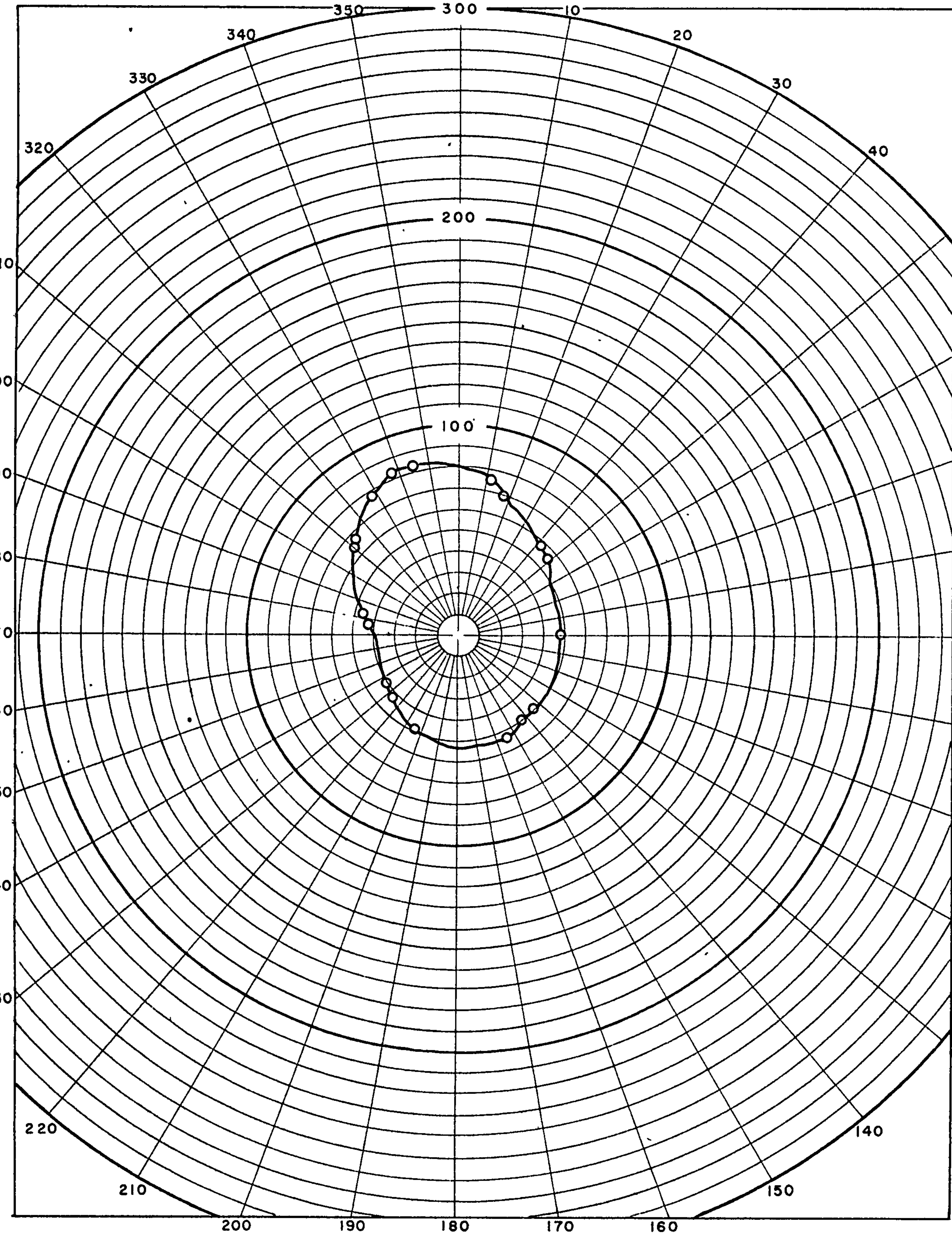

LUMINOUS PATH FUNCTION $B_{*}(17200, 90°, \phi)$

FOOT LAMBERTS PER NAUTICAL MILE

PHOTOPIC RECORD, 17200 FT. 0945 CDST

FIGURE 74
FLIGHT NO. 120
JUNE 21, 1958
CENTRAL MINNESOTA

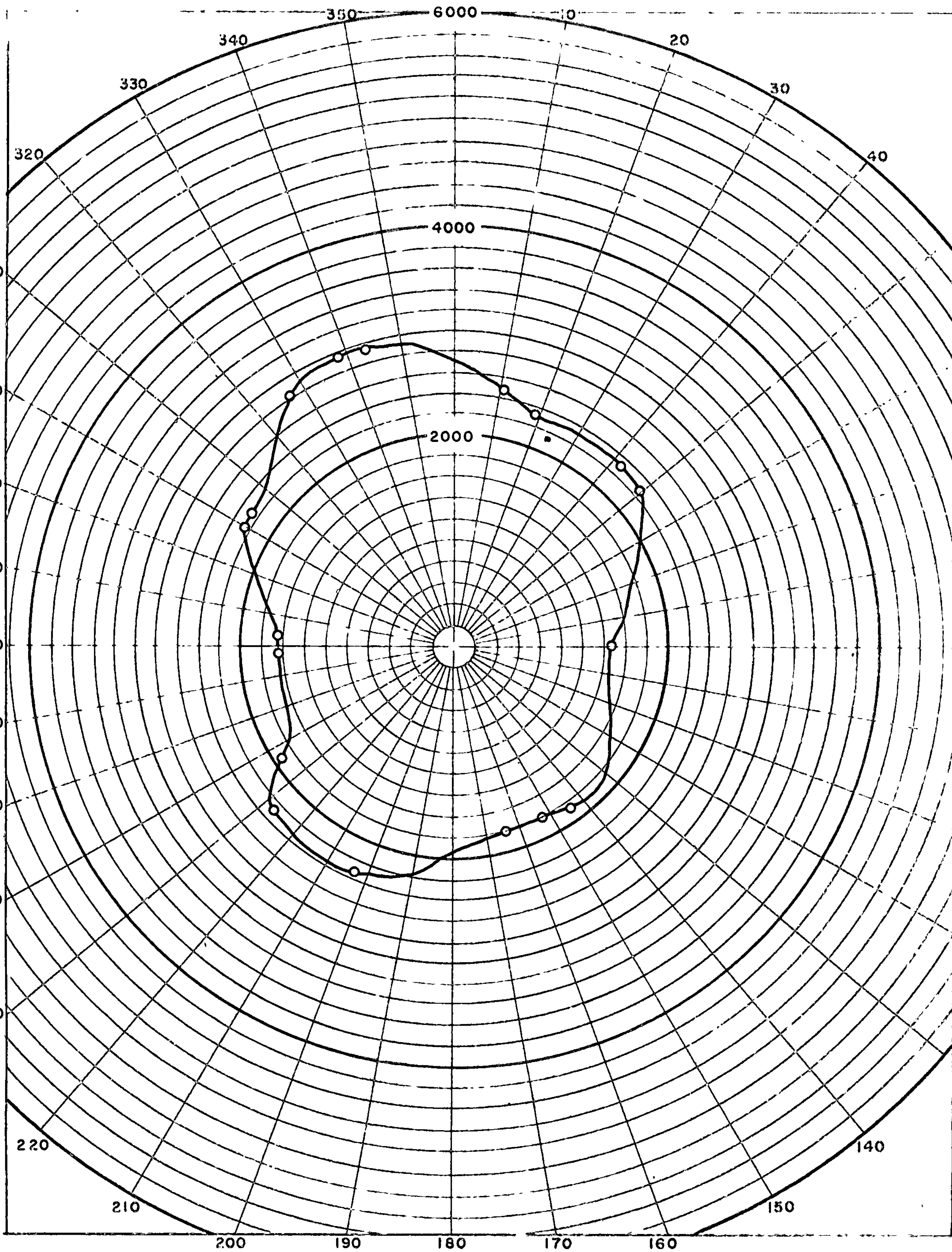

LUMINANCE, HORIZONTAL B(17200, 90°, ϕ)
FOOT LAMBERTS
PHOTOPIC RECORD, 17200 FT. 0945 CDST

FIGURE 75
FLIGHT NO. 120
JUNE 21, 1958
CENTRAL MINNESOTA

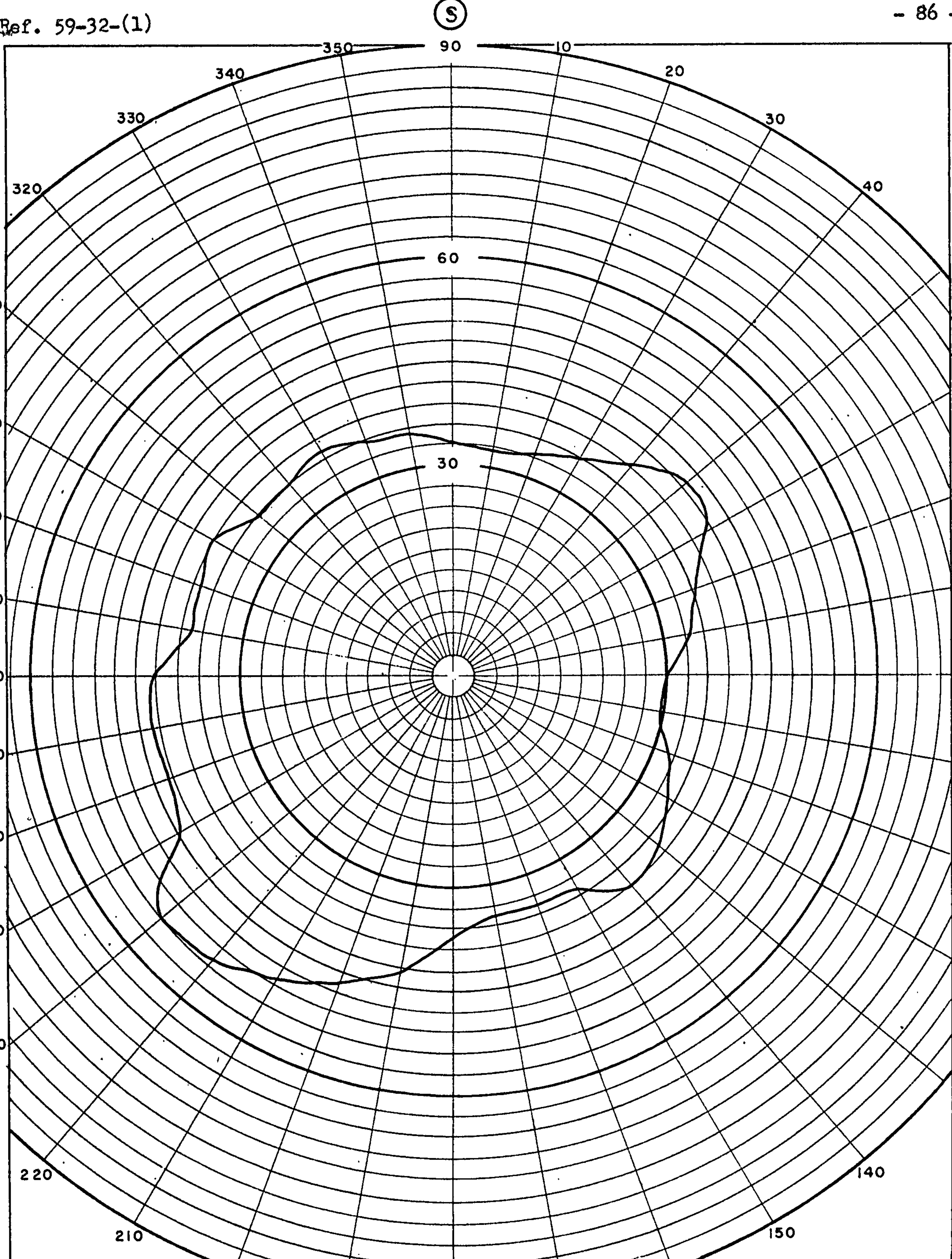

APPARENT ATTENUATION LENGTH $L_A(17200)$
NAUTICAL MILES
PHOTOPIC RECORD, 17200 FT. 0945 CDST

FIGURE 76
FLIGHT NO. 120
JUNE 21, 1958
CENTRAL MINNESOTA

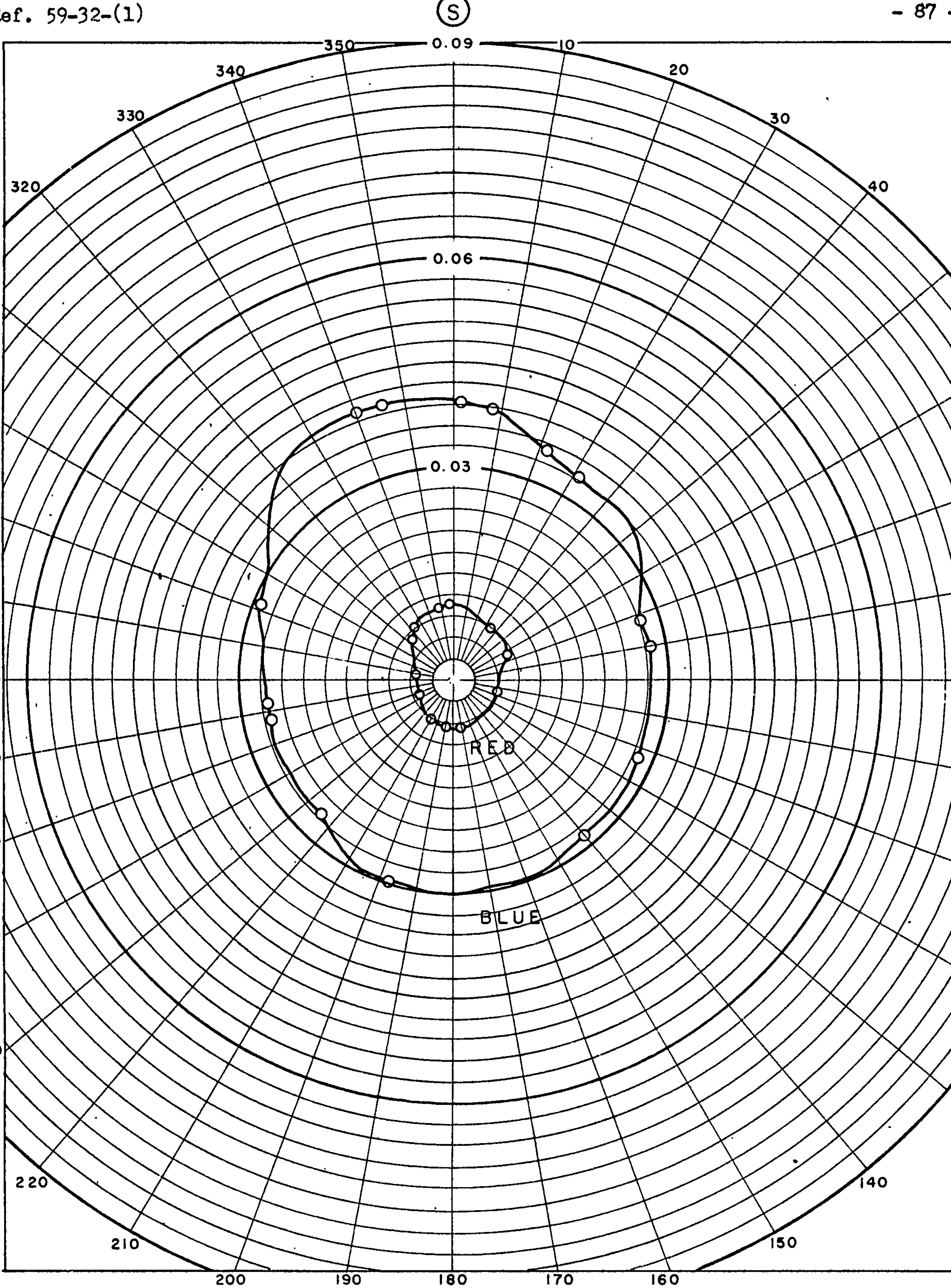

RADIANT PATH FUNCTION $N_*(17200, 90^\circ, \phi)$

WATTS $\Omega^{-1}\, FT^{-2}$ PER NAUTICAL MILE

BLUE AND RED RECORDS, 17200 FT. 0945 CDST

FIGURE 77
FLIGHT NO. 120
JUNE 21, 1958
CENTRAL MINNESOTA

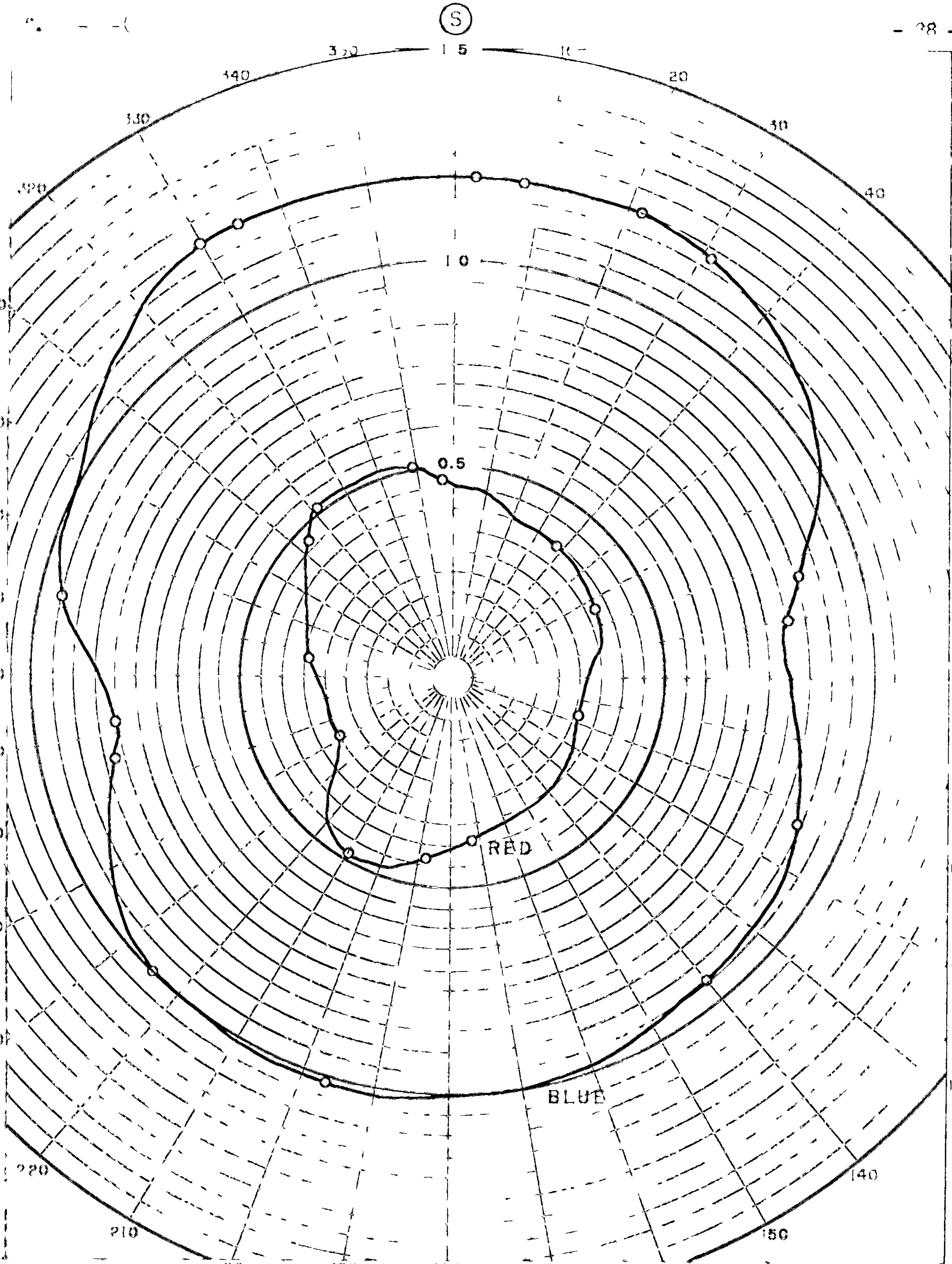

RADIANCE, HORIZONTAL N(17200, 90°, ϕ)
WATTS Ω^{-1} FT^{-2}
BLUE AND RED RECORDS, 17200 FT 0945 CDST

FIGURE 78
FLIGHT NO 120
JUNE 21, 1958
CENTRAL MINNESOTA

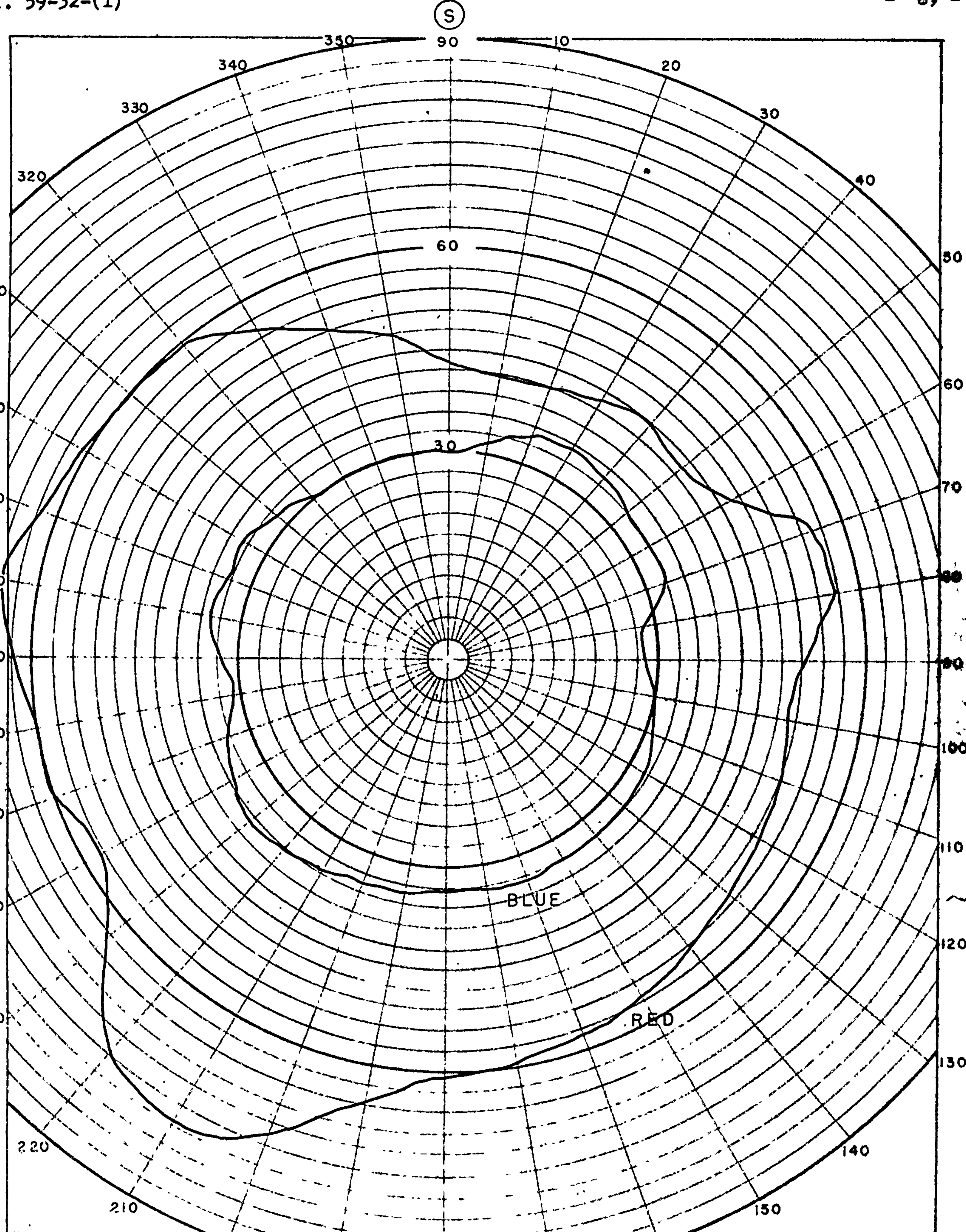

APPARENT ATTENUATION LENGTH L_A(17200)
NAUTICAL MILES
BLUE AND RED RECORDS, 17200' FT 0945 CDST

FIGURE 79
FLIGHT NO. 120
JUNE 21, 1958
CENTRAL MINNESOTA

DISCUSSION

Preface

The Visibility Laboratory of the University of California, La Jolla Campus, has been engaged for several years in an on-going research program concerning image transmission through the atmosphere. This program is discussed in "Image Transmission by the Troposphere I". [1] A reprint of this article is included in this report as Appendix I. Of special interest in Appendix I in connection with this report are notation, discussion of path function, attenuation length, and the concept of equilibrium radiance (and luminance).

Notation and Instrumentation

The notation used at the Visibility Laboratory is discussed in detail in Appendix I. This report follows that notation.

The photometric quantities illuminance and luminance are designated by E and B, respectively; the radiometric quantities irradiance and radiance are designated by H and N, respectively. In the parentheses following the basic symbols, z specifies altitude in feet, " - " indicates downwelling flux, " + " indicates upwelling flux, θ specifies the zenith angle of the path of sight of the photometer, and ϕ the azimuth angle of the photometer. In this report the azimuth angle is with respect to the sun.

1. S. Q. Duntley, A. R. Boileau, and R. W. Preisendorfer, "Image Transmission by the Troposphere I", Journal of the Optical Society of America, 47, pp. 499-506, (1957).

The photometric quantities are those recorded with a phototube-filter combination having the spectral sensitivity of the standard luminosity curve for the daylight-adapted human eye. This is shown in Figure 80. In this report this response is designated as the "photopic" response.

The phototubes are also filtered to respond to radiant energy in the blue end of the spectrum in accordance with the blue spectral sensitivity curve in the above mentioned Figure. Similarly, they are filtered to respond to radiant energy in the red end of the spectrum in accordance with the red spectral sensitivity curve in the same Figure. In this report these two sensitivities and responses to radiant energy recorded through these two filters are referred to as "blue" and "red" sensitivities and responses.

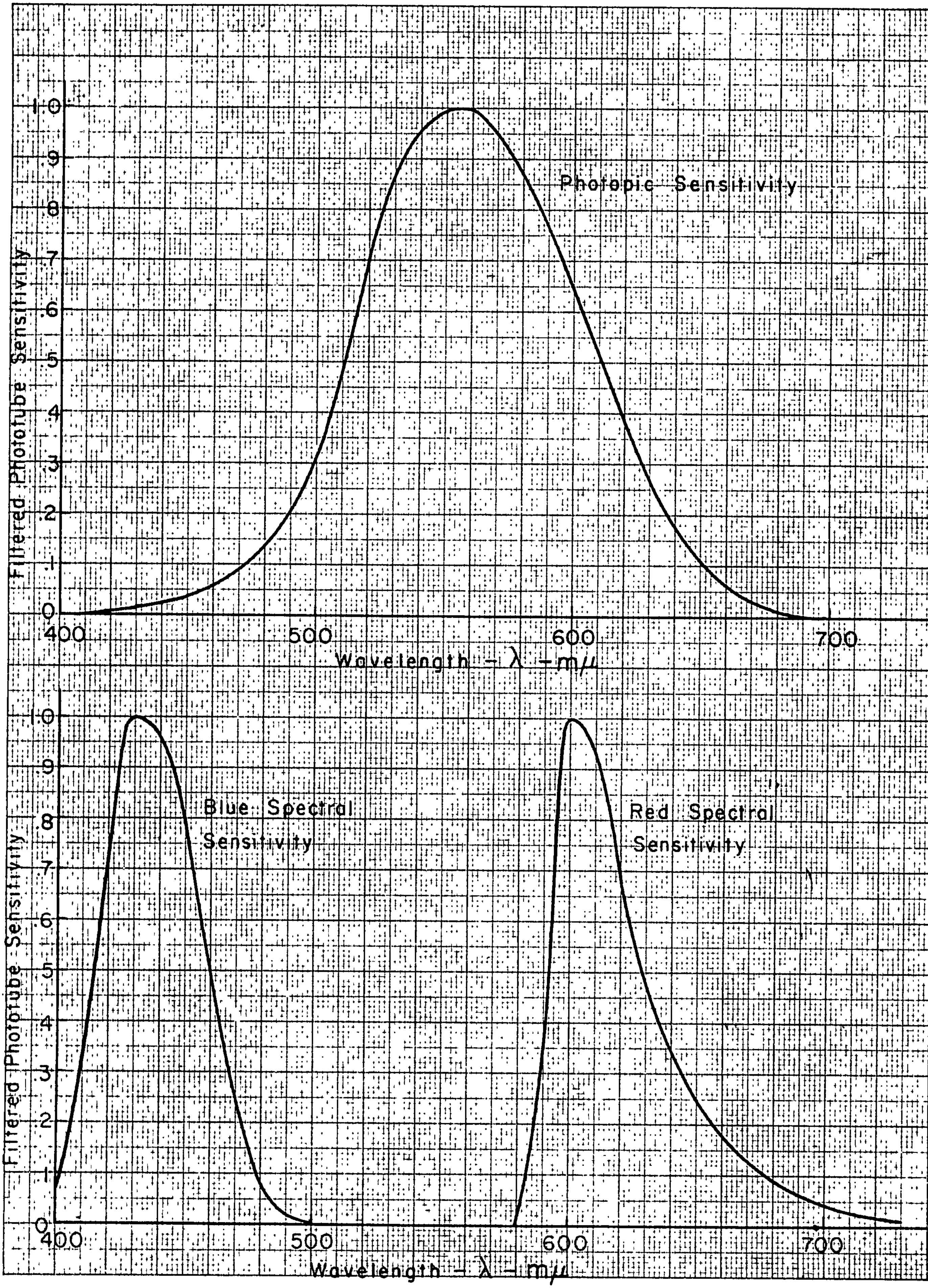
Photopic Sensitivity
Filtered Phototube Sensitivity
1.0
.9
.8
.7
.6
.5
.4
.3
.2
.1
0
400
500
600
700
Wavelength - λ - mμ
Blue Spectral Sensitivity
Red Spectral Sensitivity
Filtered Phototube Sensitivity
1.0
.9
.8
.7
.6
.5
.4
.3
.2
.1
0
400
500
600
700
Wavelength - λ - mμ

Figure 80

The filters used to provide the three filtered phototube spectral sensitivities are interposed in the flux path successively in each instrument by the action of a ratchet solenoid driving a wheel in which the filters are mounted. The ratchet solenoids are so controlled from the project engineer's station that all instruments have the same filter in position at any one time. The normal order of interposition of filters is photopic, blue, and red.

Recorded Optical Quantities

The following optical quantities were recorded during Flight 120:

Quantity	Symbol	Instrumentation
Illuminance, Downwelling Irradiance, Downwelling	E (z,-) H (z,-)	Measured on a horizontal flat plate collector.* A rotating device shadows the collector plate from the sun's rays twice each revolution, thus giving a measure of illuminance from diffuse sky light.
Illuminance, Upwelling Irradiance, Upwelling	E (z,+) H (z,+)	Measured on a horizontal flat plate collector.*
Luminance, Zenith Radiance, Zenith	B (z,0,0) N (z,0,0)	Measured by zenith telephotometer. Instrument is mounted so that when airplane is level it measures the average luminance (or radiance) of a 1° circular cone of zenith sky.
Luminance, Nadir Radiance, Nadir	B (z,180°,0) N (z,180°,0)	Measured by nadir telephotometer. Instrument is duplicate of zenith telephotometer. Mounted to measure the average luminance (or radiance) of a 1° circular cone of nadir sky.

---

* The flat plate collectors are made from translucent opal plastic. The plate is ground to a fine mat surface until the incident radiation is accepted in proportion to the cosine of the angle of incidence.

Luminance, Horizontal Radiance, Horizontal	$B\ (z,90^{\circ},\phi)$ $N\ (z,90^{\circ},\phi)$	Measured by equilibrium radiance telephotometer of attenuation meter. (See Figure 4, p. 503, in Appendix I.) This telephotometer measures average luminance or radiance of $\frac{1}{2}^{\circ}$ circular cone.
Horizontal Luminance Path Function Horizontal Radiant Path Function	$B_{*}(z,90^{\circ},\phi)$ $N_{*}(z,90^{\circ},\phi)$	Measured by path function telephotometer of attenuation meter. (See Figure 4, p. 503, in Appendix I.)
Luminance, Upper Sky Radiance, Upper Sky	$B\ (z,\theta,\phi)$ $N\ (z,\theta,\phi)$ $0 \leq \theta \leq 90^{\circ}$	Measured by upper hemisphere scanning telephotometer. This instrument measures the average luminance (or radiance) of a 5° circular cone of sky as it sweeps from horizon to horizon through the zenith, making 10° steps in azimuth between each elevation sweep. A complete map of upper sky is made in 18 sweeps in 90 seconds.
Luminance, Lower Sky Radiance, Lower Sky	$B\ (z,\theta,\phi)$ $N\ (z,\theta,\phi)$ $90^{\circ} \leq \theta \leq 180^{\circ}$	Measured by lower hemisphere scanning telephotometer. This instrument is similar to upper hemisphere scanning telephotometer in that it has a 5° acceptance angle and makes a comple lower sky map in 90 seconds; it is dissimilar to the upper scanning telephotometer in that its elevation sweep and azimuth movement are combined, the scanne swinging in azimuth at a constant rate of ten degrees for each 180° elevation sweep.

Computed Optical Property

The following optical property is computed from two measured quantities:

Apparent Attenuation Length [2]	$L_A(z)$	Computed from path function, photometric or radiant, and horizontal luminance or horizontal radiance as follows:

$$L_A(z) = \frac{B(z,90^\circ,\phi)}{B_*(z,90^\circ,\phi)} \quad \text{or} \quad \frac{N(z,90^\circ,\phi)}{N_*(z,90^\circ,\phi)}$$

---

2. The measured horizontal radiance, $N(z,90^\circ,\phi)$, if the atmosphere is sufficiently clear, will have a lesser numerical value than the horizontal equilibrium radiance, $N_q(z,90^\circ,\phi)$. This is due to the curvature of the earth and its atmosphere. This causes the ratio of measured horizontal radiance to radiant path function, $N(z,90^\circ,\phi) / N_*(z,90^\circ,\phi)$, to be less than the ratio of horizontal equilibrium radiance to radiant path function, $N_q(z,90^\circ,\phi) / N_*(z,90^\circ,\phi)$. This second ratio is defined as attenuation length,

$$L(z) = N_q(z,90^\circ,\phi) / N_*(z,90^\circ,\phi)$$

The first ratio is defined as apparent attenuation length,

$$L_A(z) = N(z,90^\circ,\phi) / N_*(z,90^\circ,\phi)$$

Because $N(z,90^\circ,\phi)$ on a clear day is less than $N_q(z,90^\circ,\phi)$, the apparent attenuation length is less than attenuation length, i.e., $L_A(z) < L(z)$.

The report "Theory of Attenuation Measurements in Planetary Atmospheres", R. W. Preisendorfer, Scripps Institution of Oceanography, University of California, La Jolla Campus, SIO Ref. 58-81, of 24 November 1958 discusses this in detail.

Subsequent to Flight 120 a scanning device was installed on the horizontal radiance telephotometer by which the differences between measured horizontal radiances and horizontal equilibrium radiances could be determined by means of equations developed in the above mentioned report (SIO Ref. 58-81). Only one test flight using this technique was possible prior to the decommissioning of the airplane. The differences were found to be negligible for the blue response, and not over 5% for the photopic and red responses and this only at altitudes of 10000 to 20000 feet.

Operational Procedure

To record the measurements of the various optical quantities three different flight patterns are normally used. In sky mapping the airplane is maintained in straight and level flight for 90 seconds; during this time the filters are not changed. Path function measurements for 360° in azimuth require a left hand circular flight path at 30° bank; during this time the filters are cycled to permit recording of comparable photometric and radiometric data. To record data as a function of altitude the airplane is held in a level attitude and by use of reduced power and extended flaps is allowed to descend. The flight procedure must be a composite of the different flight patterns to get the greatest amount of reliable data in the shortest elapsed time.

The three types of flight patterns are described in greater detail as follows:

"A" run. Airplane maintained level, at constant altitude and constant heading for duration of sky mapping. Usually two "A" runs are made in succession, 90 seconds each, with filters changed between runs. Another "A" run on reverse course with third filter selection completes sky map in photopic, blue, and red spectral sensitivities and returns airplane to starting point vicinity. During the run all other optical instruments are recording.

"B" run. Airplane is flown in a left handed, 30° bank, 360° turn during which horizontal path function and horizontal luminance (and radiance) are recorded. Each cardinal and inter-cardinal compass heading is identified by the co-pilot and indicated electrically on instrument records. Filters are cycled by hand from project engineer's position. At conclusion of "B" run airplane is put into right hand 360° turn during which time project engineer photographs sky at cardinal and inter-cardinal compass headings.

"L" run. Airplane is maintained in level attitude, on constant heading, but with altitude decreasing approximately 1000 feet per minute. (This is accomplished by lowering landing gear, extending flaps, and reducing power, the flap extension and power reduction being adjusted to give a suitable descent rate at level attitude.) All optical instruments are recording during this run except upper and lower sky scanning telephotometers. Filters are cycled by hand from project engineer's position.

The usual sequence of data-gathering runs is:

"A" runs at maximum altitude for sky maps, using successively the three optical filters.

"B" runs for path function and horizontal luminance and radiance measurement.

"B" run for photographing sky.

"L" run from maximum to middle altitude.

Repeat "A" and "B" runs at middle altitude followed by "L" run from middle to minimum altitude.

Repeat "A" and "B" runs at minimum altitude.

The "L" runs vary in length, usually because of meteorological conditions. If there are no pronounced haze layers seen during ascent, or, if no temperature inversion is apparent, the procedure would be as outlined above. If, however, there were some meteorological or other condition to warrant it, the flight procedure would be changed. For example, in Flight 120 the first part of the flight followed the usual pattern, i.e., "A" and "B" runs at 21000 feet, "L" run to 11000 feet, "A" and "B" runs at 11000 feet, "L" run to 2000 feet, "A" and "B" runs at 2000 feet. But then the pattern was changed.

After "A" and "B" runs at 2000 feet, an ascent to 6000 feet followed by an "L" to 2000 feet was made. This was done to re-record the data in case moisture had condensed on the optics of the equilibrium luminance telephotometer due to failure of the telephotometer heating system. The "A" or "B" runs were not repeated; and the airplane was taken again to 20000 feet.

Upon arrival at 20000 feet it was necessary to catch up to the balloons. During the chase the airplane climbed to 22000 feet. Also during the chase the cloud deck at 10500-16500 feet continued to fill in. After the airplane had reached the vicinity of the balloons, "A" and "B" runs were made, followed by an "L" run terminating at 16400 feet, the top of the cloud deck. This was followed by "A" and "B" runs at 17200 feet.

At the conclusion of the "A" and "B" runs at 17200 feet the airplane had been airborne for nearly six hours and because this exceeded the estimated flight time for the exercise the fuel on board was getting low. (Excess fuel adds unnecessary weight to be carried to 20000 feet so the amount of fuel at take off was that for the estimated flight time plus a safety factor.) Accordingly the airplane left the vicinity of the balloons and proceeded toward Minneapolis until a break in the clouds permitted a descent through the cloud deck. Maintaining the same course an "L" run was made below the clouds, from 10000 feet to 2000 feet, followed by three "A" runs at 2000 feet. At the conclusion of the "A" runs the exercise was terminated and the airplane continued on to Minneapolis.

Cycling of Filters

The operation of the optical filter selection mechanism is different for the three different types of runs. In the "A" runs each filter remains in the flux path until a complete sky map is obtained. In the "B" and "L" runs the filters are cycled, but at different rates. This discussion covers filter cycling during "B" and "L" runs.

In making "B" runs either of two modes of filter operation can be used. One is to cycle the filters during the 360° turn, the other is to make three 360° turns with the filters changed at the end of each turn. The advantage of the first method is that the data obtained in the three spectral ranges apply to the same air parcel. Additionally, this is accomplished in one turn of four minute duration. The main disadvantage of the method is that the data plotted as three separate curves are incomplete and missing portions of the curves must be constructed; and this has proved to be more difficult than expected.

In the second method the data recorded in each turn for each filter are complete and the data so recorded and plotted are more reliable than that obtained by the first method. There are three disadvantages, however. First, the airplane does not necessarily retain its flight path and a different sample of air is measured, secondly, at four minutes per turn the time utilized in "B" runs is extended, and thirdly, if the same flight path is followed successive turns are in air contaminated with engine exhaust products. Both of these methods have been tried and from the results obtained the decision was made to use the first method, that is, the one turn method with filters cycled during turn, during Flight 120.

The cycling of filters during the "B" runs was done on a nominal eight-second period. To identify the record by spectral response the photopic filter was used for four seconds, followed by blue for two seconds and red for two seconds.

The cycling of the filters for the "L" runs is a must if comparable spectral data are to be recorded. The method of making several "L" runs with one filter for each run introduces relatively large time variations with changes of sun's elevation, and air movement taking place such that the instrument probes during two successive runs cannot possibly be sampling the same air. The period of cycling during the "L" runs is dictated by the rotation of the shadowing device on the upper hemisphere illuminometer, it being very desirable to get one shadowed reading during each filter positioning. This established the filter cycling period of about sixteen seconds, i.e., eight seconds on photopic response, and four seconds each for the blue and red responses. Since ten, five, and five are easier to see on a watch dial this was the cycling pattern.

Because the atmosphere is stratified the data recorded by the various measurements do not plot as simple curves but show considerable structure. In the cases of the instruments looking upward or downward and those receiving illuminance or irradiance the effect of the stratification is to show gradual changes. In these instruments cycling of filters can be tolerated. In the case of the instruments with a horizontal line of sight, specifically the path function meter and the equilibrium luminance telephotometer, the stratification has a pronounced effect as the instruments are moved vertically. The measurement made through the filter which is in the flux path as the stratum is entered is the accurate one; the other two filtered quantities are measured before and after entering the stratum. To plot graphs of these two quantities it has been necessary to accept the shape of the graph of the recorded quantity.

To overcome the disadvantages of cycling the filters in the horizontally seeing instruments the path function meter and equilibrium telephotometers are being redesigned to record simultaneously the three spectral quantities through beam-splitting prisms and three separate filter-phototube combinations.

APPENDIX I

Reprinted from JOURNAL OF THE OPTICAL SOCIETY OF AMERICA, Vol. 47, No. 6, 499–506, June, 1957
Printed in U. S. A.

Image Transmission by the Troposphere I*

SEIBERT Q. DUNTLEY, ALMERIAN R. BOILEAU, AND RUDOLPH W. PREISENDORFER
Scripps Institution of Oceanography,† University of California, La Jolla, California

(Received November 15, 1956)

Quantitative treatment of the apparent luminance of distant objects and the reduction of apparent contrast along inclined paths of sight through real atmospheres has been accomplished by means of optical data taken from an aircraft in flight. Sample data from a single flight are used to illustrate some of the principles involved. Correlation has been found between the humidity profile of the atmosphere and its optical properties.

INTRODUCTION

DISTANT objects are usually viewed, photographed, or televised by means of some path of sight through the atmosphere. Conventional principles of geometrical and physical optics suffice to describe the nature of the final image except for effects due to the atmosphere. In most circumstances, however, the configuration of the image and its information content is affected, often seriously, by its transmission from the object to the receiver. The atmosphere can be regarded as a transmission link in the object-to-image chain and the concomitant effect of the pertinent optical atmospheric properties can be regarded as governing its *image transmission.*

This paper is intended as the first of a series describing the results of an extensive on-going research program which has already been in progress for several years. Results from numerous theoretical and experimental investigations of image transmission phenomena are ready to be reported and further research of many kinds is in progress. Experimental results from a single flight comprise the factual content of this first paper and the equations are limited to certain general relations needed for the practical utilization of the data; this is in keeping with the scope of the oral version of the paper as presented at the Cambridge meeting of the International Commission on Optics.

The specially instrumented B-29 aircraft used to collect the data reported in this paper has, on other flights, secured data up to 30 000 ft under several different atmospheric and lighting conditions; and subsequent papers in the series will present data from these and other flights. The optical properties of the troposphere are of special interest because most viewing takes place through it. Roughly three-fourths of the atmosphere lies within the troposphere and because this lower air often contains haze, clouds, dust, and rain it seriously affects image transmission more frequently than do the higher strata. Exploration of image transmission phenomena in the stratosphere must await an opportunity to instrument a vehicle having greater altitude capability.

SOME GENERAL PRINCIPLES‡

Introduction

In the absence of appreciable atmospheric boil[1] the apparent radiance of any distant object is the sum of two independent components: (1) residual image-forming light from the object that has traversed the atmospheric path without having been scattered or absorbed; (2) radiance created by the scattering of ambient light throughout the path of sight, including sunlight, skylight, earth-shine, etc. Only the first component contains information about the object, for the second is the result of scattering processes throughout the path of sight and is, therefore, independent of the nature of the object. In this paper the image transmission of any path of sight will be specified in terms of the transmittance of the entire path and the path radiance. No theoretical model for the atmosphere is needed; consequently, nearly all restrictive assumptions are avoided and the equations can be used to describe any path of sight through all real isotropic atmospheres with any lighting condition. To be useful in practice, these equations must be supplied with data and these are becoming available as a result of the flight research program now in progress.

Notation

The notation used in this paper has been adopted with great care and on the basis of experience accumulated over many years. It is designed to fulfill many

* Presented at the Fourth Congress of the International Commission of Optics, held in Cambridge-Boston, Massachusetts, March 28–April 3, 1956. Published with financial assistance from UNESCO and the International Union of Pure and Applied Physics.

† Contribution from the Scripps Institution of Oceanography, University of California, New Series No. 921. This work has been supported by the Geophysical Research Directorate of the Air Force Cambridge Research Center and the Bureau of Ships of the U. S. Navy under contracts NObs-43356, NObs-50274, NObs-72039, and NObs-72092.

‡ The principles presented in this paper and in subsequent papers of this series were formulated in unpublished lecture notes used within the Visibility Laboratory of the Scripps Institution of Oceanography which include, generalize, and extend earlier work by the authors and others (R. W. Preisendorfer, "Lectures on photometry, hydrological optics, atmospheric optics," Fall, 1953, Vol. I).

[1] Duntley, Culver, Culver, and Preisendorfer, J. Opt. Soc. Am 42, 877A (1952); publication of this paper is planned.

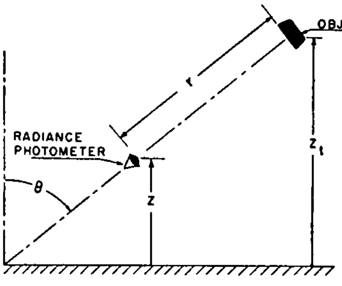

FIG. 1. Illustrating the geometry of the path of sight.

requirements: It is suited to the terrestrially-based system of altitudes and directions in which flight data must be taken and it is fully compatible with the more powerful vector notation required for the generalized theoretical treatments of image transmission and radiative transfer phenomena to follow It is compatible also with the notation commonly used in several mathematically allied fields of physics, as for example, neutron diffusion theory. It is extendable to hydrological optics, a natural counterpart of meteorological optics, in which the authors of this paper are deeply interested.

The basic symbol employed for the spectral radiance is N, and the symbol for luminance is B. The altitude of the photometer is denoted by z, the height above mean sea level. The direction of any path of sight is specified by a zenith-angle θ and an azimuth angle ϕ, the photometer being directed upward when $0\leq\theta<\pi/2$, as in Fig. 1; z, θ, and ϕ are always written as parenthetic attachments to the parent symbol. When the post subscript r is appended to any symbol, it denotes that the quantity pertains to a path of length r. The subscript 0 always refers to the hypothetical concept of a photometer located at zero distance from the object, as, for example, in denoting the *inherent* radiance of a surface. Pre-subscripts identify the object, thus the pre-subscript b refers to background, and t to object or visual target. Thus, the (monochromatic) *inherent spectral radiance* of an object t at altitude z_t as viewed in the direction (θ,ϕ) is ${}_tN_0(z_t,\theta,\phi)$ and the corresponding apparent radiance observed in the direction (θ,ϕ) at any other altitude z is ${}_tN_r(z,\theta,\phi)$ where $z_t=z+r\cos\theta$. A post-superscript *, or post-subscript $_*$ is employed as a mnemonic symbol signifying that the radiometric quantity has been generated by the scattering of ambient light reaching the path from *all directions*. Thus $N_r^*(z,\theta,\phi)$ is the spectral path radiance observed at altitude z in the indicated direction, and $N_*(z,\theta,\phi)$ is used to denote *path function*, a quantity defined later in this paper.

The (monochromatic) *apparent spectral radiance* of any distant object t is

$$ {}_tN_r(z,\theta,\phi)=T_r(z,\theta,\phi)\ {}_tN_0(z_t,\theta,\phi)+N_r^*(z,\theta,\phi), \quad (1)$$

where the first term on the right is the residual image-forming light from the object and the second term is the path radiance due to scattering processes throughout the path. $T_r(z,\theta,\phi)$ is the spectral transmittance of the path for image-forming rays; it includes the factor $[n(z)/n(z_t)]^2$ required by geometrical optics whenever the index of refraction of the medium at the observer $[n(z)]$ differs from the index of refraction of the medium at the target $[n(z_t)]$. In the case of paths of sight through the troposphere the departure of $[n(z)/n(z_t)]^2$ from unity is negligible. The transmittance of the path is a property of the atmosphere throughout the path and is independent of the distribution of the ambient lighting; in the case of any path of sight through the troposphere it is the same for upward or downward transmissions, thus $T_r(z,\theta,\phi)=T_r(z_t,\pi-\theta,\pi+\phi)$ where $z_t=z+r\cos\theta$. Because forward scattering generally exceeds backward scattering, reversibility is not true of the path radiance $N_r^*(z,\theta,\phi)$ except for a few symmetrical lighting conditions, such as (1) horizontal paths of sight under a uniform overcast, and (2) a horizontal path at right angles to the plane of the sun provided both the radiance distributions of the sky above and the earth below the path are symmetrical with respect to the plane.

The image transmitting properties of the atmosphere can be separated from the optical properties of the object by the introduction of the *contrast* concept:

The *inherent spectral contrast* $C_0(z_t,\theta,\phi)$ of an object is, by definition,

$$C_0(z_t,\theta,\phi)=[{}_tN_0(z_t,\theta,\phi)-{}_bN_0(z_t,\theta,\phi)]/{}_bN_0(z_t,\theta,\phi). \quad (2)$$

The corresponding definition for *apparent spectral contrast* is

$$C_r(z,\theta,\phi)=[{}_tN_r(z,\theta,\phi)-{}_bN_r(z,\theta,\phi)]/{}_bN_r(z,\theta,\phi). \quad (3)$$

The apparent and inherent background radiances are related by the expression

$${}_bN_r(z,\theta,\phi)=T_r(z,\theta,\phi)\ {}_bN_0(z_t,\theta,\phi)+N_r^*(z,\theta,\phi). \quad (4)$$

Theorems

Subtracting Eq. (4) from Eq. (1) yields the relation

$$[{}_tN_r(z,\theta,\phi)-{}_bN_r(z,\theta,\phi)] = T_r(z,\theta,\phi)[{}_tN_0(z_t,\theta,\phi)-{}_bN_0(z_t,\theta,\phi)]. \quad (5)$$

Thus, radiance differences are transmitted along inclined paths with the same attenuation as that experienced by each image-forming ray.

If Eq. (5) is divided by the apparent radiance of the background ${}_bN_r(z,\theta,\phi)$ and combined with Eq. (3), the result can be written:

$$C_r(z,\theta,\phi)=T_r(z,\theta,\phi) \times[{}_tN_0(z_t,\theta,\phi)/{}_bN_r(z,\theta,\phi)-{}_bN_0(z_t,\theta,\phi)/{}_bN_r(z,\theta,\phi)]. \quad (6)$$

When the inherent radiance of the background is very dark, as in the case of an object at high altitude, the second term in the brackets on the right side of Eq. (6) may be negligible.

Combining Eqs. (2) and (6) yields the expression

$$C_r(z,\theta,\phi)/C_0(z_t,\theta,\phi) = T_r(z,\theta,\phi)\ {}_bN_0(z_t,\theta,\phi)/{}_bN_r(z,\theta,\phi). \quad (7)$$

The right-hand member of Eq. (7) is an expression for the *contrast transmittance* of the path of sight; it is independent of the optical properties of the object. Equation (7) is the law of contrast reduction by the atmosphere expressed in its most general form.[2]

An interesting variant of Eq. (7) formed by combination with Eq. (4) is the following expression in which *contrast transmittance* is characterized in terms of path radiance and apparent background radiance:

$$C_r(z,\theta,\phi)/C_0(z_t,\theta,\phi) = 1 - [N_r^*(z,\theta,\phi)/{}_bN_r(z,\theta,\phi)]. \quad (8)$$

The apparent indeterminateness of Eqs. (7) and (8) when applied to the case of objects outside the atmosphere can be avoided by the use of the limiting form of Eq. (6), as follows:

$$C_r(z,\theta,\phi) = T_r(z,\theta,\phi)\ {}_tN_0(z_t,\theta,\phi)/{}_bN_r(z,\theta,\phi). \quad (9)$$

It should be emphasized that Eqs. (1) through (9) are completely general; they apply rigorously to any path of sight regardless of the extent to which the scattering and absorbing properties of the atmosphere or the distributions of lighting exhibit nonuniformities from point to point. No theoretical model of the atmosphere is involved and no restrictive assumptions have been made. The equations can be used in treating all real atmospheres and all real lighting conditions. This is in sharp distinction to treatments of the subject which are based upon theoretical models of the atmosphere which invariably involve major assumptions such as horizontal uniformity, exponential lapse rate of air density, vertical uniformity of particle size distribution, negligible earth curvature, etc.

Equation of Transfer

Image-forming light is lost by scattering and absorption in each elementary segment of the path of sight and contrast-reducing path radiance is generated by the scattering of the ambient light which reaches the segment from all directions. The quantitative description of this scattered component of path-segment radiance involves a quantity called the *path function* and denoted by the symbol $N_*(z,\theta,\phi)$, where the mnemonic subscript symbol $_*$ is used both to suggest light reaching the path segment from all directions and to denote that the quantity is a point function. The parenthetical symbols (z,θ,ϕ) indicate that the path function depends upon the direction of image transmission and upon the location of the segment in the path of sight. The path function depends upon the directional distribution of

[2] Equation (7) is a generalization of Eq. (15) on p. 183 of Q. Duntley, J. Opt. Soc. Am. 38, 179 (1948).

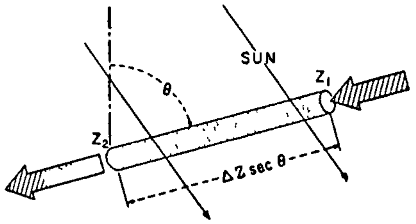

FIG. 2. Illustrating the derivation of the equation of transfer. Δz is defined as z_1-z_2, so that $\Delta r=\Delta z\sec\theta$ is always non-negative. The difference $\Delta N(z,\theta,\phi)$ between output and input is $N(z_2,\theta,\phi)-N(z_1,\theta,\phi)$.

the lighting on the segment due to its surroundings; it can be operationally defined in terms of the (limiting) ratio of the path radiance associated with a short path to the path length by the relation $N_*(z,\theta,\phi)=\lim(\Delta r\rightarrow 0)\times N_{\Delta r}^*(z,\theta,\phi)/\Delta r$. In experimental practice, the path length Δr should be sufficiently short that no change in the ratio can be detected if Δr is made shorter. Apparatus for path function measurement has been built and will be described elsewhere.

The loss in image-forming light due to attenuation by scattering and absorption within any path segment is proportional to the amount of image-forming light present; the coefficient of proportionality will be written in the reciprocal form $1/L(z)$, and $L(z)$ will be referred to as the *attenuation length*. $L(z)$ is a function of position within the path of sight; it does not depend upon the image transmission direction unless the aerosol is anisotropic, as sometimes occurs in the case of falling snow; it is independent of the manner in which the path segment is lighted by the sun or sky; it is a physical property of the atmosphere alone. Attenuation includes loss of image-forming radiance by absorption and by scattering. Absorption refers to any thermodynamically irreversible transformation of monochromatic radiant energy including, primarily, conversion of light into heat but also fluorescence phenomena, photochemical processes, etc. Attenuation by scattering results from any change of direction sufficient to cause the radiation to fall outside the summative radius of the detector mosaic.

In any path segment of length $\Delta r=\Delta z\sec\theta$, as illustrated by Fig. 2, the difference $\Delta N(z,\theta,\phi)$ between output and input radiance is attributable to a gain term $N_*(z,\theta,\phi)\Delta r$ and a loss term $N(z,\theta,\phi)\Delta r/L(z)$, so that $\Delta N(z,\theta,\phi)=N_*(z,\theta,\phi)\Delta r-N(z,\theta,\phi)\Delta r/L(z)$. This relation may be rewritten

$$\Delta N(z,\theta,\phi)/\Delta z\sec\theta = N_*(z,\theta,\phi) - N(z,\theta,\phi)/L(z). \quad (10)$$

In conformity with usage in other fields of physics Eq. (10) will be referred to as the incremental form of the *equation of transfer*. It is implicit in this equation that Δz must be taken sufficiently small so that over this interval $L(z)$ and $N_*(z,\theta,\phi)$ may be regarded as constants within the precision of experimental data.

Equation (10) is a steady-state equation of continuity,[3] based upon the conservation of energy principle; it refers only to nonemitting atmospheres, since an additional term would be needed to represent emission of radiation in the path, as by fluorescence, recombination phenomena, particle excitation, etc. Self-radiosity within the visible spectrum appears to be of negligible importance in the troposphere. Equations (1) and (4) may be regarded as integral forms of the equation of transfer.

The equation of transfer and the concepts of attenuation length and path function share the same generality as the concepts associated with Eqs. (1) through (9): No theoretical model atmosphere has been employed; each of the equations in this paper is applicable to all real isotropic atmospheres, all lighting conditions, and all paths of sight. The use of the equation of transfer in numerical summation procedures involving experimental data will be illustrated in a later section of this paper. Only when Eq. (10) is simulated by a differential equation and an analytic integration performed does the introduction of a theoretical model for the atmosphere become necessary; this will not be done in the present paper.

Equilibrium Radiance

Many image transmission phenomena are most clearly understandable in terms of the concept of *equilibrium radiance*. This concept is a natural consequence of the equation of transfer, which indicates that some unique *equilibrium radiance* $N_q(z,\theta,\phi)$ must exist at each point such that the loss of radiance within the path segment is balanced by the gain, i.e., $\Delta N_q(z,\theta,\phi)=0$. Thus

$$0=N_*(z,\theta,\phi)-N_q(z,\theta,\phi)/L(z), \quad \text{so that}$$

$$N_q(z,\theta,\phi)=N_*(z,\theta,\phi)L(z) \tag{11}$$

and the equation of transfer (10) may be rewritten as follows:

$$\Delta N(z,\theta,\phi)/\Delta z \sec\theta=[N_q(z,\theta,\phi)-N(z,\theta,\phi)]/L(z). \tag{12}$$

Equation (11) shows that each segment of every path of sight has associated with it an equilibrium radiance, and Eq. (12) states that the average space rate of change in image-forming radiance caused by the path segment is in such a direction as to cause the output radiance to be closer to the equilibrium radiance than is the input radiance. This segment-by-segment convergence of the apparent radiance of the object to the dynamic equilibrium radiance is illustrated by the data in Fig 6 of this paper.

[3] The equation of transfer has been generalized to the transient case, and rigorously derived for an arbitrary optical medium, using the concepts of measure theory. R. W Preisendorfer, "A mathematical foundation for radiative transfer theory," Doctoral dissertation, U C.L.A., May 1956. An exposition of this theory has been submitted for publication in the Journal of the Optical Society of America.

When the path of sight is horizontal and optically uniform both in terms of the composition of the aerosol and its lighting, the equilibrium radiance is identical with the apparent radiance of the horizon. The apparent radiance of distant objects inherently more radiant than the equilibrium value decreases toward the equilibrium radiance as an asymptote; conversely the apparent radiance of any dark distant object approaches the same asymptote.

Equilibrium Contrast

Many of the foregoing equations can be rewritten in terms of *equilibrium contrast*, $C_q(z,\theta,\phi)$, which is defined by the relation

$$C_q(z,\theta,\phi)=[{}_tN_r(z,\theta,\phi)-N_q(z,\theta,\phi)]/N_q(z,\theta,\phi). \tag{13}$$

Notation of the type defined by Eq. (13) enables the equation of transfer (10) to be written

$$\Delta C_q(z,\theta,\phi)/\Delta z \sec\theta=-C_q(z,\theta,\phi)/L(z) \tag{14}$$

or

$$\Delta C_q(z,\theta,\phi)/C_q(z,\theta,\phi)=-\Delta z \sec\theta/L(z), \tag{15}$$

provided that the equilibrium radiance $N_q(z,\theta,\phi)$ is constant on the segment of path under discussion. In this case the fractional change in equilibrium contrast depends only upon the ratio of the length of the path segment to the attenuation length. The negative signs throughout Eqs. (14) and (15) signify that equilibrium contrast decreases in absolute magnitude in the segment.

EXPERIMENTAL METHODS

Introduction

The apparent radiance of any distant object can be computed by means of Eq. (1) if the transmittance of the path of sight and the path radiance are calculated from experimental data. This can be done from profiles of attenuation length and path function for the path of sight by means of the relations

$$T_r(z,\theta,\phi)=[n(z)/n(z_t)]^2\prod_{i=1}^{m}\exp\{-\Delta r/L(z_i)\}$$

$$=[n(z)/n(z_t)]^2\exp\{-\Delta r\sum_{i=1}^{m}1/L(z_i)\} \tag{16}$$

and

$$N_r^*(z,\theta,\phi)=\Delta r\sum_{i=1}^{m}T_{r_i}(z,\theta,\phi)N_*(z_i,\theta,\phi), \tag{17}$$

where the vertical height $|z_t-z|$ of the path is divided into m equal segments of length Δz, and $\Delta r=\Delta z \sec\theta$. $L(z_i)$ and $N_*(z_i,\theta,\phi)$ are the mean values of L and N_* in the ith segment. $r_i=(i-1)\Delta r$, $i=1,\cdots,m$.

Attenuation Profile

An experimental technique for measuring the vertical profile of attenuation length in horizontally uniform atmospheres has been devised around an air-borne version of an instrument based upon principles described earlier.[4,5] Figure 3 shows this attenuation meter mounted on the B-29 aircraft used by the Visibility Laboratory in its flight research program. The optical system is shown diagrammatically in Fig. 4. The for-

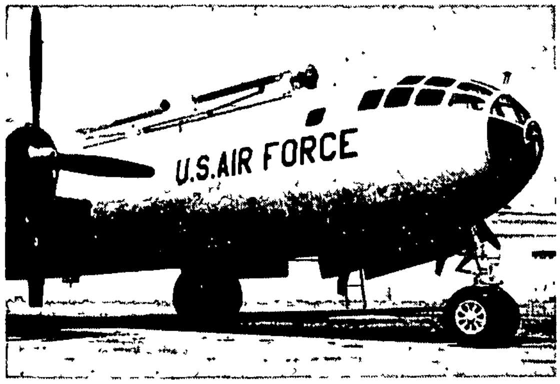

FIG. 3. Specially instrumented B-29 aircraft used to collect the data presented in this paper. The long cylindrical apparatus on top of the fuselage is the *attenuation meter*, shown schematically in Fig. 4. The smaller cylindrical device which appears slightly forward of the attenuation meter is the sky-scanning telephotometer. It consists of an end-on type multiplier phototube mounted at the focal point of a parabolic front-surfaced mirror 12 in. diam. Scanning is accomplished automatically by means of a turret and trunion mounting; scanning time for the entire hemisphere is 90 sec. Field of view, adjustable by means of interchangeable field stops, was circular, 5° in angular diameter in the case of the data shown in Fig. 6. Sensitivity is sufficient to map even the darkest high-altitude night skies. Spectral response is controlled by absorption filters. A similar (downward-viewing) telephotometer is mounted beneath the aircraft but is not shown by this photograph.

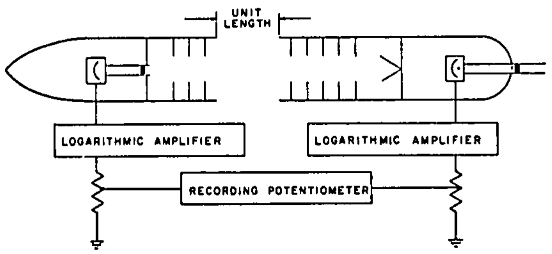

FIG. 4. Schematic diagram of the air-borne attenuation meter. The forward photoelectric telephotometer measures the equilibrium radiance; the rear telephotometer measures the radiance of a path of unit length. The latter radiance is numerically equal to the horizontal path function in the direction of flight. Multiplier phototubes and Sweet-type logarithmic circuits enable direct recording of the ratio of these radiances, i.e., of the attenuation length [see Eq. (11)]. Wind-tunnel tests of the aerodynamic design showed ambient pressure throughout the unit path. Light trap design, stray-light treatment, and photoelectric sensitivity are sufficient to enable measurement of attenuation lengths up to 200 nautical miles when the phototube spectral sensitivity is rendered photopic by means of absorption filters.

[4] S. Q. Duntley, U. S. Patent No. 2,661,650.
[5] S. Q. Duntley, J. Opt. Soc. Am. 39, 630A (1949).

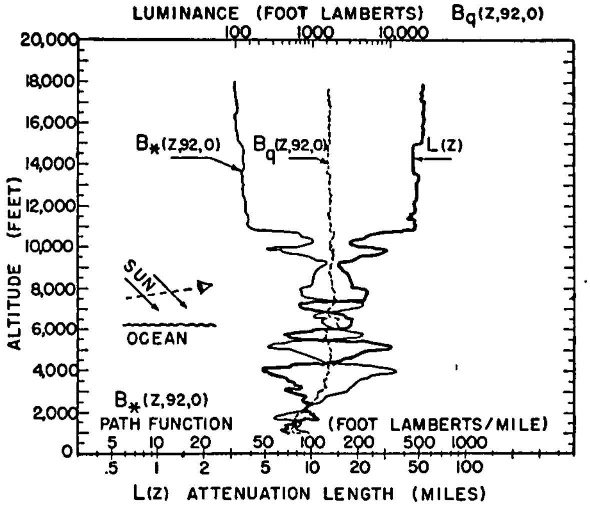

FIG. 5. Measured profiles of path function and attenuation length over the Atlantic Ocean off the coast of Florida, March 10, 1956. Flight 77. Sun position zenith angle = 48°, azimuth = 140° clockwise from true north. Path function: zenith angle $\phi = 92°$; azimuth $\theta = 0°$ from the plane of the sun. Sky condition: cloudless, blue. Approximately 36 hr after the passage of a major front. Very light ground haze with top at 4000 ft. The profile of equilibrium luminance was computed by means of Eq. (11).

ward telephotometer is directed toward the horizon and measures the equilibrium radiance of the horizontal path of sight in the direction of flight of the aircraft. The rear telephotometer measures the radiance of a path of unit length; this is numerically equal to the path function. The attenuation length is the ratio of the equilibrium radiance to the path function, as shown by Eq. (11). Recording potentiometers within the aircraft record the outputs of both telephotometers as well as their ratio.

Despite the use of multiplier phototubes, the low level of radiance produced by scattering processes in clear high altitude air precluded the use of narrow-band interference or absorption filters in the airborne attenuation meter. Because it was not possible to measure the spectral radiances called for by the equations given in this paper, each phototube was carefully corrected by means of specially constructed absorption filters to measure luminous quantities. For reasons of rigor the equations in this paper are written with the symbol N, denoting spectral radiance, but it will be understood that these same equations have been used with N replaced by B, denoting luminance, in the treatment of the illustrative data shown in Figs. 5 through 8.

During the flight for which data is given in this paper, the aircraft maintained a constant (southerly) heading and a fixed attitude which held the attenuation meter pointed at the desired portion of the horizon sky while making a controlled, rapid descent from 18 000 ft to 1000 ft at a rate of approximately 1500 ft per min. The resulting profiles of path function, equilibrium luminance, and attenuation length are shown in Fig. 5.

It will be noted that the equilibrium luminance (horizon luminance) was nearly independent of altitude. Repeated descents have demonstrated that the major details of these curves are repeatable.

The transmittance of any inclined path of sight having terminal altitudes between 1000 and 18 000 ft can be calculated from the attenuation profile in Fig. 5 by means of equations corresponding to Eq. (16).

Path Function Profiles

The aircraft is not equipped for the direct measurement of path functions for vertical and inclined paths of sight. It is capable, however, of measuring the radiance of the sky in any direction, above or below, during flight. A photoelectric telephotometer is located in a trunion mounting on top of the fuselage near the forward end of the attenuation meter, as shown in Fig. 3. This instrument performs an automatic scan of the entire sky above the aircraft in approximately 90 sec. Another telephotometer in a fixed vertical mount provides a continuous record of the radiance of the zenith during the controlled rapid descent described in the preceding section. A corresponding pair of telephotometers is mounted on the bottom of the fuselage. Figure 6 shows zenith luminance data secured by the fixed telephotometer during the same descent to which Fig. 5 applies. Similar profiles of sky luminance for any upward path of sight inclined at angles θ, ϕ can be constructed from the record of the sky-scanning telephotometer, which is designed to be operated continuously during the descent.

The profile of the path function for any path of sight can be calculated from the sky radiance profile and the attenuation profile by means of Eq. (10) after rearrangement as follows:

$$N_*(z,\theta,\phi)=\Delta N(z,\theta,\phi)/\Delta z\,\sec\theta+N(z,\theta,\phi)/L(z). \quad (18)$$

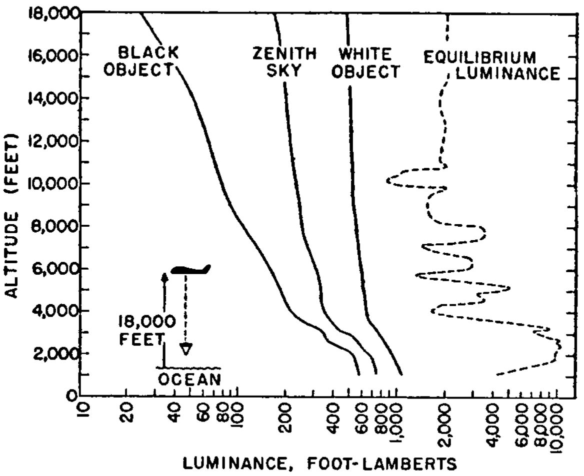

FIG. 6. Measured profile of the luminance of the zenith sky. Flight 77. Calculated profiles of the apparent luminance of black and white objects at 18 000 ft. Calculated profile of vertical equilibrium luminance.

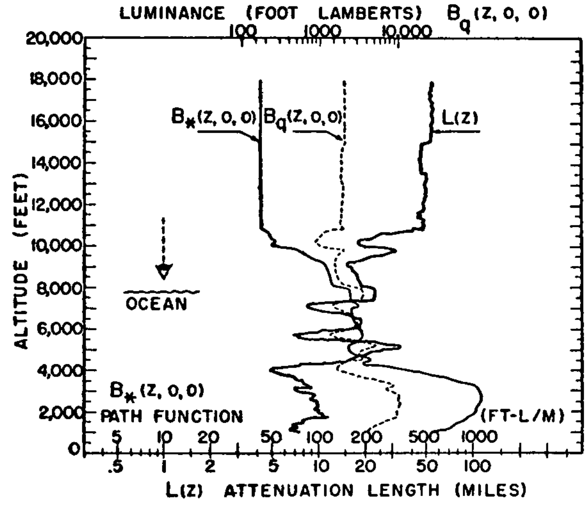

FIG. 7. Calculated profiles of vertical path function and vertical equilibrium luminance. Flight 77. The profile of attenuation length is identical with that in Fig. 5.

Figure 7 shows the result of such a calculation for the vertical path of sight which corresponds with the zenith luminance profile given in Fig. 6.

Equilibrium Radiance Profiles

An expression for the equilibrium radiance for each element of any path of sight can be found by combining Eqs. (11) and (18) as follows:

$$N_q(z,\theta,\phi)=L(z)(\Delta N(z,\theta,\phi)/\Delta z\,\sec\theta)+N(z,\theta,\phi). \quad (19)$$

Figure 6 shows the result of the use of Eq. (19) for a calculation of the equilibrium luminance profile for the upward vertical path of sight; the same profile appears in Fig. 7.

In every case the radiance of the sky $N(z,\theta,\phi)$ as observed from any altitude z is the path radiance generated by the portion of the path above the observer. That is, $N(z,\theta,\phi)=N_\infty{}^*(z,\theta,\phi)$, where $0\leq\theta<\pi/2$. Because $N(z,\theta,\phi)=0$ outside the atmosphere (except for light from the stars) and $N(z,\theta,\phi)>0$ within, it follows from Eq. (19) that the equilibrium radiance exceeds the apparent radiance of the clear sky and, therefore, the measured radiance of a clear sky increases as the photometer descends.

When clouds are present or when the image transmission direction is upward, the apparent radiance reaching any particular path segment may exceed the equilibrium radiance for that segment, so that a decrease of apparent radiance is possible. In such cases it often happens that the apparent radiance of highly radiant objects decreases while that of objects of small inherent radiance increases. Illustrative data for upward-transmitting paths of sight are planned for presentation in a subsequent paper.

Profiles of Apparent Object Luminance

Profiles of the apparent luminance of any specific object can be calculated for any path of sight provided that the inherent luminance of the object in the direction of interest is known. Two such profiles appear in Fig. 6; they refer to hypothetical "black" and "white" objects, respectively, located at a fixed altitude of 18 000 ft and viewed from directly below on the occasion to which the data in this paper applies. The profiles were calculated by means of Eq. (1). Alternatively, they could have been generated step-wise by successive applications of either Eq. (10) or Eq. (12). The complexity which characterizes the attenuation, path function, and equilibrium luminance profiles is scarcely noticeable in these vertical profiles of apparent object luminance. In the case of paths of sight inclined at large zenith angles, however, the object luminance profiles exhibit the complexities due to atmospheric structure much more prominently.

Profiles of Apparent Contrast

Figure 8 shows profiles of apparent object contrast generated by means of Eq. (3) from the apparent luminance profiles in Fig. 6. The same profiles could have been generated by use of the Eq. (7).

METEOROLOGICAL CORRELATIONS

The complex profiles of attenuation length and path function can only be the result of sharply defined layers of scattering particles. Repeated descents have demonstrated that the major features of the profiles are reproducible in space and time; the layers must, therefore,

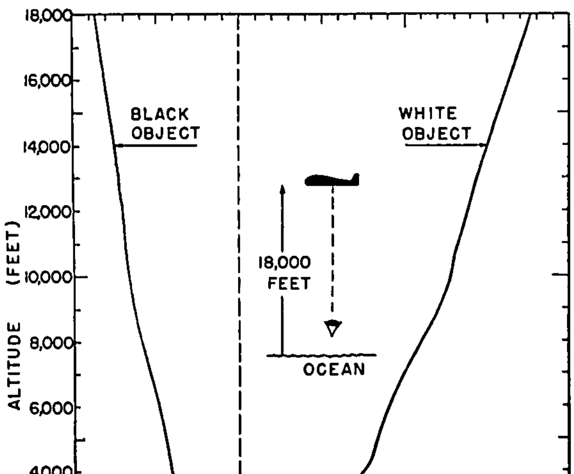

FIG. 8. Calculated profiles of the apparent contrast of black and white objects at 18 000 ft. Flight 77.

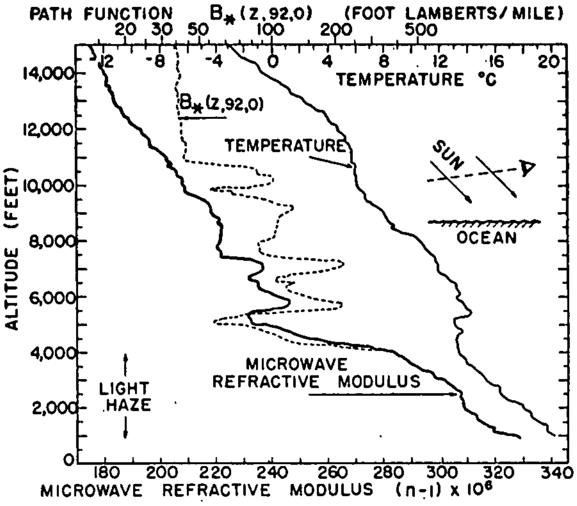

FIG. 9. Profiles of microwave refractive modulus, path function, and free air temperature. Flight 77. Correlations between the profiles of microwave refractive modulus and path function can be noted.

be horizontal strata of great extent which characterize the air mass. Such strata must also be observable in terms of nonoptical meteorological phenomena. Initial attempts to discover correlations with the temperature and humidity profiles produced routinely by the meteorological services from radiosonde observations met with failure. This was attributed to the long time constant associated with the humidity sensing elements carried by the balloons. It was believed necessary to measure the humidity profile during the controlled rapid descent of the B-29 with equipment having a fractional second time constant in order to record faithfully the presence of strata only a few feet in thickness. This was accomplished by means of an airborne microwave refractometer[6] of the type described by Crain and Deam.[7] The microwave refractive index recorded by this instrument is governed primarily by the water vapor concentration in the atmosphere; it is related to pressure, temperature, and the partial pressure of water vapor by an equation derived by Debye and discussed by numerous authors in connection with microwave propagation.[8] An expression for the partial pressure of water vapor obtained from the usual microwave approximation of Debye's equation is:

$$\epsilon=\frac{(\text{microwave refractive modulus})(\text{Kelvin temp.})^2}{(77.6)(4810)}-\frac{(\text{total pressure})(\text{Kelvin temp.})}{4810}.$$

[6] The authors are indebted to Mr. Thomas J. Obst, Director of Range Development, Patrick Air Force Base, for suggesting the use of the microwave refractometer and for arranging for the availability of this equipment for the flight experiment described in this paper.

[7] C. M. Crain and A. P. Deam, Rev. Sci. Instr. **23**, 149 (1953).

[8] E. K. Smith, Jr., and S. Weintraub, J. Research Natl. Bur. Standards **50**, 39 (1953).

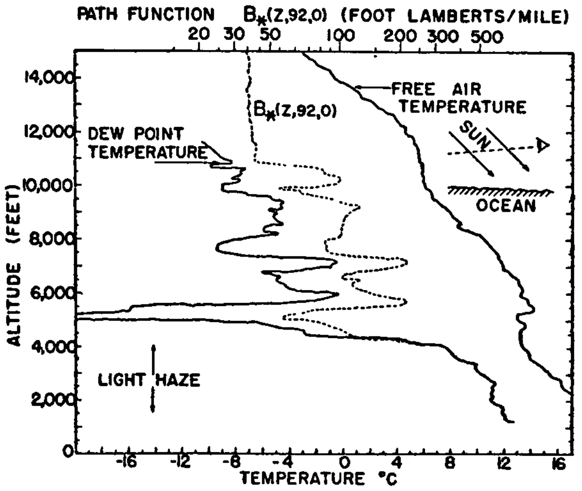

FIG. 10. Profile of dew point temperature calculated by means of Debye's equation from the profile of microwave refractive modulus in Fig. 9. Profiles of path function and free air temperature are identical with those in Fig. 9. Correlations between profiles of dew point temperature and path function are obvious.

In this equation ϵ is in millibars, the Kelvin temperature is of the stratum, the total pressure is in millibars, and the *microwave refractive modulus* of the stratum for microwaves is defined by the expression $(n-1)\ 10^6$, where n is the refractive index of the stratum.

An Air Force C-131 equipped with a microwave refractometer flew in formation with the B-29 throughout the descent during which the optical data reported in this paper was secured. The resulting profile of microwave refractive modulus is shown in Fig. 9. The profile of horizontal path function from Fig. 5 also appears in Fig. 9 for purposes of comparison.

Debye's equation was used to calculate a humidity profile from the microwave data. This profile, expressed in terms of dew-point temperature, is given in Fig. 10. The close correlation between humidity and path function is obvious.

The following speculations on the reasons for the observed correlation are offered: In terms of visible light water vapor exhibits virtually no absorption and it contributed only molecular scattering, the magnitude of which is too small to be responsible for the observed effects. The atmosphere invariably contains, however, suspended material such as sea-salt ions, silica, ammonia, or oxides of nitrogen and sulfur which can form condensation nuclei for water droplets. A tenuous haze of these tiny droplets will form in any stratum having a water vapor content above some critical minimum. These droplets will grow until the vapor pressure just outside the curved surface of the drop equals the partial pressure of water vapor in the surrounding air.[9] Liquid droplets ranging from 4×10^{-7} to more than 10^{-4} cm are known to be present in the atmosphere.[10] In the case of spherical water droplets small in diameter compared with a wavelength of light that component of the scattering coefficient which is due to droplets increases as the sixth power of their diameter,[11] assuming the number of droplets per unit of volume to remain fixed. In view of this, the observed correlation between the path function and the humidity within tenuous haze layers appears to be understandable.

ACKNOWLEDGMENTS

The number of individuals involved in an experimental program of the complexity, scope, and duration of the flight research partially described by this paper is too great to be listed properly here. Special mention should be made, however, of the technical contributions of Brig. Gen. Victor A. Byrnes, USAF, through whose efforts the program was initiated; Lt. Col. George E. Long, USAF; Major Joseph X. Brennan, USAF; and research pilot Capt. Robert L. Baron, USAF. Important contributions to the detailed design of the apparatus were made by John M. Hood, Roswell W. Austin, W. Joseph Woodside, Thomas H. Glenn, Romuald Anthony, Merril D. Hobt, and David J. A. Hooton.

[9] W. E. K. Middleton, *Vision through the Atmosphere* (Toronto Press, Toronto, 1952), Chap. 3.
[10] C. Junge, *Nuclei of Atmospheric Condensation*, Compendium of Meteorology (American Society for Metals, Cleveland, 1951).
[11] Lord Rayleigh, Proc. Roy. Soc. (London) A90, 219 (1914).

REFERENCES

1. Duntley, S. Q., A. R. Boileau, and R. W. Preisendorfer, "Image Transmission by the Troposphere I", Journal of the Optical Society of America, 47, pp. 499-506, (1957).

2. Preisendorfer, R. W., "Theory of Attenuation Measurements in Planetary Atmospheres", SIO Ref. 58-81, Scripps Institution of Oceanography, University of California, La Jolla Campus, 24 November 1958.

ACKNOWLEDGMENTS

While the assistance of all who have helped in this work is fully appreciated special mention is made of the crew of the B-29, No. 4224725, Capt. Ben V. Walker, USAF, Aircraft Commander, Capt. Louis Prestwood, USAF, Co-pilot, and Air Force Cambridge Research Center Test Support Group.